AN INVESTIGATION OF GALACTIC STRUCTURE

NEAR $(l,b) = (140^{\circ},0^{\circ})$

RICHARD JOHN DODD B.Sc. (St. Andrews)

Ph.D. Thesis

UNIVERSITY OF EDINBURGH

1973 August

Je m'en vais chercher un grand peut-être.

François Rabelais (1494-1553)

"ABSTRACT OF THESIS"

The nature of the discontinuity near the galactic equator at longitude 140° was investigated by studying the apparent surface distribution, the mean density functions and the proper motions of stars within an area of approximately 16 square degrees centred on $(\ell,b) = (140^{\circ},0^{\circ})$.

The suitability of the GALAXY machine for measuring precise stellar positions was tested. It was found that, after corrections for proper motions, the mean residuals between the catalogue and computed positions, from a Schmidt camera plate, for 430 stars in the Pleiades were $+0^{s}.002 \pm 0^{s}.009$ in right ascension and $+0''.03 \pm 0''.13$ (standard deviation) in declination. The standard deviations of these residuals correspond to 1μm on the plate. No magnitude or colour dependence was found for the GALAXY measures in the ranges of these variables considered.

UBV photoelectric magnitudes for 53 stars and RI magnitudes for 20 stars were measured. The magnitudes are given in the Johnson system.

Measurements were made of two plates taken 53 years apart to determine the proper motions of 553 stars common to both plates. U, B and V magnitudes for each of the stars were measured and the secular parallaxes of distinct groups of stars, in preselected magnitude intervals, in

.../

the two colour diagram were derived in an attempt to identify possible stellar members of the α-spiral arm defined from HI observations by Verschuur. Other than late type giants the only group of objects whose distance corresponded to that of this arm was a small group of reddened early type stars.

Star counts in unit B and I magnitude intervals were made in nine regions, each 1.75 square degrees in area, distributed about $(l,b) = (140^{\circ},0^{\circ})$. The apparent surface distribution of the stars was examined using equal number density contour diagrams. The mean density function and the mean variation of interstellar absorption with distance for the various areas were determined using a combination of theoretical and observed cumulative Wolf diagrams. This analysis showed that the considerable change in the number of stars observed with galactic longitude is due, not to increased interstellar absorption, but rather, to a real reduction in the number of stars per unit volume of space.

CONTENTS

Chapter 1. Introduction

1.1 Galactic Structure

The Galaxy of stars to which the sun belongs is spiral in structure. It consists of four main arms located, in part, in the constellations Perseus, Orion, Sagittarius and Norma and the so called 3 kpc arm. The sun lies on the inside of the Orion arm with the Perseus arm lying further from the galactic centre and the Sagittarius, Norma and 3 kpc arms lying nearer the galactic centre. The location and shape of the spiral arms may be defined optically by the spatial distribution of OB stars, Be stars of early type, HII regions, young galactic clusters, and less strongly by late B and early A main sequence stars, and the classical cepheids. All these Population I objects are young relative to the rotation period of the Galaxy, implying that they have not moved far from their place of formation.

Optical observations are severely restricted by interstellar absorption. Radio observations are not so affected and the spiral structure may be mapped by use of the 21cm line of atomic hydrogen. The HI distribution obtained depends on certain main assumptions, namely that the gas clouds have a circular motion about the galactic centre, that their temperature is uniform everywhere, and that they are optically thin.

.../

1.2 Distribution of Stars and Interstellar Matter near $(\ell, b) = (140^{\circ}, 0^{\circ})$

It was originally suggested by Reddish (1967) that a discontinuity in galactic structure occurred near the galactic plane at $\ell = 140^{\circ}$. The observational evidence cited was: the abrupt change in number density distribution at this longitude of such objects as Wolf-Rayet stars, dust embedded stars and globules, a rotation of the polarization vectors of galactic radio waves, and a variation in the wavelength dependence of the position angles of interstellar polarization of starlight.

The distribution of OB stars in the galactic plane was examined by Sim (1968a), who showed that there was a significant fall in OB star numbers at $\ell = 140^{\circ}$. This conclusion was strengthened by the work of Humphreys (1970a) which was based on all supergiants of spectral type B5 and earlier and all those later than B5 with luminosity classes brighter than Ib. These objects traced the Perseus arm from $\ell = 100^{\circ}$ to 140° at distances from 2 to 3 kpc. The arm appears as a relatively broad feature about 800 pc wide with a large concentration from $\ell = 125^{\circ}$ to 135°. Counts of B8 - A3 stars to a limiting magnitude V = 13 along the galactic plane from $\ell = 50^{\circ}$ to 150° between b + $\pm 5^{\circ}$ were made from objective

.../

prism plates by McCuskey and Houk (1971). Histograms of stars in the region b = $\pm 3^{o}$ show that the total A-star population does not fluctuate greatly with galactic longitude. The number of A stars increases with latitude through the galactic plane at $\ell = 140^{o}$. The angle with respect to the galactic equator between the minimum of the number of A stars present at $(\ell, b) = (140^{o}, -2^{o})$ and the maximum at $(\ell, b) = (136^{o}, +2^{o})$ is approximately 50^{o} which compares well with 45^{o} for OB stars (cf. Sim 1968a). An increase in space density for $\ell > 140^{o}$ between r = 1.5 and 2 kpc was noted implying that the Perseus arm had been reached.

The potential of M supergiants as tracers of spiral structure using infrared wavelengths was exploited by Humphreys (1970b). With low dispersion objective prism surveys these stars can be detected at distances as great as 10 kpc. In the Perseus arm ($\ell = 100^{o}$ to 140^{o}) the M supergiants show the same spiral features as other Population I objects. In the (ℓ, r) plane they show a strong concentration between $\ell = 130^{o}$ and 143^{o} and r = 3 to 5.5 kpc. Between $\ell = 143^{o}$ and 168^{o} no M supergiants were observed. Other M type and Mira variable stars show no number dependence on galactic longitude (Mavridis 1966), but for $|b| \leq 2^{o}$ Mavridis (1971) has shown that the distribution of carbon stars exhibits peaks at $\ell = 120^{o}$ and 170^{o} with a minimum at about $\ell = 140^{o}$.

.../

Smith (1968) found that there appeared to be a complete lack of Wolf-Rayet stars in the directions between $\ell = 140^{\circ}$ and 220°. On the basis of Khavtasi's (1960) atlas of dark nebulae, which implies that interstellar absorption is comparatively slight in these directions, Smith concludes that the gap in the Wolf-Rayet distribution is real and that the Perseus arm ends at about $\ell = 150^{\circ}$. Kraft and Schmidt (1968) tentatively arrived at a similar conclusion from a consideration of the galactic distribution of classical cepheids. This result is contradicated by Fernie (1968) using the catalogue of Fernie and Hube (1968), their (ℓ,r) plot shows no discontinuity at or near $\ell = 140^{\circ}$.

The usefulness of cepheids as spiral arm tracers was investigated by Tammann (1970) who found that the positional correlation between cepheids with $P \geq 15$ days and other Population I objects was reasonably good but weakened with decreasing period. The significance of the results of Smith, Tammann and Kraft and Schmidt is questioned by Rohlfs (1967) who on the basis of objective statistical tests doubts that cepheids or Wolf-Rayet stars are reliable in delineating spiral structure.

A survey of young open clusters whose brightest main sequence member was of spectral type B2 or earlier, was

.../

made by Moffat and Vogt (1973). In the (ℓ,r) plane a vector drawn from the sun and rotated through the direction $\ell = 140^{o}$ shows a drop in the number of clusters passing through that line of sight with increasing longitude. The change is most marked at a distance of approximately 2.5 kpc.

No obvious discontinuity at or near $\ell = 140^{o}$ is observed in the distribution of planetary nebulae (cf. Perek and Kohoutek 1967), for these objects there is a gradual fall in numbers away from the galactic centre and increased dispersion in galactic latitude. An emission Hα Schmidt camera survey was made by Kohoutek (1972) to find faint planetary nebulae in the region $70^{o} \leq \ell \leq 146^{o}$, b = $\pm 10^{o}$. 32 new nebulae were found. Their distribution is not homogeneous in galactic longitude and there are more north of the galactic plane than south. No faint planetary nebulae were discovered between $\ell = 135^{o}$ and 140^{o}. Racine and van den Bergh (1970) have found good agreement between the spiral arms outlined by R associations (i.e. stars embedded in reflection nebulae) and those obtained by other methods.

Using the 2μm sky survey of Neugebauer and Leighton (1969) Hughs et al (1969) have shown that the concentration of infrared objects increases strongly to within $\pm 2^{o}$ of the galactic equator for $355^{o} \leq \ell \leq 140^{o}$. Outside this

.../

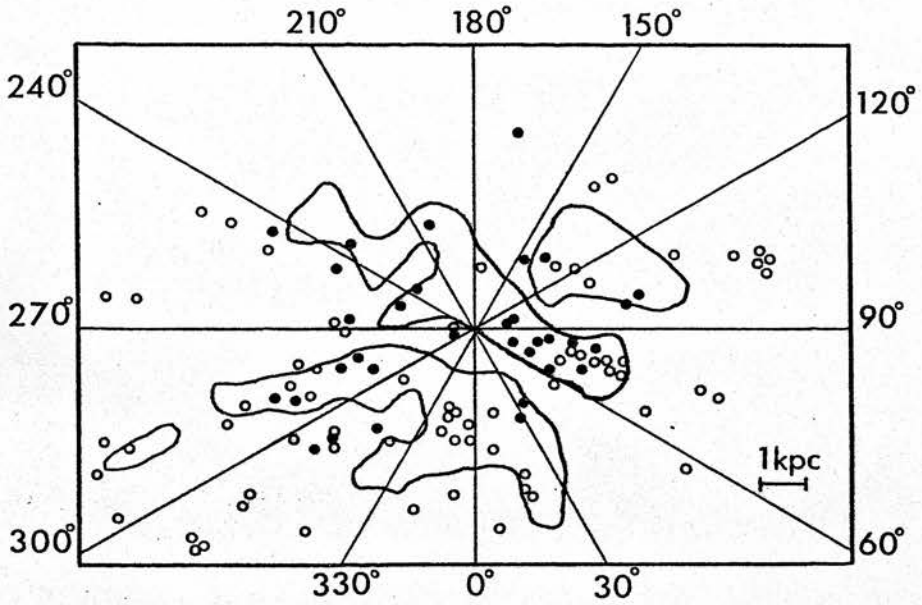

Fig 1.1 Galactic structure based on different spiral arm tracers (after Moffat and Vogt, 1973).

Enclosed areas were delineated by HII regions, supergiants, Be stars and young open star clusters.

○ Wolf-Rayet stars.

● Cepheids with $P \geq 15^d$

zone the surface density of objects tends to reach a maximum at about b = $\pm 10^{o}$ and then decrease towards the equator.

Measurements by Cooke et al (1969) and Schwartz (1969) have shown that the X-ray (2.15 kev) brightness of the sky exhibits a slight enhancement along the galactic ridge with a broad maximum in the direction of the galactic centre. Ryter (1970) has plotted the distribution of observed X-ray sources in the (ℓ,r) plane, which shows a gap between about $\ell = 135^{o}$ and $\ell = 185^{o}$. According to Deupree (1969) the positions of galactic X-ray sources appear to correlate well with novae, supernovae and planetary nebulae (Population II objects). The absence of sources in the $\ell = 140^{o}$ direction is confirmed by results from the UHURU satellite which found no discrete X-ray objects in the 2-6 keV energy range from $\ell = 130^{o}$ to $\ell = 165^{o}$ (cf. Seward 1973).

Georgelin and Georgelin (1971) using both optical and radio techniques have shown that there is a drop in the number of HII regions as a vector centred on the sun in the galactic plane sweeps through 140^{o} in the direction of increasing longitude. The number density gradient, however, is less steep than for OB or Wolf-Rayet stars or for young galactic clusters. A discussion on the relative merits of optical and radio observations of HII regions is given by Mezger (1970) who points out that the distribution of optically observed HII regions and

.../

OB stars with galactic longitude indicates that it is primarily determined by interstellar dust extinction. This implies that optical observations can at best only reveal local structure in the solar vicinity. Radio observations are not affected by dust and can therefore be used for more remote structural investigations. Such an investigation at the distance of the Perseus arm revealed no HII regions from $\ell = 140^{\circ}$ to 160°.

A map of the distribution of HI in the Galaxy based on Schmidt's (1965) model is given by Kerr and Westerhout (1965). No discontinuity in the galactic plane in the HI density is evident. A more detailed investigation of neutral hydrogen in the Perseus arm based on the Maryland-Green Bank galactic 21cm line survey was made by Sato (1970).

Goss (1967) found that the distribution of OH agrees with the spiral arms as delineated by HII regions. In many cases for which an OH absorption line was found in the direction of a galactic HII region, the velocity of one of the OH absorption lines and the velocity of the nebulae agreed quite closely. No absorption line OH sources were found between $\ell = 140^{\circ}$ and $\ell = 180^{\circ}$.

The variation of interstellar absorption with galactic longitude has been investigated by several authors

.../

in various ways. Neckel (1967) used 4700 measurements of stars and clusters in order to derive the extinction A(r) as a function of r, taking R = 3.1 as the ratio of total to selective absorption. He plotted the value of A_v within 1 kpc of the sun along the galactic equator to b = $\pm 6^o$. At $\ell = 140^o$ the absorption from $b = -1^o$ to b = $\pm 6^o$ lies between the limits $1^m.4 \leq A_v \leq 2^m.2$. Between $\ell = 140^o$ and 260^o A_v (r $\leq$ 1 kpc) is smaller than for the rest of the Milky Way, which may indicate that the absorbing matter is concentrated at the inner edge of the local arm. FitzGerald (1968) using photoelectric magnitude measures found that reddening was not present in the Perseus arm up to $\ell = 140^o$ but that beyond this longitude and at a greater distance from the sun than the arm itself reddening began. If these observations are correct they lend support to Dixon's (1967) theory that non-gravitational forces, which act only on the interstellar gases and materials, cease to act on material that has condensed to form stars and, as a consequence, newly formed stars fall away from the gases in which they were produced. The stars then fall towards the mean galactic plane and towards the galactic centre.

The ratio R of total to selective extinction was derived by Crézé (1972) from a comparison of spectroscopic and photometric data with the kinematical parallaxes compiled from radial velocities, through a model of galactic differential rotation. HII regions, Population I Cepheids

.../

and open clusters were used for the study. R was found to depend both on galactic longitude and colour excess. R decreases from 4.5 at $\ell = 90^{o}$ to a minimum of 3.1 at $\ell = 145^{o}$, corresponding to decreasing thickness of the local spiral arm in the line of sight. After $\ell = 145^{o}$ the value of $\left| dR/d\ell \right|$ becomes much greater. Another indication of a change in the properties of the interstellar obscuration at about $\ell = 140^{o}$ is provided by Brück et al (1968) on the basis of variations in the observed spectrophotometric ratio UV slope/BV slope. Kostjakova (1970) however, found no unusual feature in the spectrophotometric gradient of the integrated spectrum of the Milky Way at and around $\ell = 140^{o}$. Equivalent widths, as published by Seddon (1968), for the diffuse interstellar absorption band at λ6180 were compared by Rudkjøbing (1970) with photoelectric λ4430 indices for ten stars in the northern Milky Way. The intensity ratio was found to be dependent on galactic longitude and showed a maximum at about $\ell = 150^{o}$.

In conclusion, evidence of a material galactic discontinuity at or near $\ell = 140^{o}$ is provided by OB stars, Wolf-Rayet stars, carbon stars, M supergiants, young open clusters, HII and OH regions, reflection nebulae, infrared and galactic X-ray sources and changes in the value of interstellar extinction.

.../

There is no discontinuity in the distribution near $\ell = 140^{\circ}$ of main sequence stars of type A and later, planetary nebulae, and neutral hydrogen gas.

1.3 Structure of Fields near $(\ell, b) = (140^{\circ}, 0^{\circ})$

The structure of the velocity field in the Perseus arm has been extensively studied. Rickard (1968) using optical data on young open clusters, HII regions, O-associations, interstellar extinction and interstellar absorption lines together with high resolution 21cm hydrogen maps found that from $\ell = 97^{\circ}$ to 150° between $b = \pm 1^{\circ}$ the Perseus arm showed peculiar radial velocities of about -25 km sec^{-1}. A distance estimate based upon the interstellar absorption lines, interstellar extinction and HII regions indicated that the gas, dust and ionised elements were situated 1.5 to 2.5 kpc from the sun. These limits contain the estimated distance, based on HI emission line profiles using Schmidt's (1965) model, of the Perseus arm at $\ell = 140^{\circ}$ of 2.2 kpc given by Velden (1970). However, this may be coincidental since Rickard's observations indicate that, within the distance range quoted, the interstellar medium is moving with a fairly uniform velocity in violation of differential rotation and contrary to Schmidt's model. This conclusion is based on the assumption that there is a strong velocity correlation between neutral hydrogen gas and interstellar NaI and CaII and the HII regions. There appears to be considerable

.../

turbulent motion within the arm, of the six O-associations studied, five have velocities systematically less negative than the HI arm. Only one lies in the major part of the arm and it is at the end of the region of peculiar motions ($\ell = 135^{o}$).

Rickard's conclusion that the velocity structure of the Perseus arm is not as predicted by Schmidt's model is contradicted by the work of Courtès et al (1970). They used radial velocities and spectrophotometric distances of HII regions to give a model of the rotation curve of the Galaxy which is identical to the Schmidt curve. From this agreement they conclude that the HII regions have the same rotational velocities as other population I components such as bright cepheids and neutral hydrogen.

Verschuur (1973) suggests that the observed peculiar velocities may be due to observing two different spiral arms while assuming there is only one. He postulates the existance of a more distant arm (the α- spiral arm) beyond the Perseus arm on the basis of neutral hydrogen observations (cf. Fig. 1.2).

An investigation of the radial velocities of all supergiants of type B5 and earlier and all those later than B5 with luminosity classes brighter than Ib in the Perseus arm from $\ell = 100^{o}$ to 140^{o} was made by Humphreys (1970a). She finds that a comparison with neutral

.../

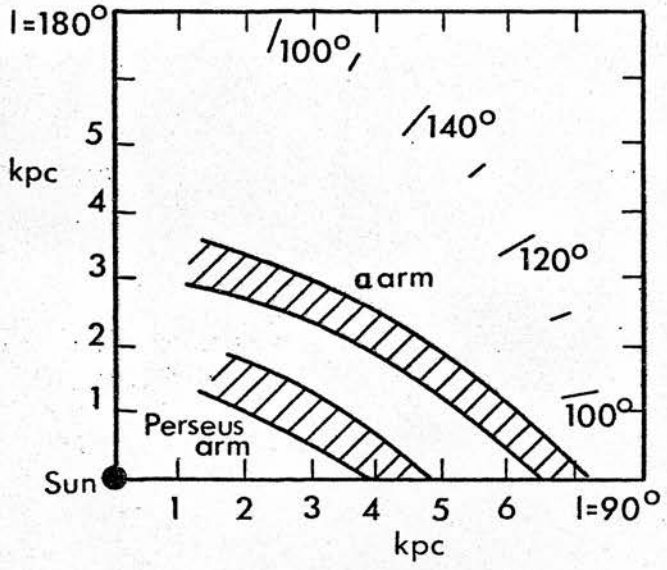

Fig. 1.2 A section of a spiral structure map for the Perseus region (after Verschuur 1973). The Perseus arm was mapped by Associations, HII regions, and open clusters as well as HI radio measurements; the α- arm was mapped by HI measurements alone.

hydrogen observations shows that in velocity space the gas and stars correlate well. In positional space the gas and stars also exhibited a fairly strong correlation. Velocity residuals between the observed radial velocity and the radial velocity predicted for the given distance using Schmidt's model were computed. These indicated a non-circular group motion which Humphreys supposed was shared by the gas in the arm. The residuals found were negative over the entire inner side of the arm, again tending to support Dixon's (1967) theory, though this result does contradict Rickard's observations which imply that the stars are moving faster than the gas in the arms.

It would appear, in conclusion, that there is not enough reliable evidence as yet to support the hypothesis that the motion of the Perseus arm is not described by Schmidt's model and that a velocity discontinuity exists at $\ell = 140^{\circ}$.

Estimates of the strength and direction of the interstellar magnetic field may be deduced from observations of the polarization of light and radio waves. Surveys of linear polarization at radio frequencies near to galactic longitude 140° have been made by Spoelstra (1972) at 1415 MHz, Berkhuijsen (1972) at 820 MHz, Baker and Smith (1971) at 410 MHz, Verschuur (1968, 1969) at 408 MHz, and Seaquist (1967) at 710 MHz. At all these frequencies a strongly polarized feature was observed near $(\ell, b) = (140^{\circ}, +6^{\circ})$ with the region on the galactic

.../

equator around $\ell = 140^{o}$ showing an anomalously low polarization. In each case the polarization vectors were aligned at right angles to the galactic equator. Seaquist found that there was a poor correlation between sky brightness and polarization measures at 710 MHz consistent with the hypothesis that the magnetic field causing the polarization is local since the greater the distance of the magnetic field the greater would be the correlation between the sky brightness and polarization measures. Verschuur has postulated that the cause of the polarization is a combination of distorted magnetic field and the ionization produced by a B2 star tunneling through an interstellar cloud. He concludes that, if the observed lack of HI and the depolarization are associated with the star, nearly all the polarized emission seen in the region of $\ell = 140^{o}$ comes from distances greater than 300 pc (the assumed distance of the star) because there is at least one very small area where the polarization observed at 408 MHz is zero.

Plots of optical polarization vectors (cf. Fig. 1.3 and 1.4) over the entire sky in various distance intervals from 0-4000 pc for 7000 stars are presented by Mathewson and Ford (1970). If most of this polarization is produced by the scattering of light by interstellar dust particles aligned by a magnetic field (Davis and Greenstein 1951) then the E - vectors may be taken to represent the

.../

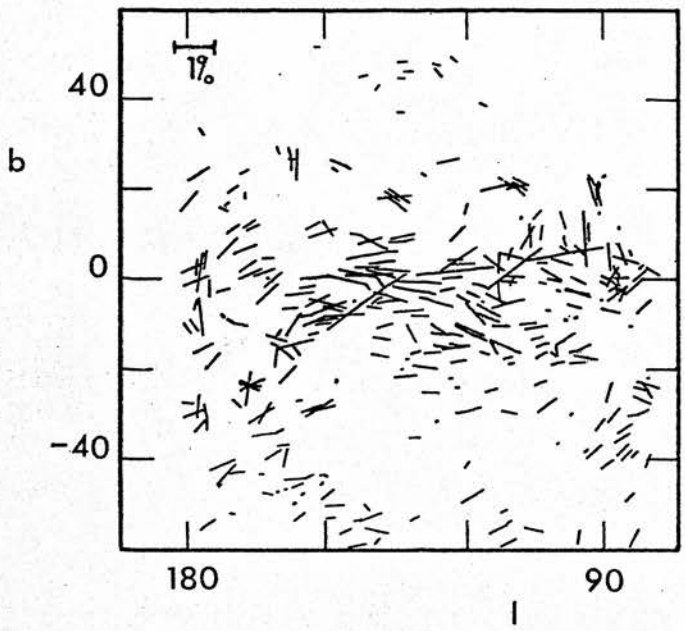

Fig. 1.3 E-vectors of optical polarization for stars from 0-600 pc distance. Adapted from Mathewson and Ford (1970).

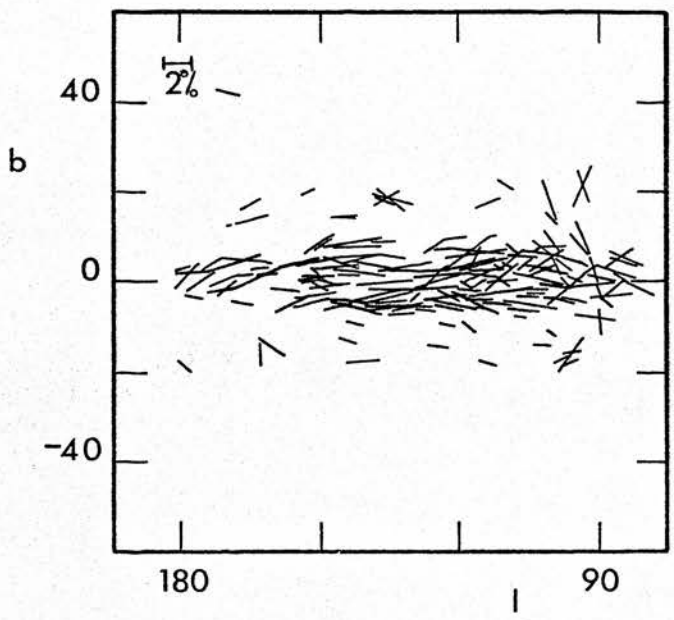

Fig. 1.4 E-vectors of optical polarization for stars from 600-4000 pc distance. Adapted from Mathewson and Ford (1970).

projection of the magnetic field on a plane perpendicular to the line of sight and thus they trace the structure of the magnetic field as revealed by the interstellar dust. For the region within 600pc of the sun the E-vectors form quite definite patterns which are best explained by a helical magnetic field (Matthewson 1968). The directions of the magnetic field determined from optical and radio polarization measurements are in good agreement. Matthewson and Nicholls (1968) found that to account for the distribution of sense of the rotation measures of extra-galactic radio sources, it was necessary to add a longitudinal field directed towards $\ell = 90^{\circ}$ to the helical magnetic field. The E-vectors of the stars at distances greater than 600 pc show the influence of this longitudinal field. Further investigations showed that the helical field is confined to the region within 500 pc of the sun whilst the longitudinal field is much more widespread. At and around $\ell = 140^{\circ}$ the E-vectors are parallel to the galactic equator, the parallelism becoming more definite with distance.

By combining measurements of the flux of primary cosmic ray electrons with the mean non-thermal emissivity of the galactic disk in the direction of $\ell = 140^{\circ}$, Bridle (1968) has estimated the strength of the interstellar magnetic field in this region for the disk. The mean emissivity derived gives a mean magnetic field strength

.../

in the line of sight of $(6 \pm 2) \times 10^{-6}$ Gauss, if the non-thermal emission is assumed to be concentrated within the spiral arms, the results imply a field strength of $(1.6 \pm 0.5) \times 10^{-5}$ Gauss.

The evidence for an irregularity in the magnetic field structure of the Galaxy around $\ell = 140^{\circ}$ is very strong and tends to point to a localized origin for the disturbance. It is therefore probable that on a galactic scale the change in the observed magnetic field structure is of little consequence and is unrelated to a possible termination of the Perseus arm at $\ell = 140^{\circ}$.

1.4 Summary

There is a considerable weight of observations in support of a galactic discontinuity at $\ell = 140^{\circ}$. However whereas studies of the spatial distribution of objects place the discontinuity at the distance of the Perseus arm (about 2 kpc), those of magnetic field structure suggest a local origin nearer than 600 pc. It would therefore seem that these discontinuities are distinct.

The object of this thesis is to provide more information about the surface and spatial distributions, and the motions, of the stars within an area of approximately 16 square degrees centred on $(\ell, b) = (140^{\circ}, 0^{\circ})$ which may help to resolve the nature of the discontinuity.

.../

Chapter 2. Measuring Machines

2.1 Introduction

Brief descriptions of the computer and photometric and astrometric measuring machines used for reducing the various photographic plates taken are given below. Observational equipment, such as telescopes, is described under the appropriate chapter heading. An account of the use of GALAXY for measuring precise stellar positions is also given.

2.2 ICL 4130 Computer

The ICL 4130 computer of the Royal Observatory Edinburgh was installed in 1967. It has a 32K 2 micro-second 24 bit word store. Peripherals include 5 magnetic tape handlers, 2 paper tape punches and readers, control teletype, line printer and on-line digital graph plotter.

2.3 Joyce-Loebl Microdensitometer

The Joyce-Loebl microdensitometer was used to prepare density with wavelength tracings of 192 stars in the $(\ell, b) = (140^{\circ}, 0^{\circ})$ region. The operational principle of this microdensitometer is based on a double-beam light system, in which two beams from a single light source are switched alternatively to a single photomultiplier. If the two beams are of different intensity, a signal is produced by the photomultiplier, which, after amplification,

.../

causes a servo-motor to move an optical attenuator so as to reduce the intensity difference to zero. In this way a continuously null balancing system is obtained in which the position of an optical attenuator is made to record the density at any particular part of the spectrum.

The position of the optical wedge, to which a direct writing pen is attached, is controlled by the amplified photomultiplier signal being applied to a servo-motor which drives the wedge until a null-balance is achieved. The plate and recording tables are driven by another servo-system at a speed proportional to the rate of change of density. These tables are directly linked by a single arm, the spectrum magnification depending on the position of the pivot used on this arm. Changes in zero point are made by adjusting a grey wedge, a series of such wedges giving a range in tracing amplitude.

2.4 Grubb Parsons Two Coordinate Measuring Machine

This machine was used to obtain (X,Y) coordinates, for GALAXY reference block stars and for stellar spectra on a prism plate. If care is taken the repeatability of the (X,Y) measures is around $\pm$ 2μm.

The plate to be measured is inserted through an opening in the top of the casing and placed emulsion side

.../

Fig. 2.1 Grubb Parsons Two Coordinate Measuring Machine.

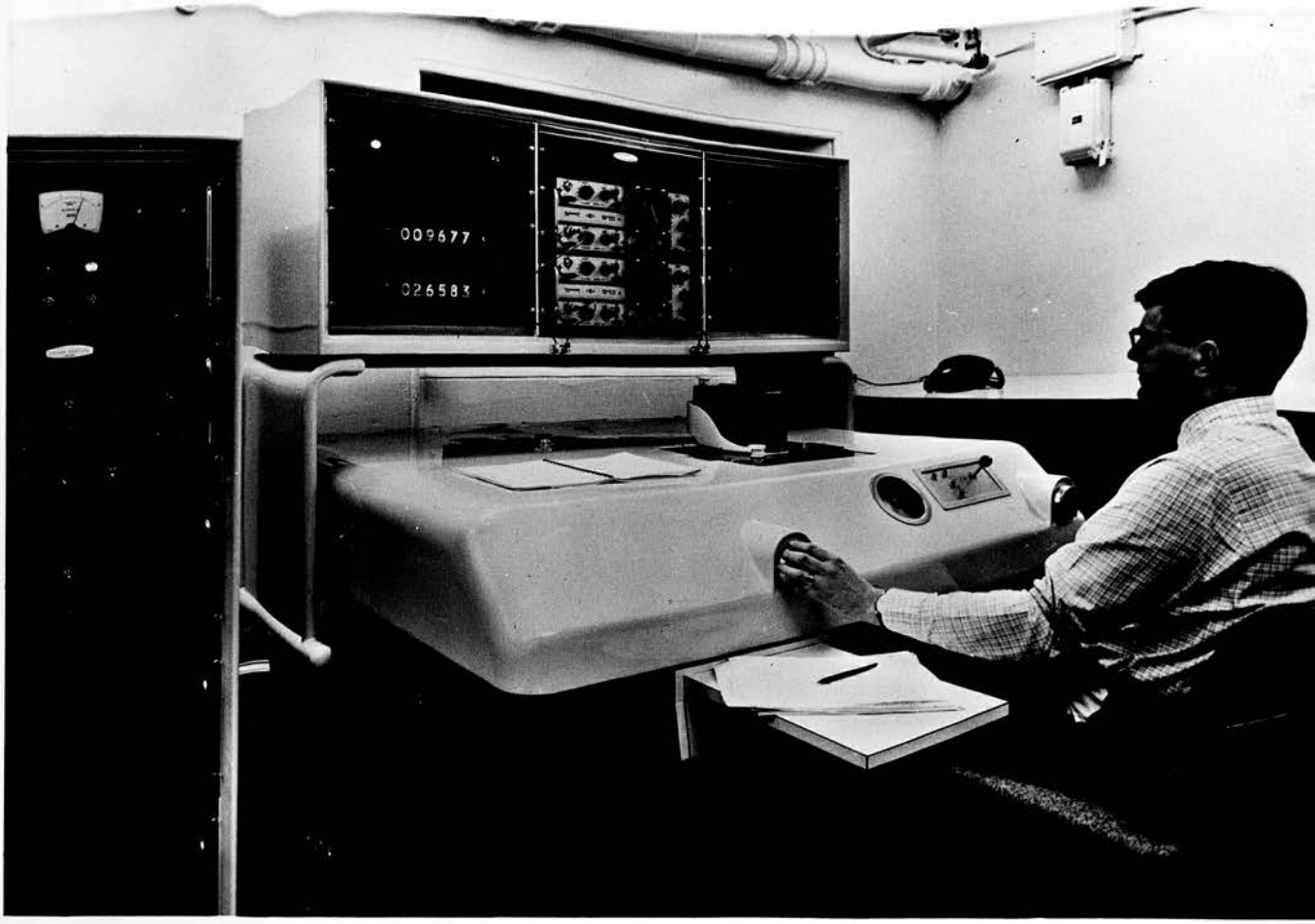
009677
026583

down on a moveable carriage. The aperture in the casing is sealed by a heavy piece of plate glass. The photographic plate and the associated measuring devices are thus contained in a totally enclosed thermostatically controlled environment. The carriage is driven in the X and Y directions by two speed electric motors using a joystick control. The general position of the plate can be seen at all times through the glass in the casing. In addition, a screen in the front of the casing shows a projected image of the area of the plate in the neighbourhood of the bisection system. The centre of screen has engraved three concentric circles into which the star image to be measured is driven. The image is then in the field of the photometric bisection scanner.

Two oscilloscopes show the absorption trace produced in X and Y coordinates for the chosen star image, together with a datum pulse. By means of hand controls the plate carriage position is finely adjusted until the star image is exactly at the measuring point; this is when the limbs of the absorption trace are of equal height with respect to the datum pulse. At this point the (X,Y) coordinates may be read directly in microns from two six figure illuminated decade counters.

2.5 Becker Iris Photometer

Descriptions of the semi-automatic iris photometer

.../

have been given by Fellgett and Seddon (1963) and Seddon and Jones (1966).

Briefly the Becker photometer compares a reference beam of light coming directly from the main lamp with that transmitted through an adjustable iris placed in the plane of a greatly magnified image of the photographic plate. A star image is centred in the iris which adjusts automatically until the light passing through the iris round and through the star image is equal to the reference beam. At this point (X,Y) coordinates accurate to approximately 100μm and iris reading may be either punched on paper tape by a foot control or read directly from decade counters. The photographic plate to be measured may be inserted into the moving (X,Y) carriage with the emulsion side either up or down. In the current work the Becker photometer was used to measure U and V magnitudes of 553 proper motion stars in the $\ell = 140^{o}$ region.

2.6 The GALAXY Machine

The GALAXY (an acronym for General Automatic Luminosity And X-Y measuring engine) machine was originally designed by Prof. P.B. Fellgett as a means of extracting, in conjunction with a digital computer, the large amount of information contained on photographic plates taken with Schmidt telescopes. A complete history of the design and development of GALAXY is given by Walker (1971).

.../

Fig. 2.2 The GALAXY Measuring Machine.

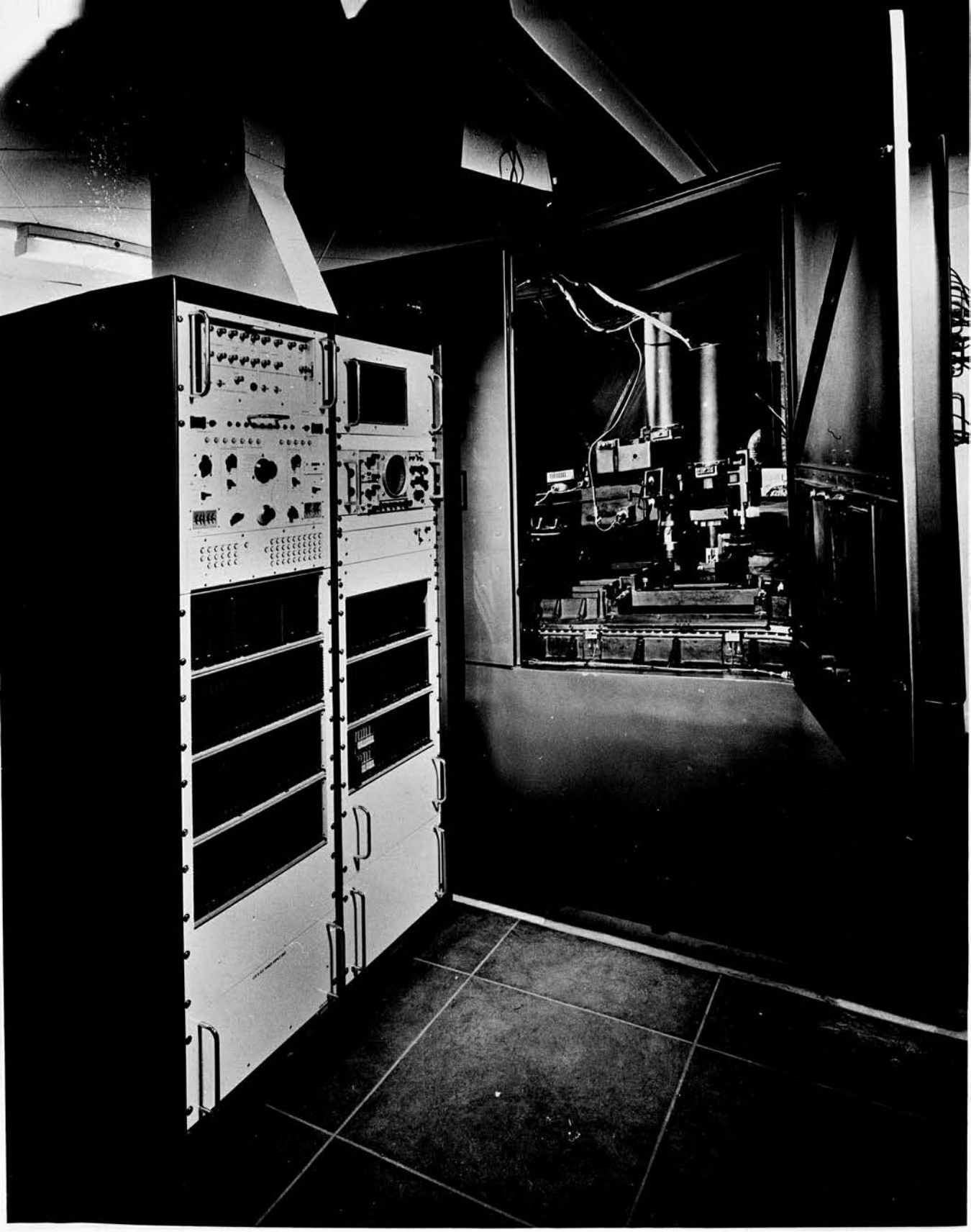

The machine consists of a hollow webbed base casting on which is mounted a carriage which is moved in X and Y on linear ball bearings by two hydraulic rams. The photographic plate to be measured is fitted into a heavy plateholder which has three ball-ended screws for locating in three V-grooves on the carriage. Two micro-spot cathode-ray tubes with their scanning assemblies and optical systems are rigidly mounted on a bridge casting over the carriage, so that the plate can be positioned relative to their optical axes. The variation in light transmitted when the plate moves being detected by two photomultipliers mounted below the carriage level. X and Y movements are measured to 1μm using a Moire grating system. The whole machine is kept in a temperature, humidity and dust controlled atmosphere.

GALAXY has two modes of operation, known as the search phase and the measurement phase. In the search phase a small spot of light (8, 16, 32 or 64μm in diameter) projected from one of the optical systems scans the selected area of the plate in a raster pattern. A photo-electric cell monitors the light transmitted through the plate and detects the reduction in brightness when the light spot falls on a star image. The speed at which the plate is scanned depends on the spot size setting, being 30 square mm per minute for 16μm. The star coordinates are punched out on paper tape at a rate of 10000 per hour for the 16μm spot.

.../

The paper tape prepared during the search phase is used as the control input for the measurement phase. The machine drives to the approximate coordinates of each star and scans the plate with a spot one micron in diameter in a pseudo spiral pattern (i.e. 1024 concentric circles reduced optically by either 240, 75 or 30 times, with the X240 optical system the projected diameter on the emulsion of the largest circle is 256μm). If the star image is not centred, a photo-electric cell monitoring the transmitted light detects more light coming through one side of the pseudo spiral than the other, which produces a current that drives the plate carriage, through servo-motors, until the star image is centred and no off-balance current is produced. To measure the apparent size of the image a comparison is made between the observed transmission profile of the image and a group of 1024 idealized profiles. When both the centring and image profile conditions are satisfied, the image centre coordinates (X,Y) and the number of the nearest matching profile (M) are punched onto paper tape. The rate of measurement of star images is 900 per hour.

Since the search and measurement optics are distinct it is necessary to use a 'datum' plate to relate the coordinates as measured by the different systems. The datum plate contains a clear pin hole (50μm in diameter) in a black background, the coordinates of this pin hole

.../

are set equal in both the search and measurement modes. To check GALAXY measures for consistency a reference block of star images is specified (normally about 100 images) which is measured after every 900 programme star images. The coordinates of the reference block star images are measured initially with the Grubb Parsons measuring machine. Two reference block star images on each plate are chosen. The (X,Y) coordinates of these reference stars are measured by GALAXY in a manual mode. The GALAXY coordinates are compared with the Grubb Parsons coordinates to determine the constants of translation and rotation needed to convert Grubb Parsons coordinates to GALAXY coordinates. The coordinates of all the reference stars are then converted to GALAXY coordinates using the computed translational and rotational constants.

Tests on the positional and photometric accuracy of GALAXY were made by Pratt (1971). For Edinburgh Schmidt plates a difference in M number of 1 was found to correspond to $0^{m}.016$ which is smaller than variations in the background fog of $\pm\ 0^{m}.05$. The mean value of the coordinate drift was $\pm$ 0.48μm.

2.7 Precise Stellar Positions from GALAXY Machine Measures

The reduction procedures outlined below were developed for use with the GALAXY measuring machine. (cf Dodd 1972).

.../

The photographic plate used for testing the reduction method was taken with a Schmidt camera, since the recent work by Andersen (1971) has confirmed the earlier work of Dixon (1963), Dieckvoss and de Vegt (1966), Dieckvoss (1955, 1960) and Barney (1955) that this type of telescope is suitable for astrometric purposes. The reduction from Cartesian to equatorial coordinates was achieved using the positions of all the reference stars in a least squares fit to determine the plate constants for the entire region under consideration. The residuals between the positions computed for the reference stars, using the calculated plate constants, and the catalogue positions were used via a weighted inverse squared error function to correct further the reference and programme star positions. It was considered valid to use such a function in this case as the source catalogue errors were very much smaller than the measurement error in arc seconds. The idea of using the information contained in the residuals to correct the positions of the programme stars is due to Debehogne (1968).

The equatorial coordinates of catalogue stars, for a given epoch, were corrected for their proper motions for the time difference between the plate and catalogue epochs. The coordinates and component proper motions of the reference stars were input to an updating computer program in the form of pseudo-decimals, e.g. $12^h\ 28^m\ 19^s.35$

.../

would become 12.281935. This computing convenience was suggested by Bertiau and De Graeve (1967). The coordinates were converted to radians and the following corrections made:-

$$\alpha = \alpha_i + t\,\Delta\alpha_i \qquad 2.1$$

$$\delta = \delta_i + t\,\Delta\delta_i \qquad 2.2$$

$$t = T - T_o \qquad 2.3$$

where (α_i, δ_i) are the input equatorial coordinates measured in radians

$(\Delta\alpha_i, \Delta\delta_i)$ are the proper motion corrections, also in radians

T is the epoch of the plate in years

T_o is the epoch of the source catalogue in years

and (α,δ) are the corrected equatorial coordinates of the reference stars.

.../

The standard coordinates (X,Y) of the reference stars were computed from their corrected equatorial coordinates (α, δ) and the coordinates (α_o, δ_o) of the plate centre using equations 2.4 and 2.5

$$x = \frac{\cos\delta \sin(\alpha-\alpha_o)}{\sin\delta \sin\delta_o + \cos\delta \cos\delta_o \cos(\alpha-\alpha_o)} \qquad 2.4$$

$$y = \frac{\sin\delta \cos\delta_o - \cos\delta \sin\delta_o \cos(\alpha-\alpha_o)}{\sin\delta \sin\delta_o + \cos\delta \cos\delta_o \cos(\alpha-\alpha_o)} \qquad 2.5$$

To determine the plate constants the standard coordinates were expressed as a series expansion in X and Y, the GALAXY measured coordinates, as far as the third order terms. The plate constants a_o to a_9 and b_o to b_9 are then given by equations 2.6 and 2.7.

$$x = a_o + a_1 X + a_2 Y + a_3 X^2 + a_4 XY + a_5 Y^2 + a_6 X^3 + a_7 X^2 Y + a_8 XY^2 + a_9 Y^3 \qquad 2.6$$

$$y = b_o + b_1 X + b_2 Y + b_3 X^2 + b_4 XY + b_5 Y^2 + b_6 X^3 + b_7 X^2 Y + b_8 XY^2 + b_9 Y^3 \qquad 2.7$$

.../

Since, in general, there will be more than ten reference stars per plate the a_i, b_i were determined by the method of least squares using a matrix equation of the type

$$\underset{\sim}{c} \cdot \underset{\sim}{A} = \underset{\sim}{k} \qquad 2.8$$

The solution of this set of linear equations was found by the Gauss-Jordan procedure outlined by Hawgood (1965) and modified to double the word length normally used by the Royal Observatory's ICL 4130 computer, i.e. 96 bit words of which 87 bits are the mantissa and 9 bits the exponent. In all, due to repetition in matrix $\underline{A}$, there were 47 product sums to be evaluated.

As a check on the reference stars, the first set of computer plate constants were used with the (X,Y) coordinates of these stars to give their standard coordinates and, from equations 2.9 and 2.10 below, their equatorial coordinates.

$$\tan(\alpha - \alpha_o) = \frac{x}{\cos\delta_o - y\sin\delta_o} \qquad 2.9$$

.../

$$\tan \delta = \frac{\sin \delta_o + y \cos \delta_o}{\cos \delta_o - y \sin \delta_o} \cos(\alpha - \alpha_o) \qquad 2.10$$

These values may be directly compared (in radians) with the input equatorial coordinates.

In order to compute more reliable plate constants three rejection criteria were used in succession, the first being that the difference between the catalogue and computed position in either R.A. or declination for the reference star is greater than 0.01 radian, the second being that this residual is greater than 0.0001 radian, and the third that the difference is greater than 0.000005 radian. These circular measures correspond approximately to 1^{o}, 20" and 1" of arc respectively. Reference stars whose computed positions exceeded the permitted values were rejected and not used in subsequent recomputations of the plate constants.

The set of plate constants determined after the third rejection loop in the program were used in the computation of the standard coordinate of the programme stars through equations 2.6 and 2.7 and thence their equatorial coordinates from equations 2.9 and 2.10.

.../

From the above analysis it is possible to construct a plot of the residuals in the reference star positions against their measured Cartesian coordinates. Knowing the residuals for the reference stars allows their positions to be corrected back to those of the source catalogue. For the programme stars, whose residuals are not known, a method of computing a value which may be used as a residual from the known values of the reference stars residuals is required. The one restriction which was applied to the analytical representation was that it should reproduce as nearly as possible the actual reference star residuals at the coordinates of the reference stars. The function chosen was a weighted inverse squared exponential $E_j(X_j, Y_j)$ defined by

$$E_j(X_j, Y_j) = \frac{\sum_i E_i(X_i, Y_i) \exp\left(-k\left((X_i - X_j)^2 + (Y_i - Y_j)^2\right)\right)}{\sum_i \exp\left(-k\left((X_i - X_j)^2 + (Y_i - Y_j)^2\right)\right)} \qquad 2.11$$

where $E_j(X_j, Y_j)$ is the computed value of the residual at point (X_j, Y_j)

$E_i(X_i, Y_i)$ is the actual residual of the reference star i at point (X_i, Y_i)

and k is a free parameter which enables adjustments to the shape of the function E_j to be made.

.../

In the computation of E_j the coordinates (X_i , Y_i) and (X_j , Y_j) are scaled by dividing either by the diameter of the plate (for circular plates of the type used by the Schmidt telescope at the Royal Observatory Edinburgh) or by the length of the diagonal of the plate, measured in the same units as X and Y.

A test program was written to determine, within the limits of the computer, which value of k would give the most likely distribution of programme star residuals. Figures 2.3 and 2.4 illustrate the appearance of the function E_j for $k = 10$ and $k = 1000$ respectively. In this example five test residuals of values 1,2,3,4 and 10 situated at rectangular coordinates (1,5), (5,5), (1,1), (5,1), and (3,3) were used and E_j evaluated for (0,0) (0.5, 0.5) (6,6) with a coordinate scaling factor of 10.

It was not possible to use much larger values of k than 1000 due to the size of the maximum real number available with the computer used. However, $k = 1000$ does give a reasonable representation of residuals expected and meets the one restriction mentioned above. As $k \to \infty$ the residual contour lines close together and divide the plate into domains of uniform residuals equal to the various known residuals.

.../

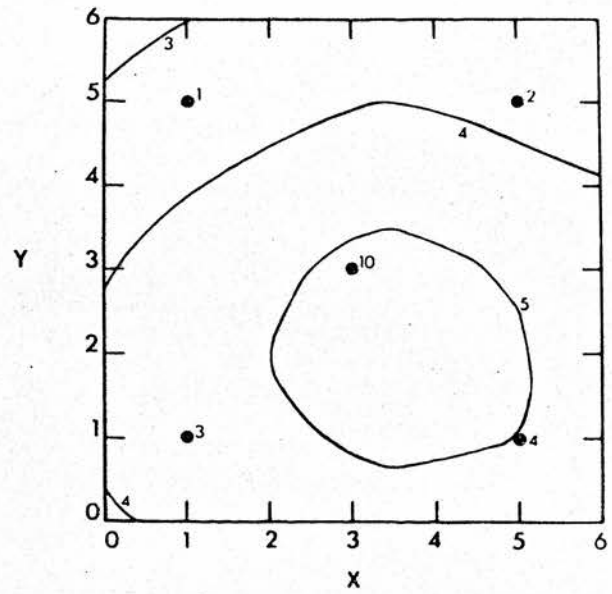

Fig. 2.3 The weighted inverse exponential function E_j (X,Y) for $k = 10$.

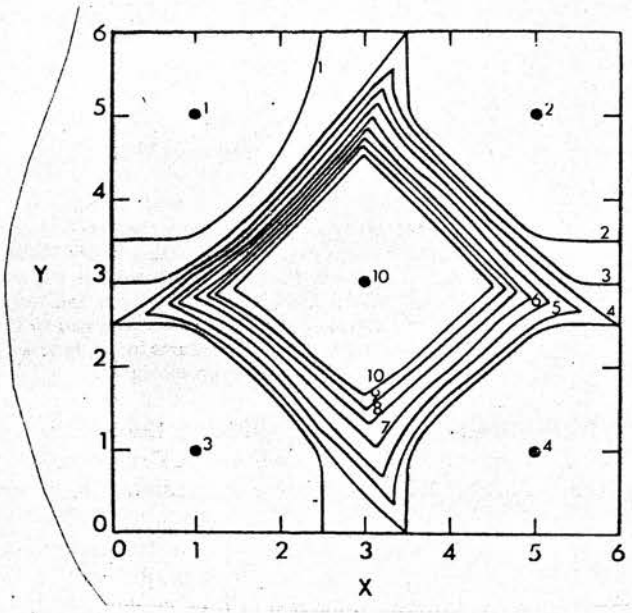

Fig. 2.4 The weighted inverse exponential function E_j (X,Y) for k = 1000.

The plate used to test both the above analysis and the suitability of GALAXY for astrometric programmes was one of the Pleiades taken at Edinburgh with the 40/60/150cm Schmidt telescope. The 20 minute exposure was obtained using a photoelectric autoguider of the type described by Adam (1971), ensuring that the images were unaffected by human guiding error. The guide star for the plate, ROE No. 1181 taken on 1971 January 19, was Hertzsprung 1349, and the local hour angle at mid-exposure ($05^h\ 32^m$ L.S.T) was $01^h\ 51^m$. (The field covered by the plate is 4^o in diameter and the plate scale is 7.4μm/arc sec.)

The emulsion used was a fine grain panchromatic Ilford R40 which in combination with a Schott GG14 filter gives a bandwidth of 1500Å centred on 5800Å.

The plate was developed for 5 minutes in a nitrogen bubble agitation tank at 20^oC using Kodak D19b developer, actively fixed for 7 minutes in Kodak Rapid Fixer, washed for one hour, and dried in an enclosed box by a forced circulation of filtered air at 20^oC in a vertical position.

The region of the Pleiades was chosen in order that positions derived from the plate could be compared directly with those given by Eichhorn et al (1970). All

.../

stars in their catalogue were identified or accounted for, the small plate scale not permitting the resolution of certain close double and multiple stars, and their rectangular coordinates measured on the Grubb Parsons measuring machine with an accuracy of $\pm 2\mu m$. On the basis of these measurements transformations from Grubb Parsons to GALAXY coordinates were made using two stars, numbers 457 and 2690 of Hertzsprung's (1947) catalogue which were measured manually with the GALAXY machine. The region measured was some 25% of the total area of the plate. The plate centre used (Hertzsprung 1349) did not coincide with the centre (Alcyone) of the region measured.

On the search tape produced 55 reference stars selected for determining the plate constants were punched out twice at the beginning to enable the rejection process of the reduction program outlined above to operate. Following these stars on the tape were the programme stars. The tape was read in three times by GALAXY and three sets of X,Y measures obtained. The total measurement time was $1\frac{1}{2}$ hours. For these runs the X240 optical system was used enabling only stars fainter than about photo-visual magnitude 8 to be measured. Elongated images (e.g. partially resolved doubles) and images lying on or inside the halation rings of the brightest stars were rejected. Altogether 72 star images were rejected leaving 430 measured.

The output tape, in octal, containing the three sets of X, Y and M (a number related to the image size) was processed to produce a tape containing the mean of the three measures in X and Y in decimal form suitable for the main reduction program. For the three sets of (X,Y) measures, the differences between the maximum and minimum X and the maximum and minimum Y readings were less than or equal to 2μm for all the reference stars except Hertzsprung 1726, which had a Y range of 3μm.

The 55 reference stars were selected from the group of 102 stars with König (1924) numbers given by Eichhorn et al (1970). Their equatorial coordinates were corrected for proper motion to the plate epoch and these values used in conjunction with their Cartesian coordinates to evaluate the plate constants. None of the 55 stars had a positional difference, when compared with the Eichhorn catalogue, of as much as 1 arc sec in either coordinate. The exclusion of the third order terms in the solution introduced an error of approximately 5μm at the edge of the field. The mean residual (Catalogue - Computed) position, and its standard deviation for the reference stars was $-0^{s}.001 \pm 0^{s}.007$ in R.A. and $-0''.01 \pm 0''.09$ in declination. The greatest residual in R.A. was $+0^{s}.018$ for Hertzsprung 344 and in declination $+ 0''.28$ for Hertzsprung 2182. After correction by the error function

.../

the mean residuals and their standard deviations were $0^{s}.000 \pm 0^{s}.004$ in R.A. and $0''.00 \pm 0''.04$ in declination.

From the computed plate constants the equatorial positions of each of the programme stars was calculated using their (X,Y) coordinates. The total computing time required for this conversion, including the error function correction, was 28 minutes.

A comparison was made between the computed programme star positions and those in the Eichhorn catalogue. The residual (Catalogue - Computed) position was corrected for proper motion using the values given by Hertzsprung (1947). Histograms of the frequency distributions of the corrected residuals in R.A. and declination are given in Figures 2.5 and 2.6. The probability that these distributions are normal is greater than 99% in each case. The mean corrected residuals and their standard deviations are $-0^{s}.002 \pm 0^{s}.009$ in R.A. and $+0''.03 \pm 0''.14$ in declination. Before correction by the error function the mean residuals and their standard deviations were $-0^{s}.001 \pm 0^{s}.012$ in R.A. and $+0''.04 \pm 0''.17$ in declination. In this case therefore, correcting positions using the error function resulted in a 15% reduction in the standard deviation of the mean residual in R.A. and an 18% reduction in the standard deviation of the mean residual in declination. Use of the F-test shows that these reductions in standard

.../

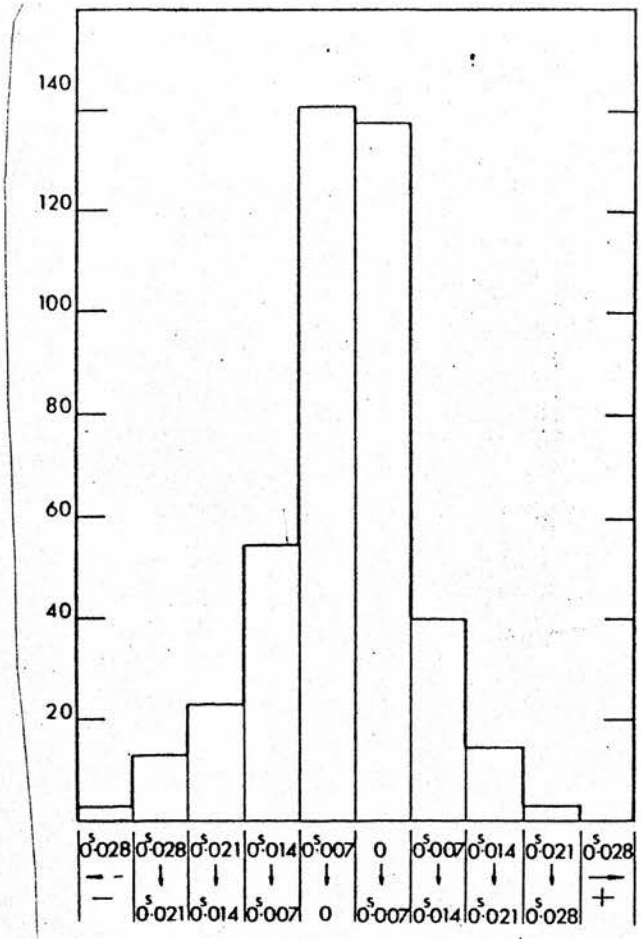

Fig. 2.5 Frequency distribution of residuals in R.A.

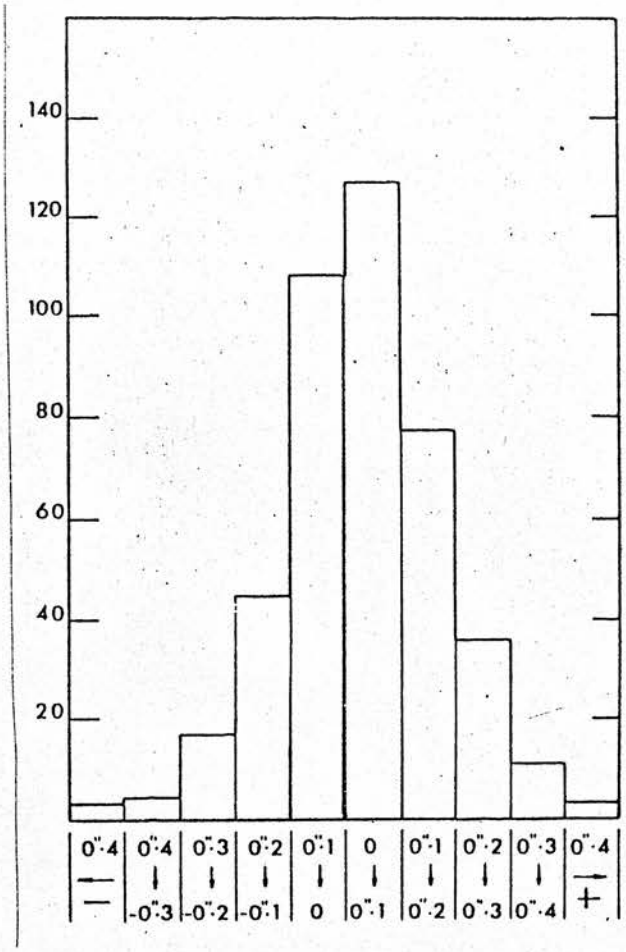

Fig. 2.6 Frequency distribution of residuals in declination.

deviation are indeed significant. In linear distance on the plate the error function corrected standard deviation for each coordinate is approximately 1μm, which is the basic unit of measurement of the GALAXY machine.

Since the equations for converting from Cartesian to equatorial coordinates contained no terms in either stellar magnitude or colour index, the possibility of a positional dependency on either of these variables was examined by plotting, for each star, its corrected residual in R.A. and declination, against its photovisual magnitude and colour index (values for these being taken from Eichhorn's catalogue. The mean corrected residuals for one magnitude ranges in magnitude and 0.25 magnitude ranges in colour index are plotted, with their standard deviations as error bars, in Figures 2.7 and 2.8 for each of R.A. and declination. From these graphs it would appear that only the corrected residual in declination plotted against magnitude shows any sign of a systematic effect, but even in this case the increase in residual between the mean position of a star of magnitude 8.5 and that of a star of magnitude 13.5 amounts to only 0.09 arc sec, which in linear terms on the plate is 0.6μm.

A plot of the vector sum of the residuals in R.A. and declination against GALAXY coordinates is given in Fig. 2.9. The vector sum residuals applied to the programme stars by the function E_j (X,Y) are shown in

.../

Fig. 2.10. The centre of each cross represents the position of a measured star, the dimensions of the cross being 0.1 x 0.1 arc sec.

A circle of radius 1cm on the plate drawn about Alcyone as centre was used to divide the field into two sectors. The mean combined residuals and their standard deviations for the inner and outer rings were $0\overset{''}{.}05 \pm 0\overset{''}{.}16$ and $0\overset{''}{.}02 \pm 0\overset{''}{.}19$ respectively. The variance ratio test revealed that there was a significant difference between the standard deviations of the inner and outer rings at the 5% level of testing but no significant difference between the means. This was to be expected as the positions of many of the stars in the outer ring were determined by extrapolation rather than interpolation from the plate constants equations. The absence of a significant difference between the means implies that there is no systematic shift of star coordinates dependent upon image position on the plate.

Measurement of the test plate was repeated using the X75 and X30 GALAXY optical systems. The X75 optics enabled stars fainter than $m_{pv} = 6$ to be measured and the X30 optical system was able to measure star images up to the 4th photovisual magnitude. Star images for measurement were selected as for the X240 optics and the same reduction method used.

.../

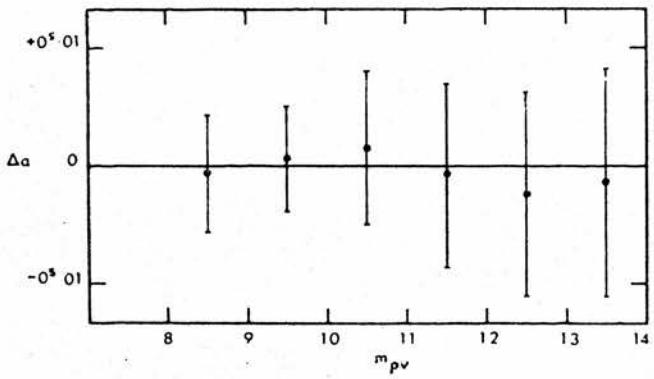

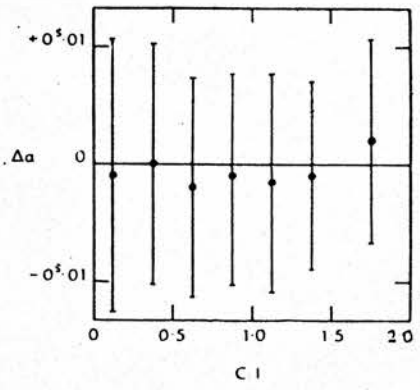

Fig. 2.7 R.A. residuals against magnitude and colour index.

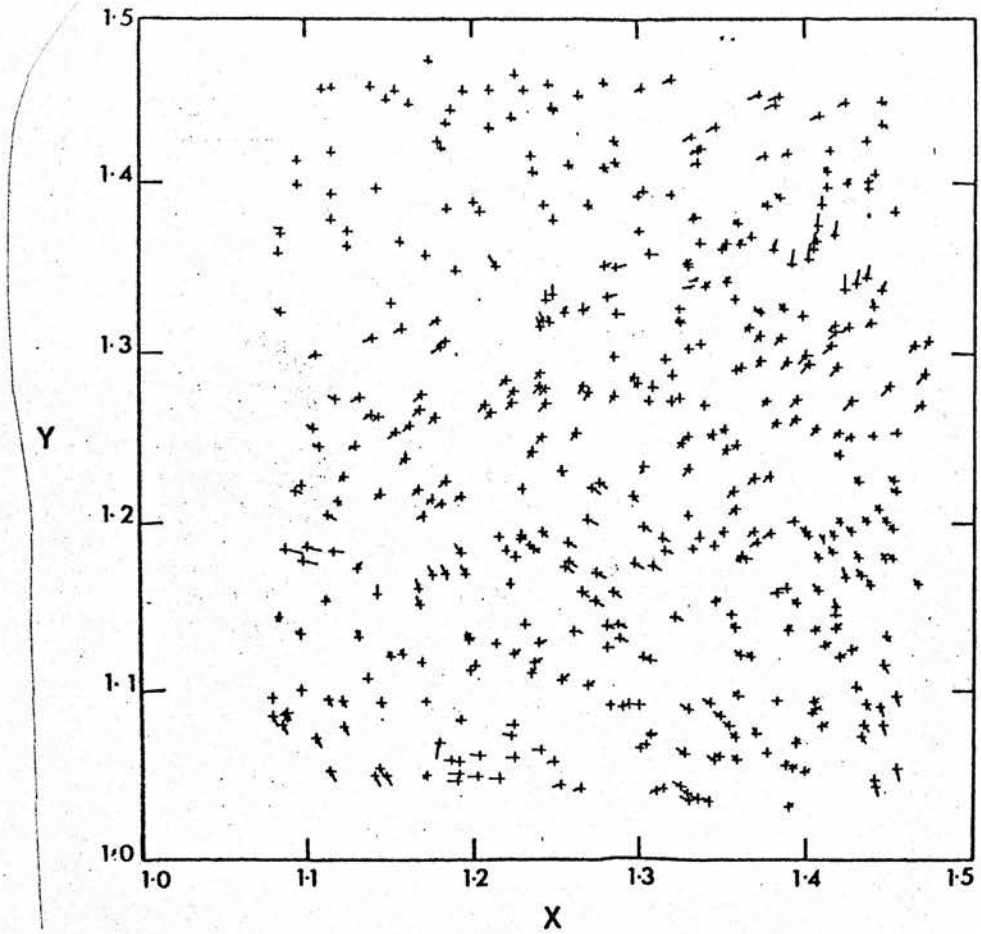

Fig. 2.10 Vector sum residuals applied to the programme stars by the function E_j (X,Y).

For the X30 optics the mean and standard deviation of residuals in R.A. were $+0^{s}.001 \pm 0^{s}.017$ and in declination $-0''.02 \pm 0''.18$. For the X75 optics the corresponding values were $-0^{s}.002 \pm 0^{s}.016$ and $-0''.03 \pm 0''.17$.

A plot of residuals in R.A. and declination against magnitude for each of the GALAXY optical systems in the range $4.5 \leq m_{pv} \leq 9.5$ is given in Fig. 2.11. The results for residuals against colour index were identical to Figures 2.8 and 2.9.

The above results show that the measurements of the star images on the Schmidt plate made by the GALAXY measuring machine were neither magnitude nor colour dependent in the ranges considered. The results also suggest that the method of analysis described works satisfactorily in the region measured for the source catalogue used.

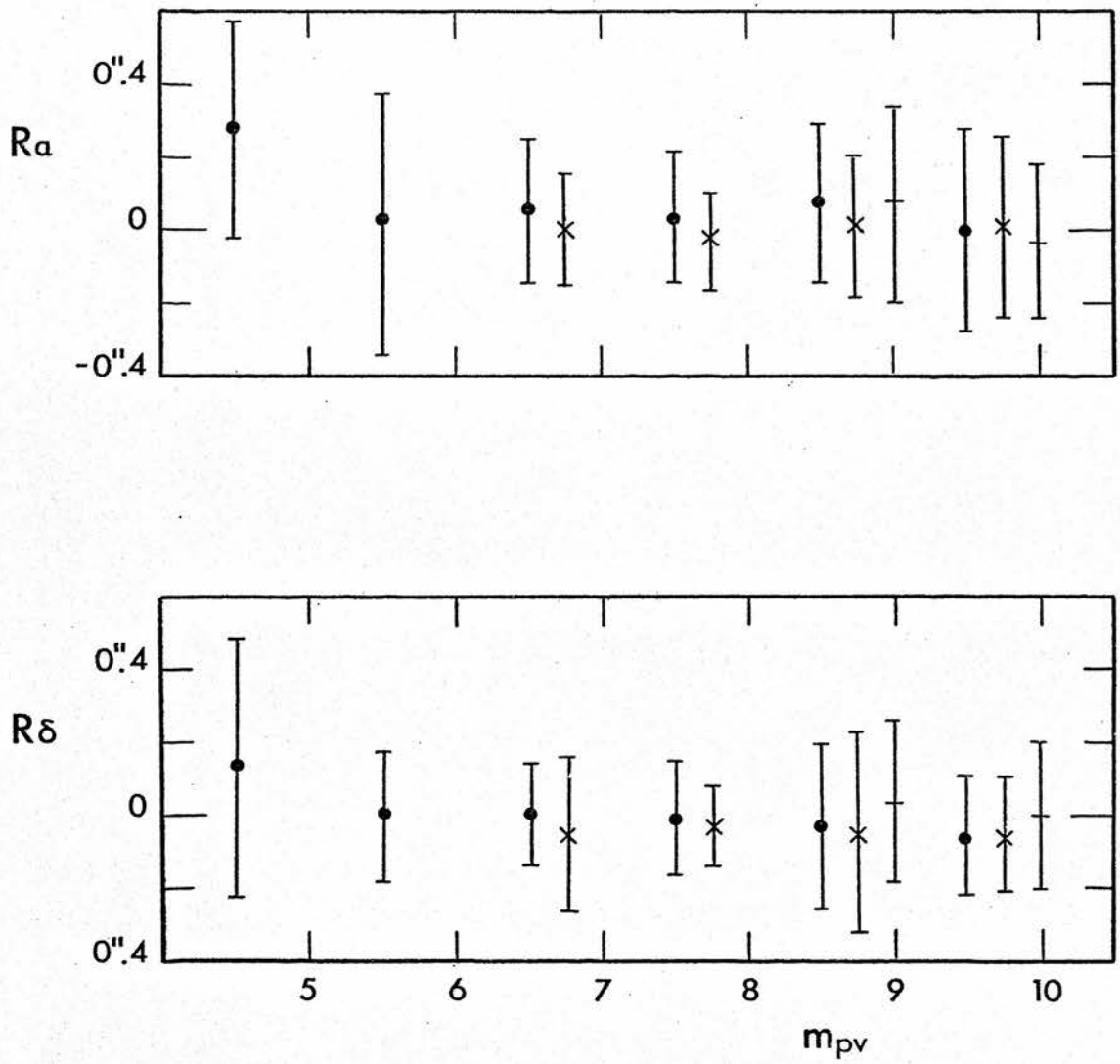

Fig. 2.11 Residuals in R.A. and declination against magnitude for X30 (•), X75 (X), and X240 (+) GALAXY optical systems.

Chapter 3 Photoelectric Photometry

3.1 Introduction

In order to calibrate the photographic photometry of the $\ell = 140^{\circ}$ region a sequence of photoelectric magnitudes from standard stars was needed. Five regions were selected from an Edinburgh Schmidt plate centred on star BD + 57° 696 at $(\ell, b) = (140^{\circ}.14, +0^{\circ}.14)$. A square of side $\frac{1}{2}^{\circ}$ centred on each of five reference stars given in Table 4.1 was drawn and the area examined to find suitable stars to give a useful magnitude range for calibrating the photographic plates.

TABLE 3.1

CENTRAL STARS

Region	ROE No.	α_{1950}	δ_{1950}	ℓ_{1950}	b_{1950}
A	13	$3^h 06^m 18^s$	59° 19'.9	139°.72	+1°.25
B	55	3 08 34	57° 48'.8	140°.74	+0°.09
C	62	2 56 40	58° 13'.3	139°.17	-0°.32
D	53	3 03 01	57° 21'.5	140°.32	-0°.67
E	43	3 05 05	58° 41'.8	139°.90	+0°.62

For each of the programme stars offsets in R.A. and declination from the central stars were calculated using the known Edinburgh Schmidt plate scale to facilitate star identification whilst observing. Fig. 3.1 shows the positions of the regions selected and the stars measured on a Schmidt plate print.

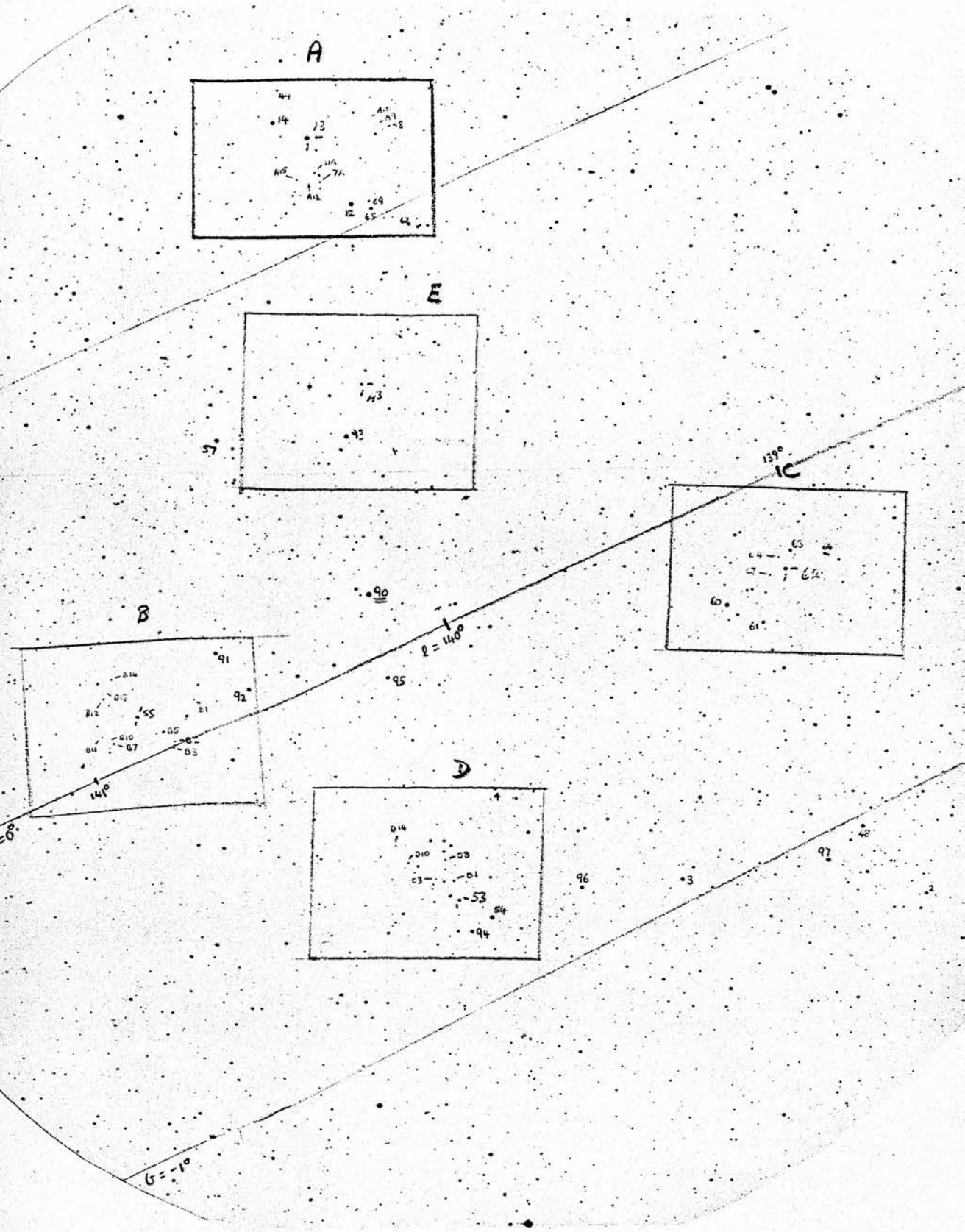

Fig. 3.1 The $\ell = 140^{\circ}$ region showing the selected areas and stars whose magnitudes were measured photoelectrically.

3.2 Observations made with an 88-inch Telescope

Descriptions of the Mauna Kea Observatory and its main telescope are given by Jefferies and Sinton (1968) and Morrison and Jefferies (1972). The photoelectric observations, directly recorded by a moving pen, of the $\ell = 140^{\circ}$ region were made by Dr. R.D. Wolstencroft of the University of Hawaii, at the f10 Cassegrain focus of the 88-inch telescope.

The pen recorder deflections were marked off on the chart, measured, corrected for sky brightness and transformed into magnitudes with the help of a table (cf. Schulte and Crawford 1961). These were then converted to observed magnitudes using the amplifier constants given in Table. 3.2.

TABLE 3.2

AMPLIFIER CONSTANTS (VALUES OF S)

	A	B	C	D
5	2.432	3.737	4.933	6.243
6	4.942	6.247	7.443	8.753
7	7.457	8.762	9.958	11.268
8	9.967	11.272	12.468	13.778
9	12.459	13.764	14.960	16.270
10	14.960	16.265	17.561	-

It was noted that, for many of the bright stars, the zero point had not been correctly set so that the recording pen came up hard against the bottom stop, thus giving readings that were too small and consequently magnitudes that were too faint.

A preliminary reduction was made to give approximate colours for working out extinctions. Using the plots in Fig. 3.2 the approximate colours were converted to effective wavelength and via Fig. 3.3 to zenith extinction in magnitudes. The extinction curve is the mean of several nights' observing at the 88-inch telescope by S. Wolff.

The instrumental magnitude m_c for a particular colour c was related to the measured chart deflection D_c, amplifier sensitivity S_c, standard sensitivity (S value at 6C which is 7.443), zenith extinction $1.086\tau_c$ and a function of zenith distance $m(z_c)$ by

$$m_c = -2.5 \log D_c + S_c - 7.443 - 1.086\,\tau_c\, m(z_c) \qquad 3.1$$

where

$$m(z_c) = \left(\sin\varphi \sin\delta + \cos\varphi \cos\delta \cos H \right)^{-1} \qquad 3.2$$

(φ = latitude of observer,
δ = declination and
H = hour angle of stars)

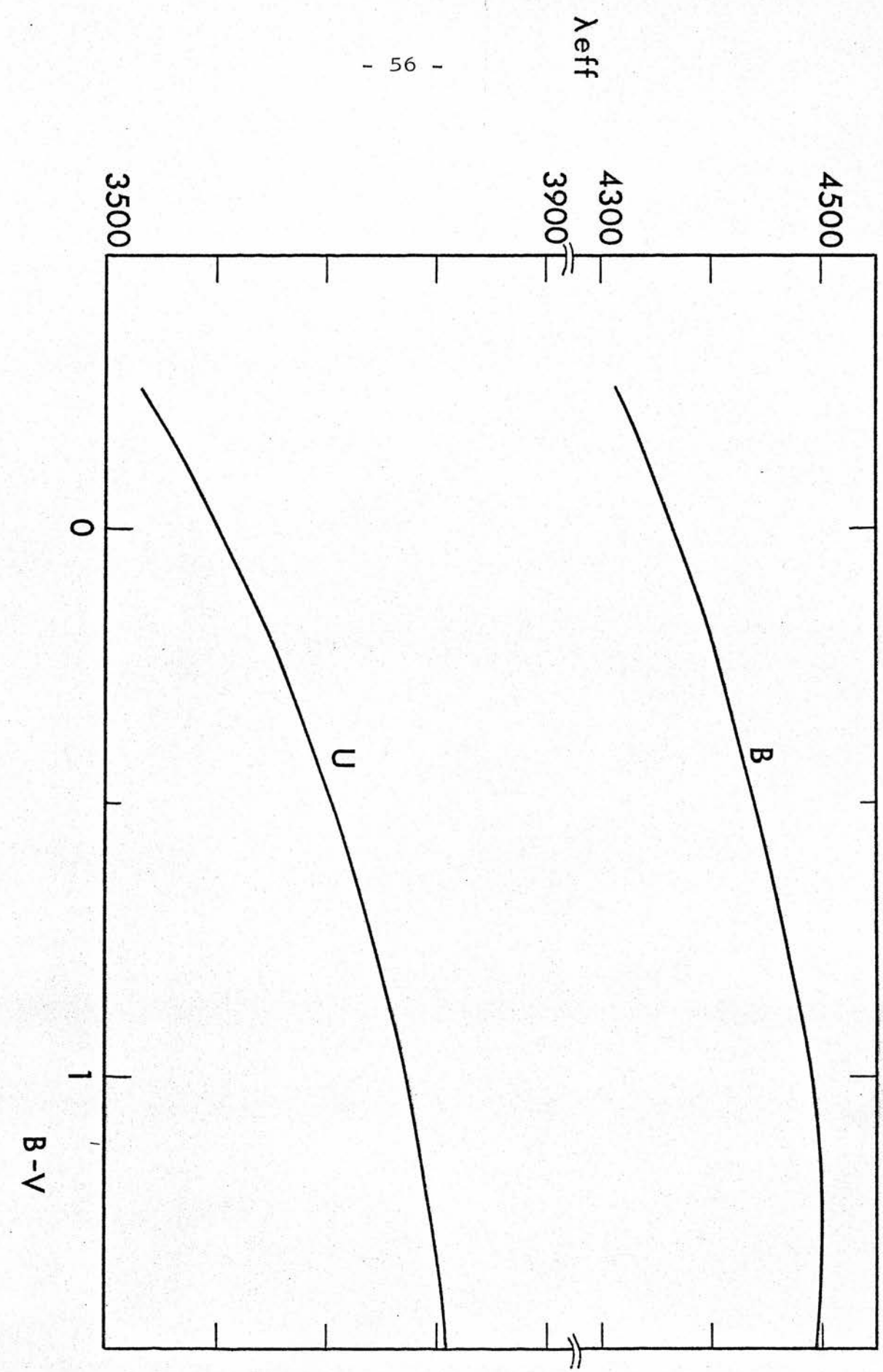

Fig. 3.2 Plots of effective wavelength for U and B filters with colour.

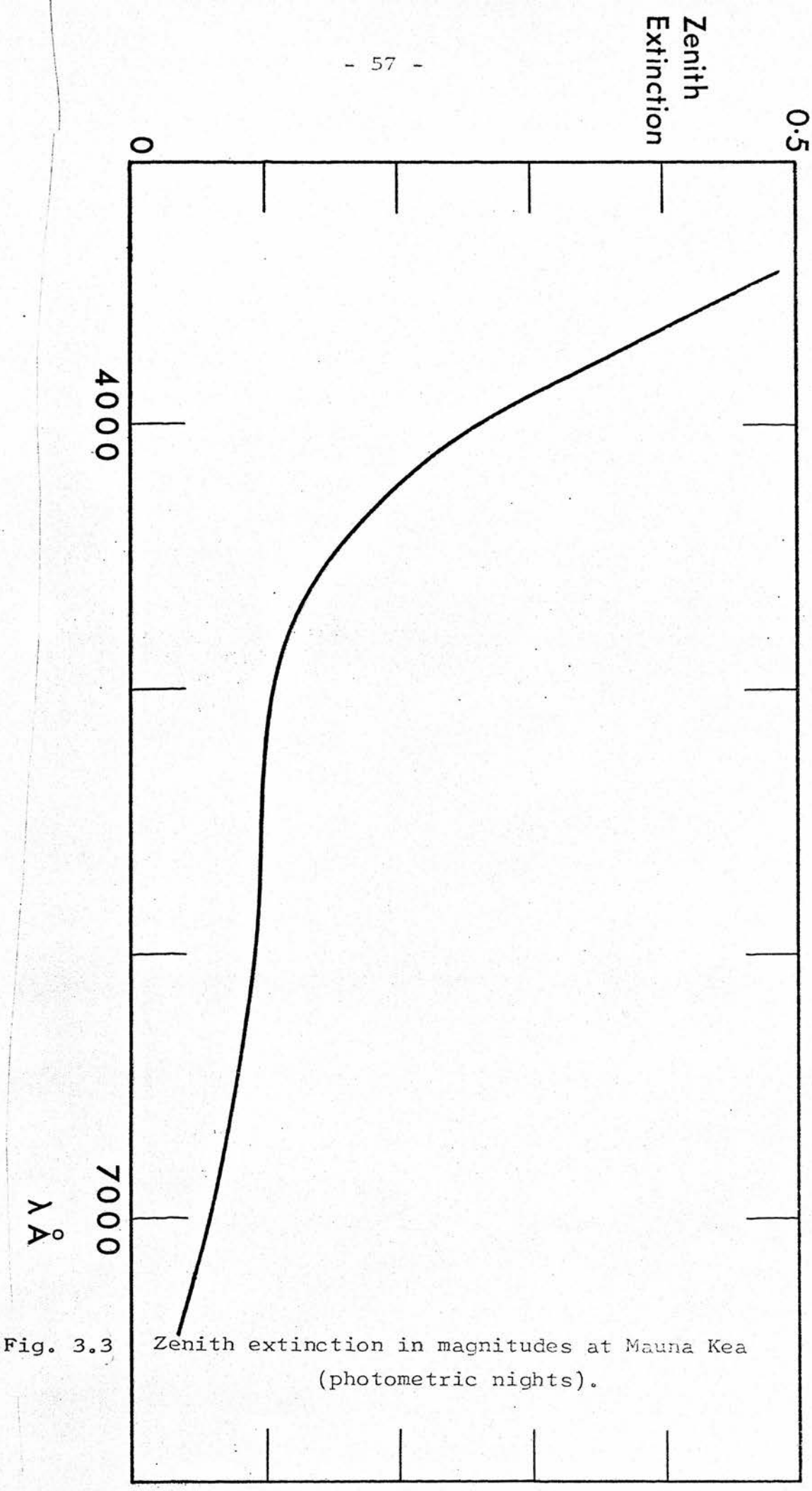

Fig. 3.3 Zenith extinction in magnitudes at Mauna Kea (photometric nights).

The magnitudes m_B and m_v were reduced to zenith. m_u was reduced to outside the atmosphere since there is a strong correlation between a star's colour and its ultraviolet extinction. The observed m_B and m_v were transformed into the Johnson (1964) colour system with the aid of small colour corrections derived from Fig. 3.4 using the standard stars, whose magnitudes, taken from Iriarte et al (1965), are listed in Table 3.3.

TABLE 3.3
PHOTOELECTRIC MAGNITUDES
OF STANDARD STARS

Star	U	B	V	B - V	U - B
ζ Cyg	4.95	4.19	3.19	1.00	0.76
ν Cyg	3.50	4.32	4.42	-0.10	-0.82
ν Cep	4.95	4.80	4.29	0.51	0.15
θ Peg	3.72	3.63	3.55	0.08	0.09
δ CMa	3.00	2.47	1.80	0.67	-0.53
δ Mon	4.18	4.15	4.15	0.00	0.03
23 UMa	4.09	4.00	3.67	0.33	0.09
24 UMa	5.69	5.33	4.56	0.77	0.36
υ^2 Hya	4.21	4.49	4.58	-0.09	-0.28

In the case of m_u (cf. Fig. 3.5), no clear correction could be discerned and it was decided to apply a straight zero point correction derived from what were considered to be the better observed results. Dr. Wolstencroft in a footnote to his observations points out that "U magnitudes

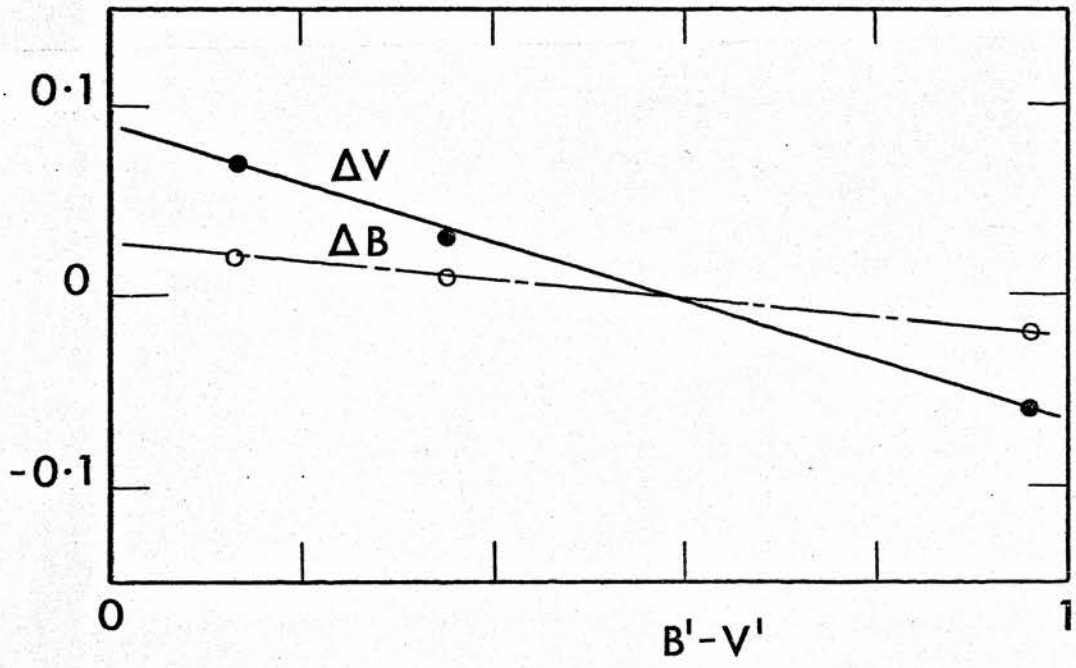

Fig. 3.4 Corrections to observed magnitudes to reduce to B, V system.

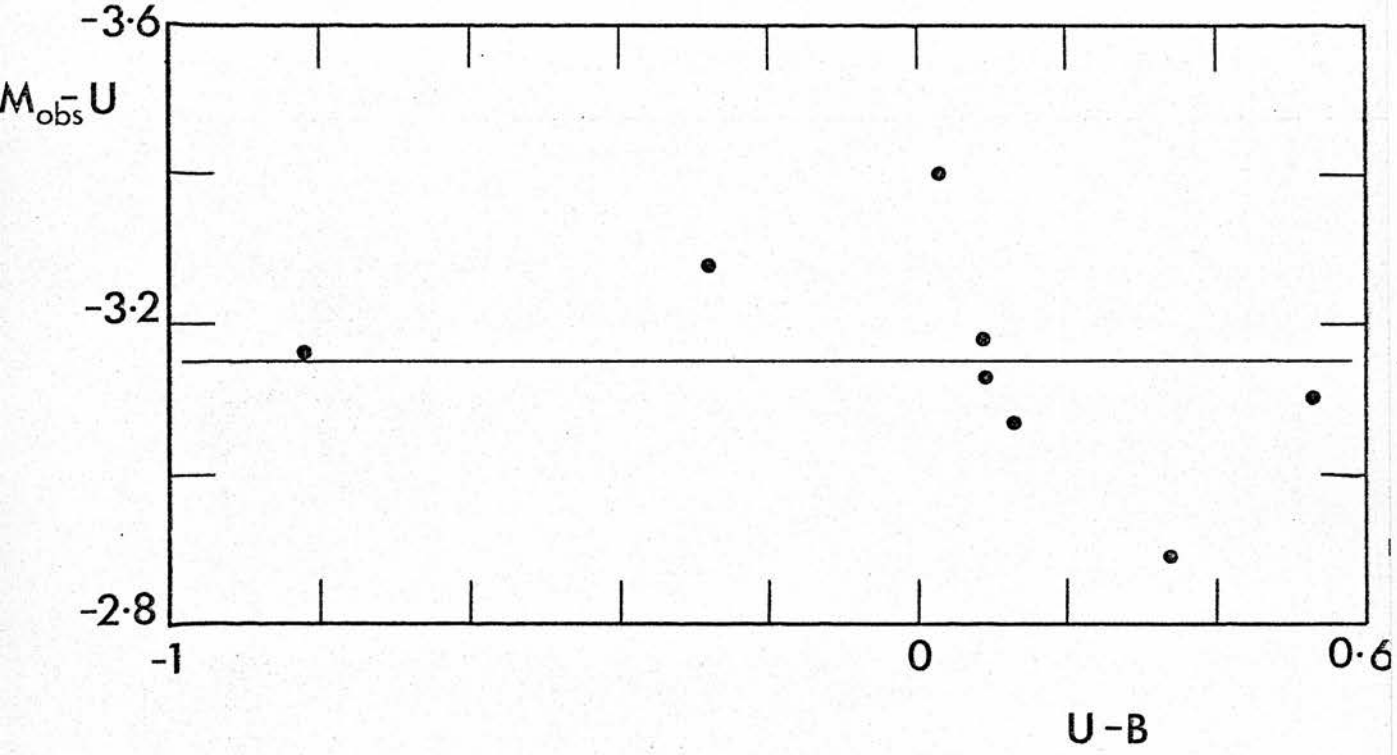

Fig. 3.5 Corrections to observed magnitudes to reduce to U system.

for red stars may be unreliable because U measures with and without a red leak filter were not made because of lack of time". Table 3.4 lists the derived UBV photoelectric magnitudes for twenty stars in the $\ell = 140^{\circ}$ region. Colons indicate uncertain measures.

TABLE 3.4

PHOTOELECTRIC MAGNITUDES IN THE $\ell = 140^{\circ}$ REGION FROM OBSERVATIONS WITH THE 88-INCH TELESCOPE

ROE Star No.	U	B	V	B - V	U - B
A13	7.91	8.26	7.97	0.29	-0.35
A8	14.50	14.55	13.79	0.76	-0.05
A9	15.07	15.46	14.50	0.96	-0.39
A10	14.86	15.00	14.05	0.95	-0.14
A7	13.44	13.60	12.75	0.85	-0.16
A11	12.88	12.79	12.20	0.59	0.11
A12	15.45:	15.59:	14.24:	1.35	-0.14
B55	10.83	10.90	10.16	0.74	-0.07
B1	14.89	14.63	13.63	1.00	0.26
B2	12.90	13.96	12.25	1.71	-1.06
B3	13.41	13.44	12.58	0.86	-0.03
B5	15.13	14.92	14.97	-0.05	0.21
B7	13.25	13.21	12.56	0.65	0.41
B10	18.48:	17.60:	15.79	1.81	0.88
B11	15.13	14.61	13.61	1.00	0.52
B12	13.46	13.55	12.67	0.88	-0.09
B13	16.86	16.03	14.95	1.08	0.83
C62	9.68	9.47	9.14	0.33	0.21
C4	14.17	14.43	13.51	0.92	-0.26
C7	14.12	14.48	13.43	1.05	-0.36

3.3 Observations made with the Twin 16-inch Telescope

A general description of the twin 16-inch telescope at the Royal Observatory Edinburgh has been given by Reddish (1966) and a more detailed explanation of its operation by Lawrence and Reddish (1965). The instrument (cf. Fig. 3.6) consists of two Ritchey-Chretien telescopes of aperture 40cm and effective focal length 610cm on the same mounting (of modified open fork design). One of the telescopes can be offset up to $\pm 5^{o}$ in R.A. and declination relative to the other, reference, telescope. Each telescope has a photoelectric photometer and the reference telescope also has a photoelectric autoguider. The reference telescope is used to guide on a reference star, and also by measuring its brightness, to monitor changes in sky transparency. The offset telescope is used to measure the brightness of the programme stars in turn, relative to the reference star being monitored simultaneously. In the photometry the reference star is thus used only as an intermediary and the result is to obtain the relative brightness of the programme stars with the effect of changes in sky transparency largely eliminated. For the measurements a pulse counting device is used with integration times of ten or fifty seconds.

Observations were made in U (UG2 filter), B (GG13 + BG12 filter) and V (GG14 filter) during the 1970/71 and

Fig. 3.6 The twin 16-inch photoelectric telescope.

1972/73 seasons and in b, y, r and i during the 1970/71 season. Preliminary magnitudes for programme stars were obtained by converting the measured pulse count into magnitudes and adding it to the known magnitude of the reference star. The 1970/71 UBV magnitudes were adjusted to the zero point of the 1972/73 observations.

Relations between the mean of five observed magnitudes and colours and those given by Iriarte et al. (1965), on the Johnson system, and Blanco et al. (1968) were derived by plotting (observed - catalogue) magnitude and colour differences against catalogue colours. Star HR1040 was taken as the primary standard and its observed V magnitude was equated to 4.55.

TABLE 3.5

PHOTOELECTRIC MAGNITUDES

OF TWIN TELESCOPE STANDARD STARS

HR No.	U	B	V	B - V	U - B
922	5.72	5.86	5.88	-0.02	-0.14
1035	4.38	4.61	4.20	0.41	-0.23
1040	5.01	5.11	4.55	0.56	-0.10
1046	5.21	5.14	5.13	0.01	0.07
1129	5.85	5.60	4.79	0.81	0.25
1204	4.76	4.93	5.02	-0.09	-0.17
1242	6.06	5.56	5.07	0.49	0.50

.../

The seven stars listed in Table 3.5, which were observed contemporaneously with the $\ell = 140^{o}$ programme stars, were used to derive the following empirical straight line equations.

$$U_{Johnson} = U_{observed} \qquad 3.3$$

$$B_{Blanco} = B_{observed} + 0.01 \qquad 3.4$$

$$V_{Blanco} = V_{observed} + 0.064 - 0.082(B-V)_{observed} \qquad 3.5$$

The relations between UBV observed with the programme telescope and the standard systems are illustrated in Figures 3.7 and 3.8. Good agreement was found between the above reduction formulae and those obtained for selected bright stars.

The b,y,r,i observations of 1970/71 were approximately reduced to the Johnson system. The y observations were converted to V by using a simple colour correction depending on (b - y) determined by comparing the observed y with the mean V from the 1970/71 and 1972/73 observations for the stars in common. r and i were reduced by converting y - r and y - i to V - R and V - I using relations found from observations of the fourteen bright stars listed in Table 3.6.

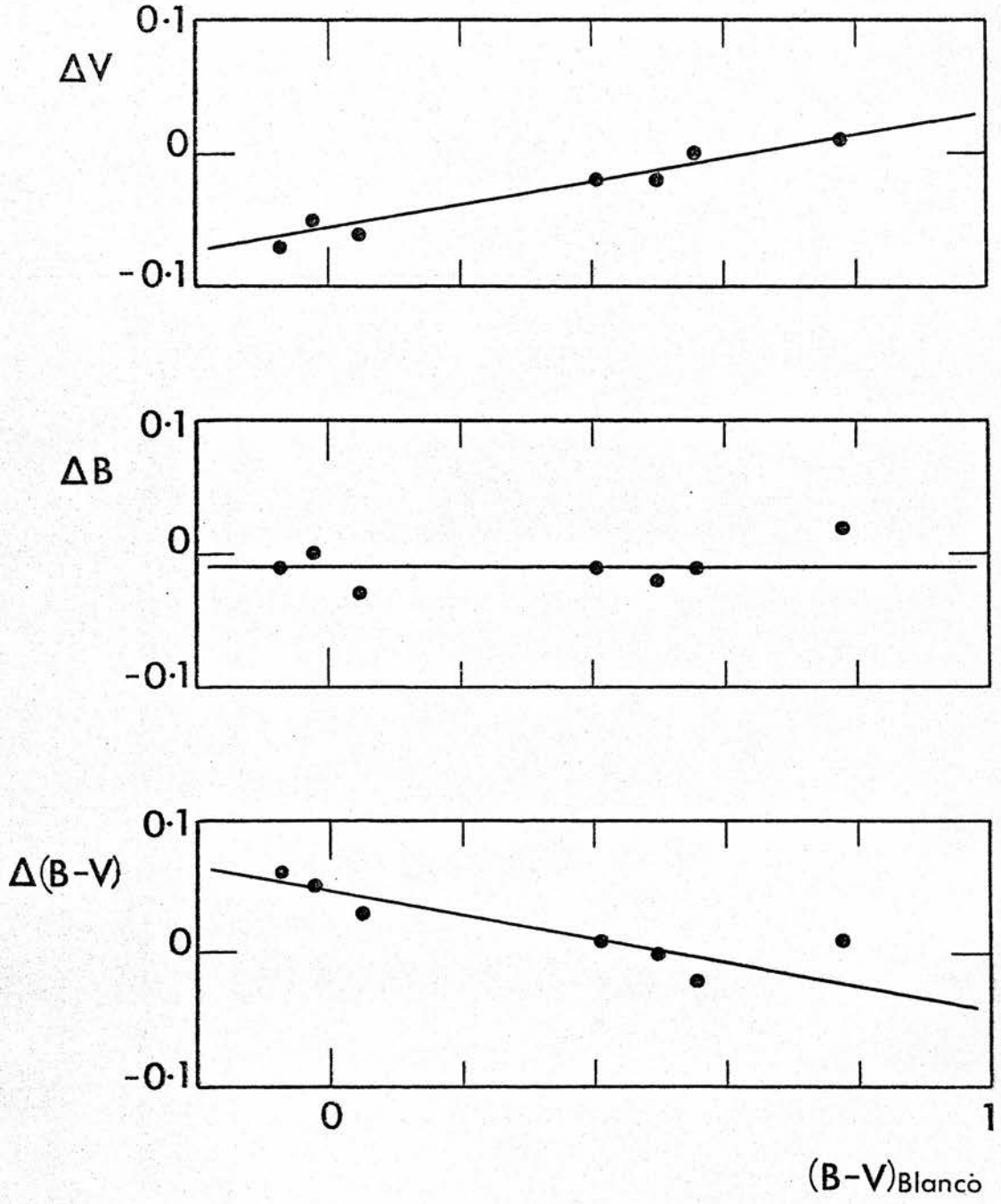

Fig. 3.7 Relations between B, V observed with 16-inch programme telescope and standard systems.

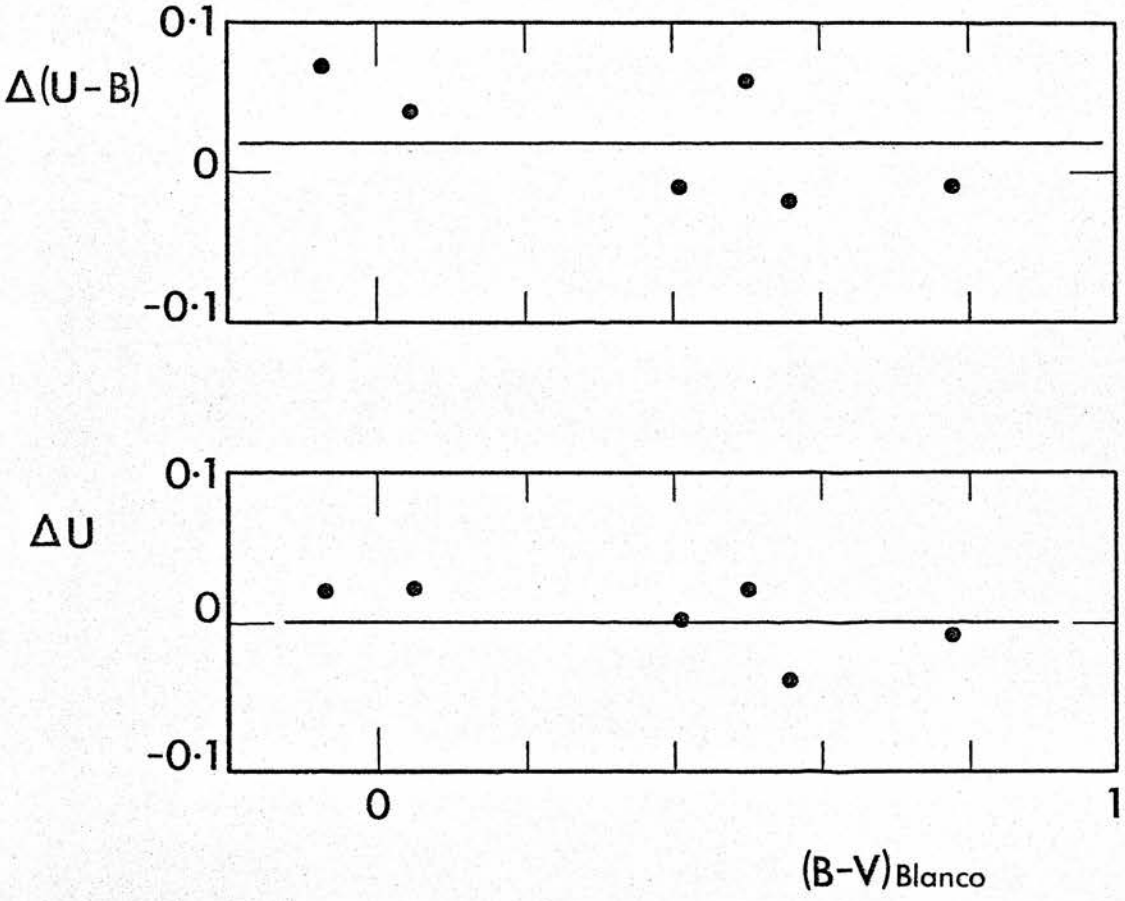

Fig. 3.8 Relations between U observed with 16-inch program telescope and standard systems.

TABLE 3.6

V, R and I
PHOTOELECTRIC STANDARDS.

HR No.	V	V - R	V - I	Sp. Type
3624	4.69	0.33	0.47	A7m
3751	4.29	1.10	1.84	K3III
3771	4.56	0.64	1.06	G2IV
3800	4.54	0.70	1.15	G8III
3815	5.40	0.62	0.99	G8IV - V
3888	3.82	0.34	0.50	F2IV
3974	4.49	0.18	0.25	A7V
4090	4.73	0.26	0.40	GOV
4301	1.80	0.81	1.39	KOIV
4335	3.01	0.82	1.41	K1III
4392	4.98	0.72	1.18	G8II
4550	6.45	0.66	1.10	G8Vp
4554	2.44	0.05	0.03	AOV

The zero points of the V - R and V - I so found were adjusted by comparing the provisional values with B - V for the same stars. The plots of y - r against V - R and y - i against V - I (Figures 3.9 and 3.10) yielded the empirical straight line relations given by equations 3.6 and 3.7.

$$(V-R)_{Johnson} = 1.19\,(y-r) + 0.26 \qquad 3.6$$

$$(V-I)_{Johnson} = 1.47\,(y-i) + 1.12 \qquad 3.7$$

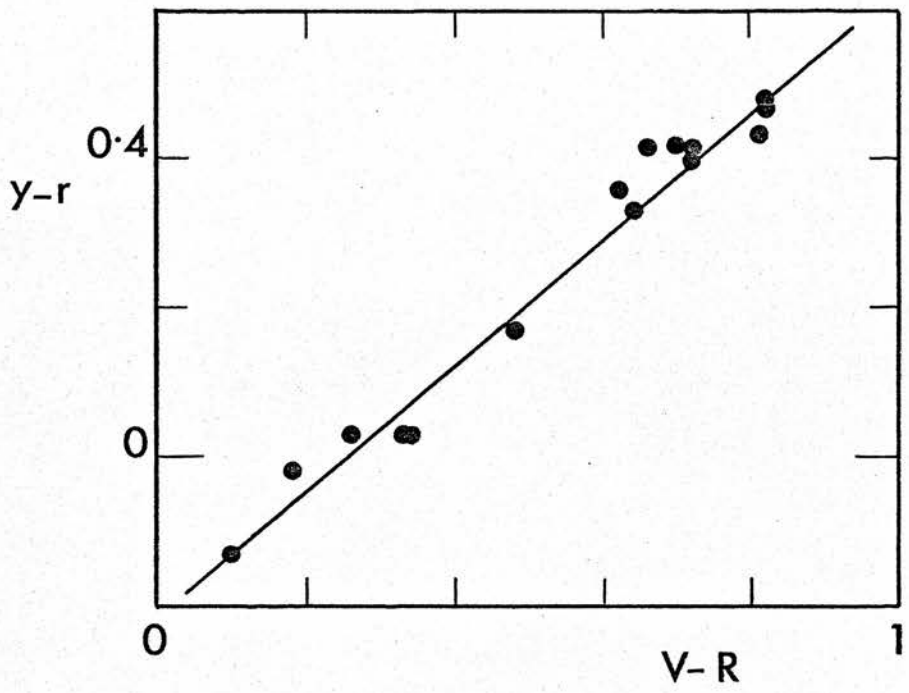

Fig. 3.9 Plot of (V - R) against (y - r) for V, R and I standards.

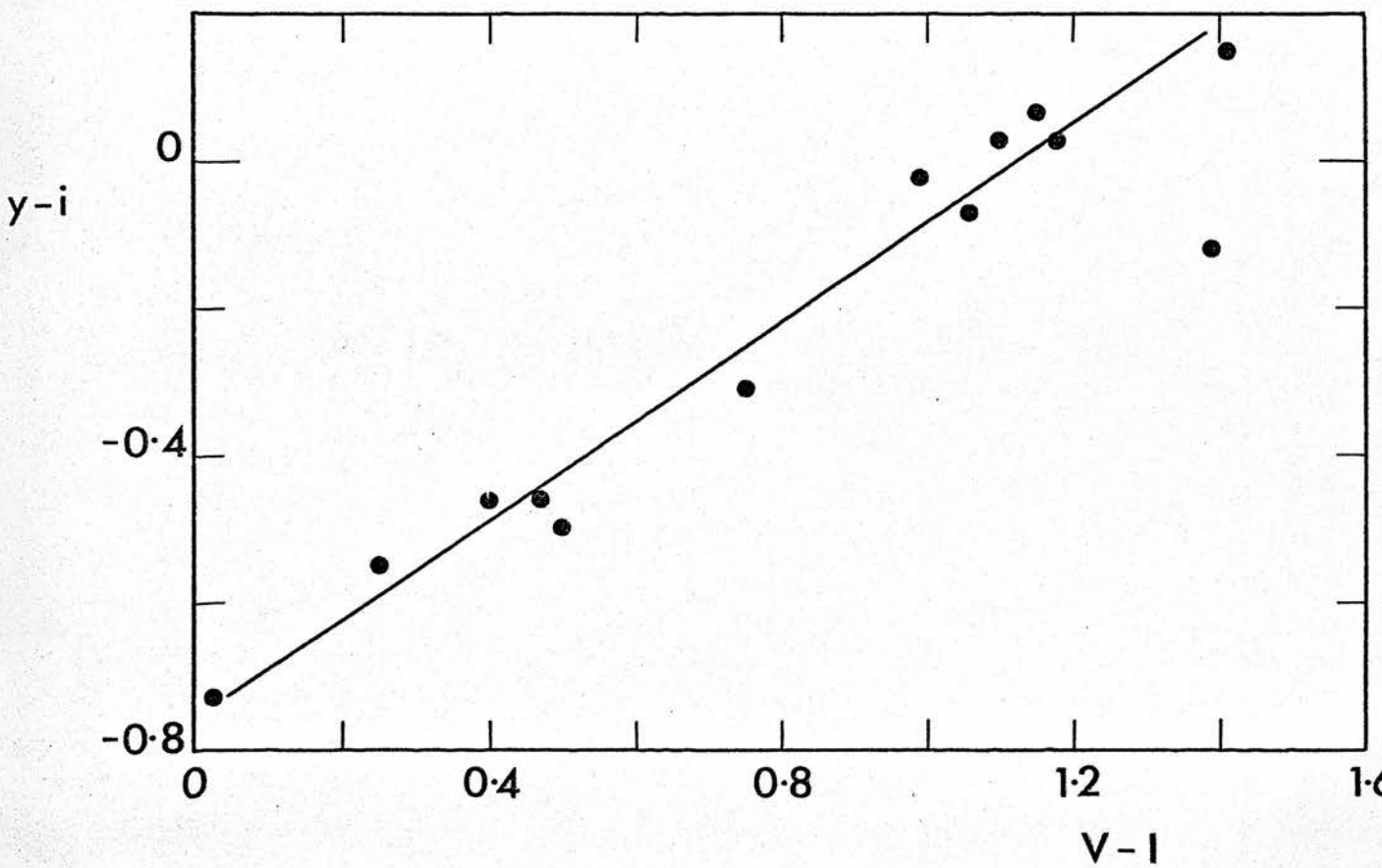

Fig. 3.10 Plot of (V-I) against (y - i) for V, R and I standards.

The R and I magnitude for the programme stars were then derived by applying (V - R) and (V - I) to V. Table 3.7 below includes the complete list of stars observed with the twin 16-inch telescope.

3.4 Comparison of results obtained with the different telescopes

Seven stars were observed by both the 88-inch telescope and the twin 16-inch telescope. In Fig. 3.11 the magnitude relations between the two instruments are plotted, these relations are represented by the following empirical straight line equations.

$$U_{16} = 1.084\, U_{88} - 0.756 \qquad 3.8$$

$$B_{16} = 0.990\, B_{88} + 0.070 \qquad 3.9$$

$$V_{16} = V_{88} + 0.070 \qquad 3.10$$

The observations made with the 88-inch telescope were transformed via these equations into the magnitude system of the twin 16-inch telescopes. The converted magnitudes are listed in Table 3.7.

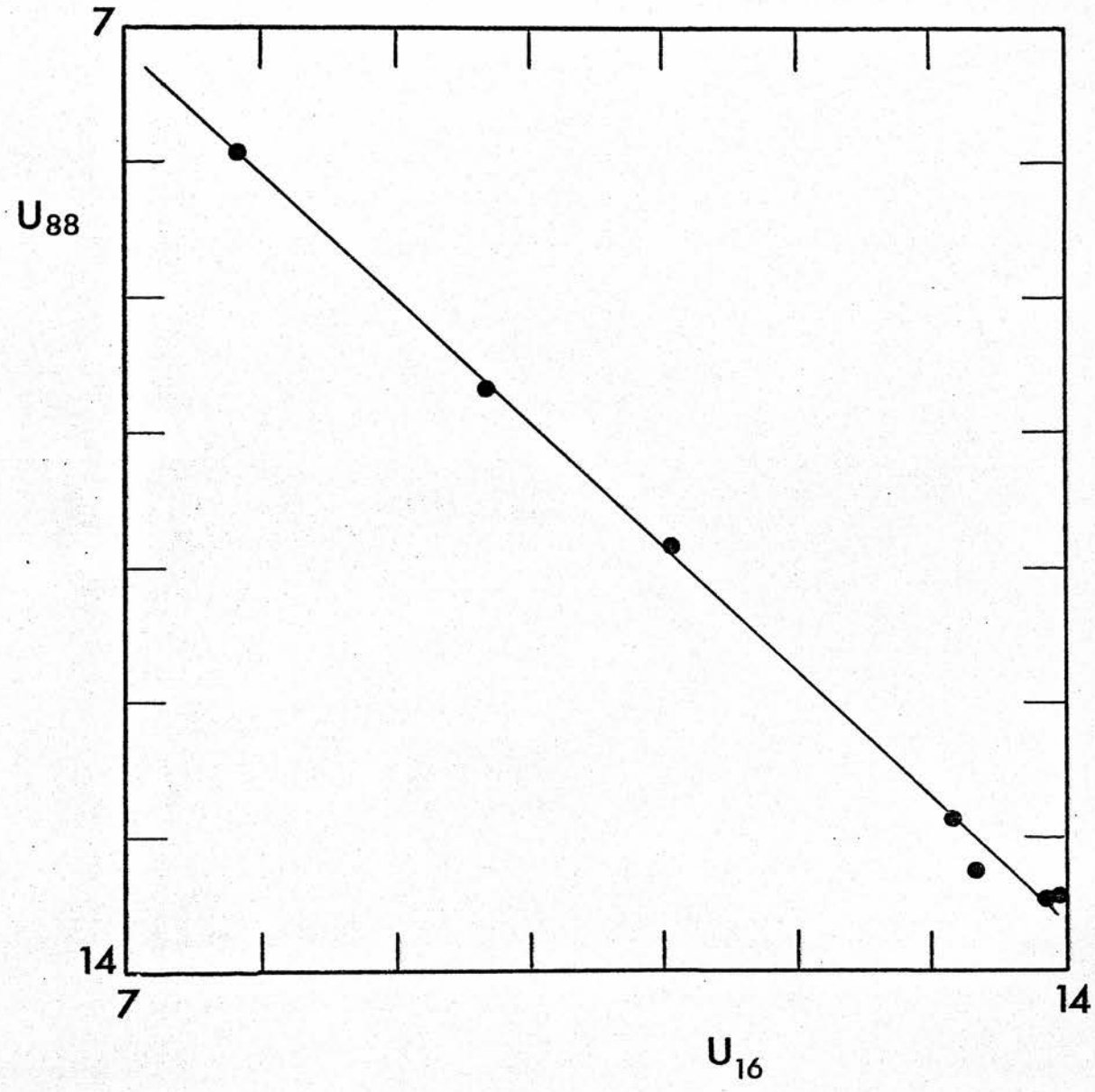

Fig. 3.11a U relations between the 88-inch and the twin 16-inch telescopes

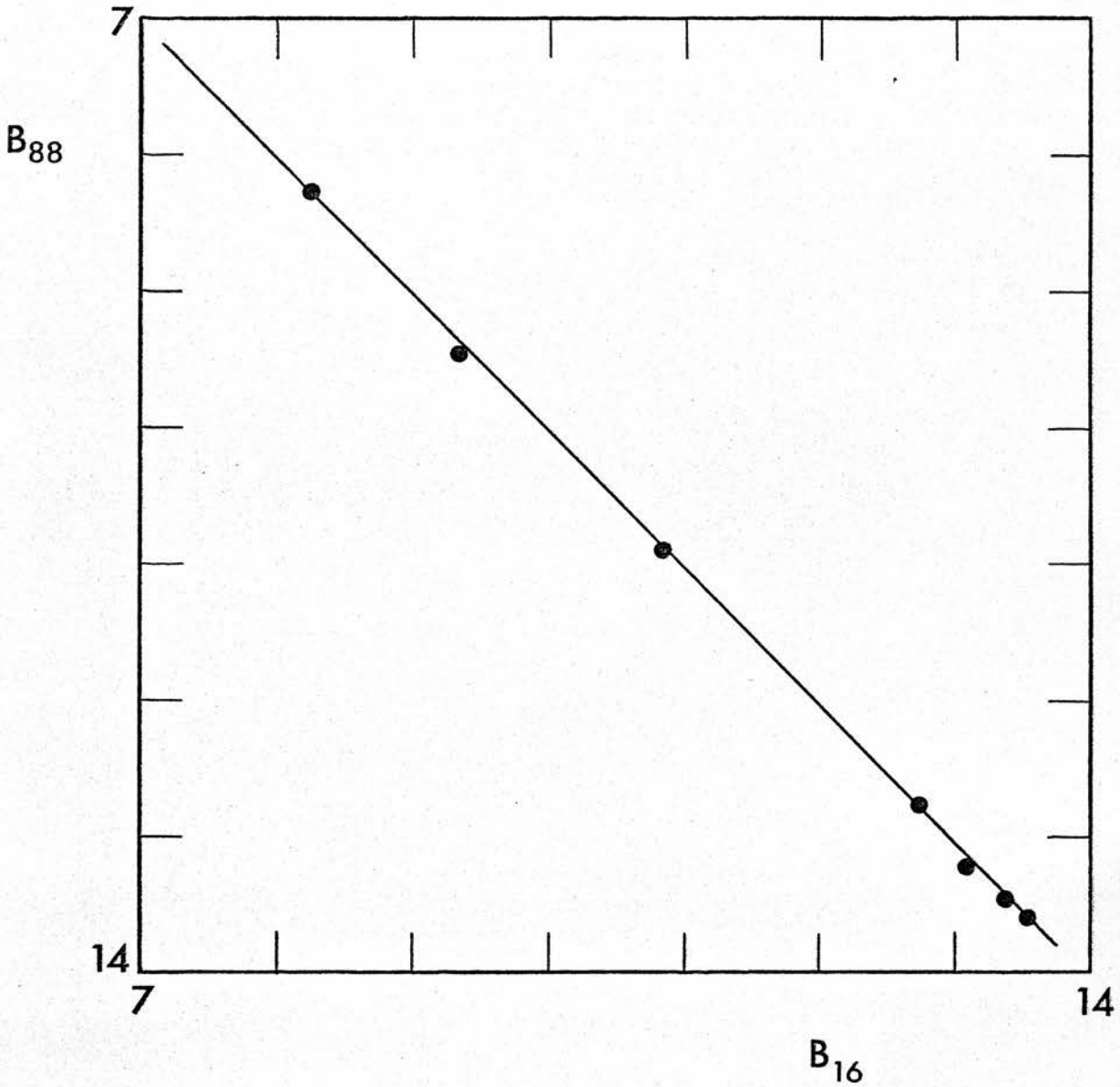

Fig. 3.11b B relations between the 88-inch and the twin 16-inch telescopes.

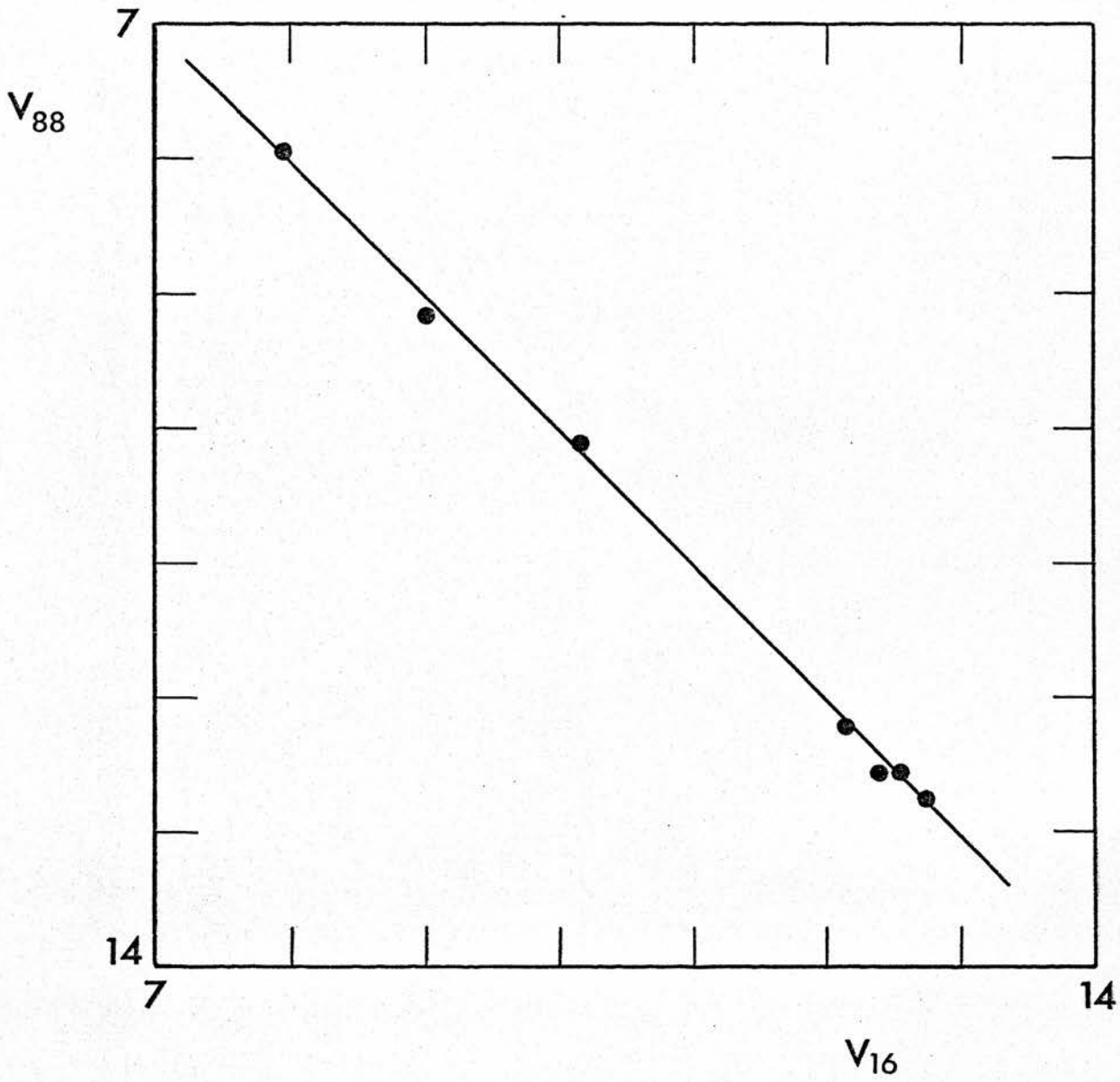

Fig. 3.11c V relations between the 88-inch and the twin 16-inch telescopes.

3.5 Summary

The UBV photoelectric magnitudes for 53 stars and RI magnitudes for 20 stars were combined to produce the following two-colour difference plots: Fig. 3.12 (U - B) - (B - V), Fig. 3.13 (B - V) - (V - R), and Fig. 3.14 (B - V) - (V - I). The standard sequences plotted are from Johnson (1966). A complete list of observed magnitudes is given in Table 3.7 and of observed colours in Table 3.8. Approximate galactic coordinates, and BD - numbers and spectral types, where available, for these stars are given in Table 3.9.

TABLE 3.7

U B V R I

PHOTOELECTRIC OBSERVATIONS

IN THE $\ell = 140^{o}$ REGION

ROE Star No.	U	B	V	R	I
3	9.08	9.43	8.81	8.28	7.93
4	10.70	10.89	10.00	9.27	8.69
12	8.08	8.22	8.11	7.92	7.96
13	7.84	8.25	7.91	7.57	7.38
14	9.30	9.34	8.99	8.60	8.36
43	10.97	10.89	10.38	9.77	9.40
44	12.90	12.43	11.90		
48	9.08	8.95	8.75	8.51	8.39
53	10.39	10.13	9.56		
54	9.15	8.57	7.93	7.35	6.76
55	11.07	10.83	10.10	9.42	9.03
56	8.70	8.64	8.11	7.68	7.41
57	8.27	8.34	8.17	7.94	7.81
60	8.50	8.79	8.45		
61	9.86	9.59	9.25		
62	9.70	9.33	9.00		
63	11.04	10.73	9.93		
64	12.54	11.50	10.12		
67	9.42	9.32	8.73		
68	11.91	10.83	9.45		
69	13.49	12.93	12.33		
90	7.96	7.78	7.45	7.12	6.98
91	9.49	9.26	8.56	7.97	7.56

TABLE 3.7 Con't

ROE Star No.	U	B	V	R	I
92	9.49	9.47	8.97	8.52	8.14
93	8.77	8.49	8.01	7.57	7.30
94	10.42	9.45	8.16	7.25	6.57
95	9.87	9.69	9.09	8.53	8.18
96	9.47	9.26	8.80	8.36	8.09
97	10.47	8.90	6.86	5.42	4.15
98	10.17	9.30	8.04	7.16	6.48
A7	13.81	13.67	12.82		
A8	14.96	14.62	13.86		
A9	15.58	15.53	14.56		
A10	15.35	15.07	14.12		
A11	13.21	12.86	12.27		
A12	15.98:	15.66:	14.31:		
A15	13.49	13.10	12.42		
B1	15.38	14.70	13.70		
B2	13.23	14.03	12.32		
B3	13.78	13.51	12.65		
B5	15.64	14.99	15.04		
B7	13.61	13.28	12.63		
B10	19.28:	17.67:	15.86		
B11	15.64	14.68	13.68		
B12	13.81	13.62	12.74		
B13	17.52:	16.10:	15.02		
C4	14.60	14.50	13.58		
C7	14.54	14.55	13.50		

TABLE 3.7 Con't

ROE Star No.	U	B	V	R	I
D1	12.98	12.52	12.05		
D3	14.48	14.02	13.31		
D8	14.26	14.12	12.98		
D10	13.12	13.34	12.36		
D14	14.57	13.85	12.47		

TABLE 3.8

DERIVED PHOTOELECTRIC COLOURS

ROE Star No.	U - B	B - V	V - R	V - I
3	-0.35	0.62	0.53	0.88
4	-0.19	0.89	0.73	1.31
12	-0.14	0.11	0.19	0.15
13	-0.41	0.34	0.34	0.53
14	-0.04	0.35	0.39	0.63
43	0.08	0.61	0.61	0.98
44	0.47	0.53		
48	0.13	0.20	0.24	0.36
53	0.26	0.57		
54	0.58	0.64	0.58	1.17
55	0.24	0.73	0.68	1.07
56	0.06	0.53	0.43	0.70
57	-0.07	0.17	0.23	0.36
60	-0.29	0.34		
61	0.27	0.34		
62	0.37	0.33		
63	0.31	0.80		
64	1.04	1.38		
67	0.10	0.59		
68	1.08	0.38		
69	0.56	0.60		
90	0.18	0.33	0.33	0.47
91	0.23	0.70	0.59	1.00
92	0.02	0.50	0.45	0.83
93	0.28	0.48	0.44	0.71

TABLE 3.8 Con't

ROE Star No.	U - B	B - V	V - R	V - I
94	0.97	1.29	0.91	1.59
95	0.18	0.60	0.56	0.91
96	0.19	0.46	0.44	0.71
97	1.57	2.04	1.44	2.71
98	0.87	1.26	0.88	1.56
A7	0.14	0.85		
A8	0.34	0.76		
A9	0.05	0.96		
A10	0.28	0.95		
A11	0.35	0.59		
A12				
A15	0.39	0.68		
B1	0.68	1.00		
B2				
B3	0.27	0.86		
B5	-0.65	-0.05		
B7	0.33	0.65		
B10				
B11	0.96	1.00		
B12	0.19	0.88		
B13				
C4	0.10	0.92		
C7	-0.01	1.05		
D1	0.46	0.47		
D3	0.46	0.71		
D8	0.34	1.14		
D10	-0.22	0.98		
D14	0.72	1.38		

TABLE 3.9

POSITIONAL AND SPECTRAL DATA

ON PHOTOELECTRIC STANDARDS

ROE No.	BD No.	ℓ_{1950}	b_{1950}	Spectral Type
3	+57° 681	139°.79	-0°.91	BO.5 Vpe
4	+57° 687	140.08	-0.48	B1 Ib
12	+58° 563	139.70	1.05	B9
13	+58° 567	139.72	1.25	B5
14	+58° 568	139.82	1.35	B7
43		139.90	0.62	B6
44		139.74	1.40	B9
48	+57° 669	139.31	-1.01	AO
53	+56° 774	140.32	-0.67	
54	+56° 771	140.27	-0.76	FOI
55	+57° 705	140.74	0.09	
56	+58° 583	140.92	1.11	F5
57	+58° 572	140.30	0.68	B9
60	+57° 678	139.35	-0.33	
61		139.75	-1.30	
62	+57° 675	139.17	-0.32	A2
63	+57° 671	139.08	-0.31	
64		138.98	-0.39	
67	+58° 560	139.60	0.93	
68	+58° 562	139.66	1.01	
69		139.65	1.04	
90	+57° 695	140.14	0.14	FO
91		140.57	0.19	G5
92		140.54	0.07	A2
93		140.00	0.53	A2
94		140.33	-0.76	KO

TABLE 3.9 Con't

ROE No.	BD No.	ℓ_{1950}	b_{1950}	Spectral Type
95		140°.24	-0°.05	F8
96		140.03	-0.79	FO
97		139.43	-1.04	K5
98		138.90	-1.02	KO
A7		139.75	1.13	
A8		139.54	1.17	
A9		139.55	1.19	
A10		139.56	1.21	
A11		139.75	1.16	
A12		139.77	1.16	
A15		139.80	1.15	
B1		140.59	0.06	
B2		140.59	-0.07	
B3		140.70	-0.03	
B5		140.72	0.03	
B7		140.83	0.06	
B10		140.83	0.07	
B11		140.84	0.09	
B12		140.79	0.17	
B13		140.78	0.19	
C4		139.17	-0.29	
C7		139.21	-0.32	
D1		140.31	-0.62	
D3		140.35	-0.60	
D8		140.31	-0.56	
D10		140.38	-0.52	
D14		140.39	-0.47	

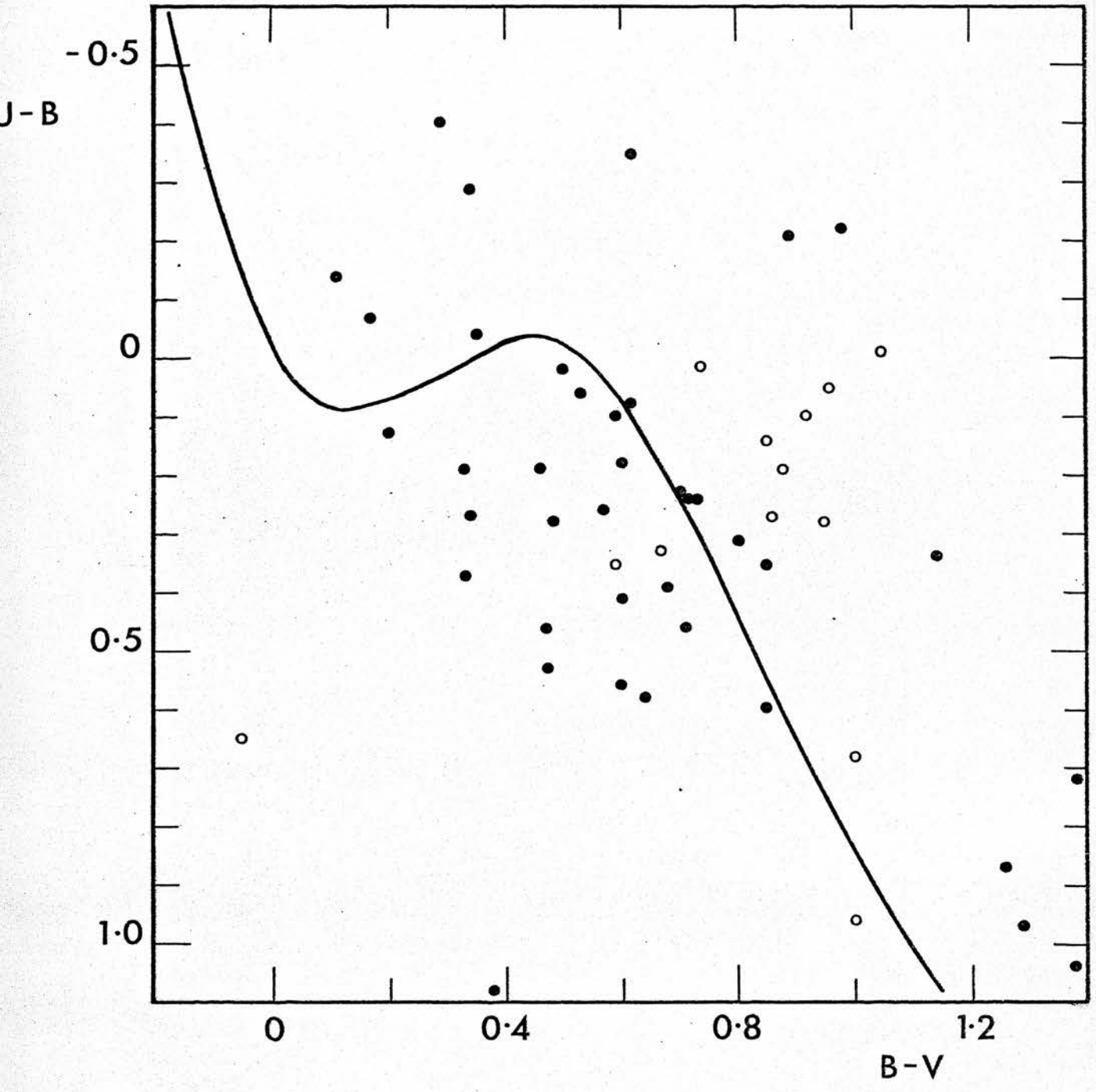

Fig. 3.12 (U - B) - (B - V) plot for observed photo-electric standards.

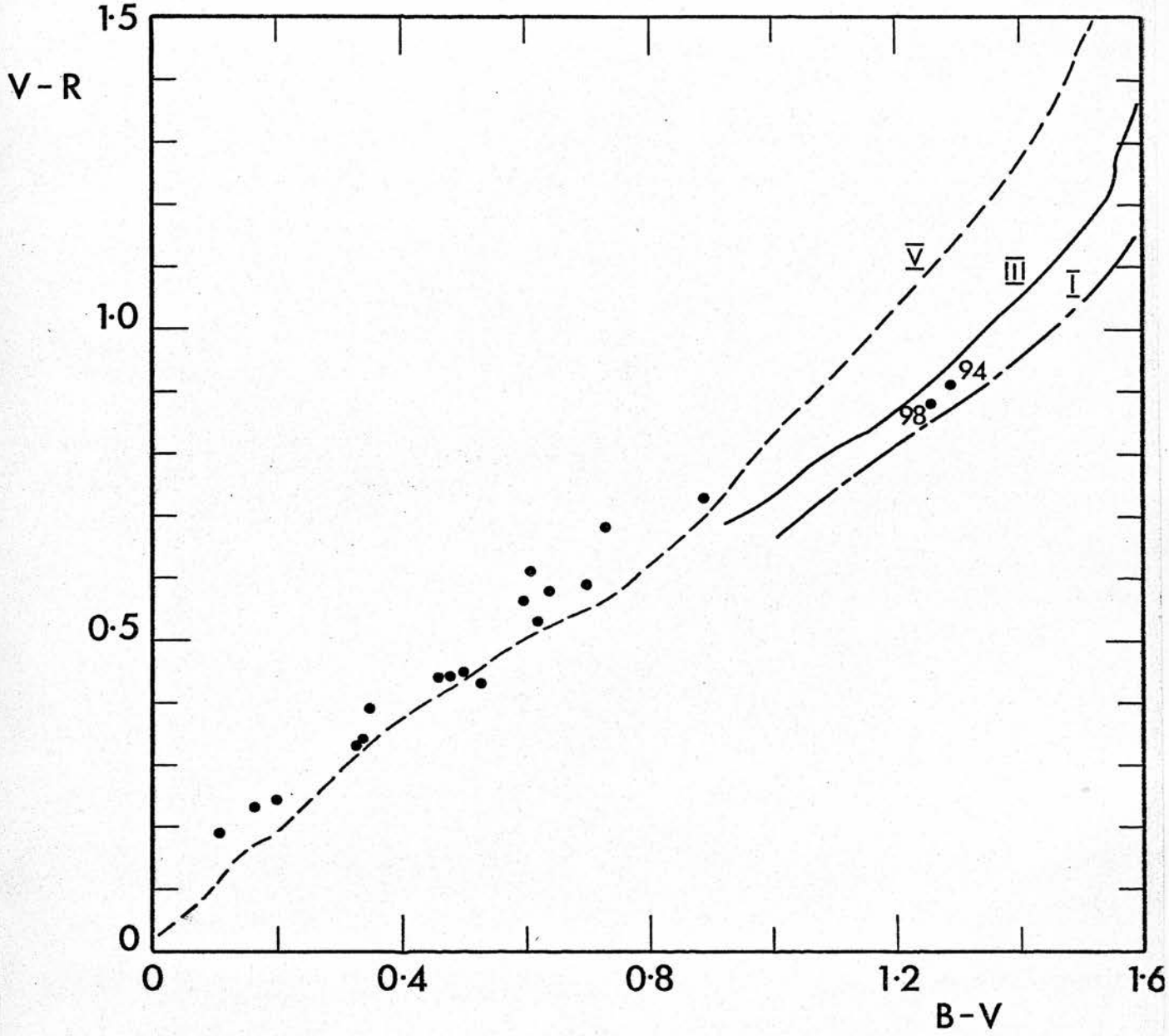

Fig. 3.13 (B - V) - (V - R) plot for observed photo-electric standards.

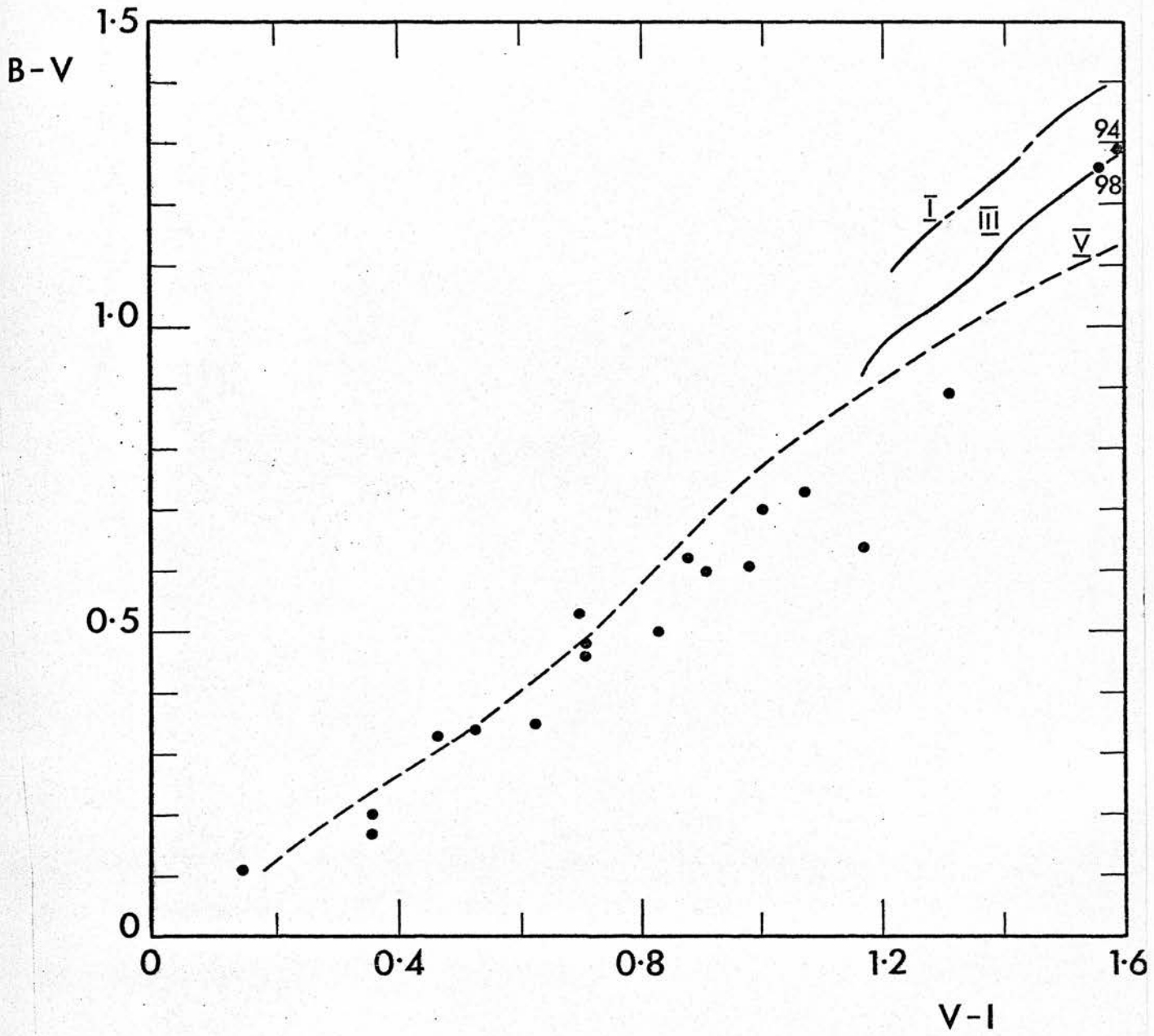

Fig. 3.14 (B - V) - (V - I) plot for observed photo-electric standards.

Chapter 4. Proper Motions

4.1 Introduction

Measurements were made of two plates taken 53 years apart to determine the proper motions of stars common to both plates. U, B and V magnitudes for each of the stars were measured and the secular parallaxes of distinct groups of stars, in preselected magnitude intervals, in the two colour diagram were derived.

4.2 Observations and Measurement

The first epoch plate (SV 1796) was taken with the 33/343cm astrograph at the Specola Vaticana as part of their contribution to the "Carte du Ciel" observational programme. The second epoch plate (ROE 741) was taken with the 40/60/150cm Schmidt telescope, shown in Fig. 4.1, at the Royal Observatory Edinburgh. The V magnitudes used were obtained from plate ROE 902 and the U magnitudes from plate ROE 748. Details of these plates are given in Table 4.1.

TABLE 4.1

OBSERVATIONAL MATERIAL

Plate No.		SV 1796	ROE 741	ROE 902	ROE 748
Date		1915 Jan 14	1967 Dec 27	1968 Dec 12	1968 Jan 3
Plate Centre	α	3^h10^m	3^h05^m	3^h05^m	3^h05^m
	δ	$+57^\circ12'$	$+58^\circ06'$	$+58^\circ09'$	$+58^\circ09'$
Emulsion		-	IIaO	IIaD	IIaO
Filter		-	GG13	GG14	UG2
L.S.T.		3^h01^m	7^h00^m	4^h30^m	2^h37^m
Exposure Time		3×40^m	5^m	3^m	40^m

The Schmidt plates were developed for five minutes in a nitrogen bubble agitation tank at 20°C using Kodak D19b developer, actively fixed for 7 minutes in Kodak rapid fixer, washed for one hour, and dried in an enclosed box by a forced circulation of filtered air at 20°C in a vertical position. No information regarding emulsion type or method of development was available for the astrograph plate.

The area of the plates common to both was selected to be measured. This area is approximately bounded by $l = 140^\circ$ to 141° and $b = -1^\circ$ to $+1^\circ$. On the astrograph plate all stars in this region which had three distinct images were noted and cross-identified on the Schmidt plate. 796 corresponding images were found. A careful visual inspection of each of the images on the astrograph

Fig. 4.1 R.O.E. 40/60/150cm Schmidt telescope.

plate was made to reject unsuitable stars such as close doubles, those misshapen by optical aberrations and those with one or more images lying on the reseau. Some stars which were resolved on the scale of the astrograph plate (60"/mm) were not resolved on the Schmidt plate (scale 140"/mm). Images rejected by the GALAXY machine were not used, neither were mean measures in which the drift between any of the GALAXY runs exceeded $\pm$ 5μm. In all 243 stars from the original block were rejected leaving 553 whose positions and motions were to be determined.

Charts were made up on which all the stars to be measured were numbered. The initial measures were made on the Grubb-Parsons two coordinate measuring machines using as the origin of the axes a fiducial point on the plate carriage, this ensured that all the (X,Y) measures had the same sign. All the programme stars on the Schmidt plate were measured, as were two diametrically opposed stars which were to be used as transformation reference points in converting from Grubb Parsons to GALAXY coordinates. Using the translation and rotation constants generated by the transformation stars the entire Grubb Parsons set of measures was converted to GALAXY coordinates by computer program GXRF which outputs a pseudo search tape for use directly with the GALAXY machine. The X75 optical system was used to allow all the images to be measured without rejection due to size (as would have happened to bright images had the X240 optics been used).

Each image was measured three times to allow corrections for drift to be made. The total time taken for GALAXY to measure all the images three times was 2^h40^m.

On the astrograph plate only the images at the apex of the triangle of three images were measured on the Grubb Parsons machine. Two stars on the north and south edges respectively of the plate were measured as transformation reference points. GALAXY coordinates were measured manually for each of the three images of the transformation stars and the translation and rotation constants thus obtained for each image applied to all the programme stars to give three distinct search tapes. All the star images on each of these tapes were measured three times and a mean value taken. The mean values for a given image from each of the three tapes were then combined to form the mean position of the centroid of the triangle of images. The total time taken for GALAXY to measure all the images three times was 8^h.

4.3 Determination of Magnitude

B magnitudes were derived by plotting a calibration curve of the GALAXY M-measures of ROE Schmidt plate 741 against photoelectrically determined magnitudes for standard stars. The curve is shown in Fig. 4.2. A least squares fit to the data has equation

$$B = 20.63 - 0.042396\,M \qquad 4.1$$

The above relationship was used to recompute the standard star magnitudes from their M-number. The standard deviation of the difference between the photoelectric and the computed magnitude was used to give an indication of the accuracy of the computed magnitudes, in this case $\sigma_B = \pm 0^m.12$

The relevant star images on the U and V Schmidt plates were measured with a semi-automated Becker iris photometer and calibration curves drawn of photoelectric magnitude against iris reading. These are also shown in Fig. 4.2 A linear least squares fit proved inadequate so a quadratic fit was made to the data with a subsequent reduction in the residual standard deviations. The quadratic least squares equations were

$$U = 19.26 - 0.028984\,I + 0.000019\,I^2 \qquad 4.2$$

$$V = 17.51 - 0.031845\,I + 0.000024\,I^2 \qquad 4.3$$

with residual standard deviations of

$$\sigma_U = \pm 0^m.14$$

$$\sigma_V = \pm 0^m.11$$

Combining the various magnitude residual standard

deviations yield the following standard deviations in measured colour

$$\sigma_{(B-V)} = \pm 0^{m}.16$$

$$\sigma_{(U-B)} = \pm 0^{m}.18$$

4.4 Proper Motion Reduction using AGK3 Stars as Reference Points

Stars from the AGK3 catalogue which appeared in the region to be measured were identified using a transparent overlay on which were printed circles corresponding to the AGK3 star positions. Each circle carried an identifying number from which, by using the catalogue, the circle could be associated with a particular catalogue star. The scale of the overlay was midway between that of the Schmidt plate finder charts and the astrograph plate finder charts, this allowed for easy identification of the AGK3 stars in small areas on either chart. The overlay was moved across the charts between identification to counteract the difference in scales. Both the overlay and the catalogue were prepared from a magnetic disc form of the catalogue, held at the Royal Greenwich Observatory, by Mr. C.A. Murray.

On the Schmidt plate there were 25 AGK3 stars in the region of interest and on the astrograph plate 24 though in the latter case some of the images were of poor quality.

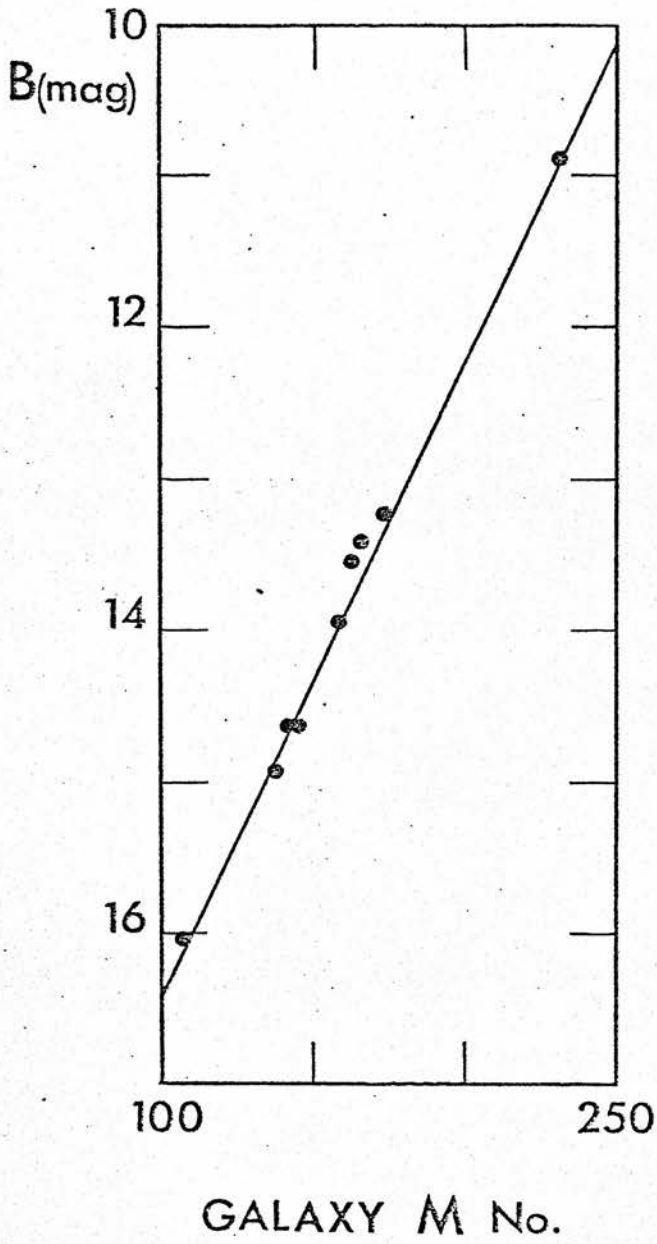

Fig. 4.2a B magnitude calibration curve

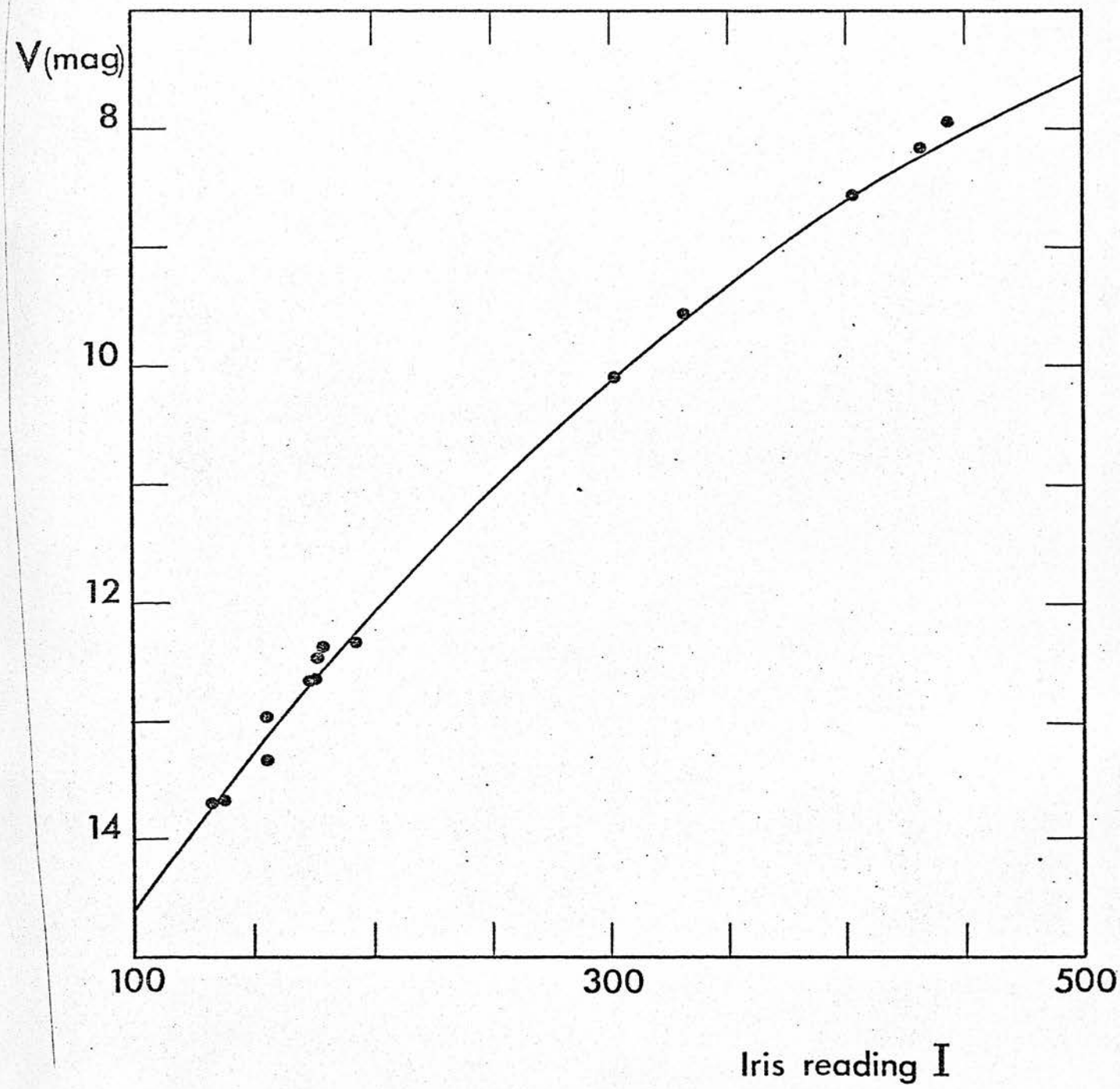

Fig. 4.2b V magnitude calibration curve.

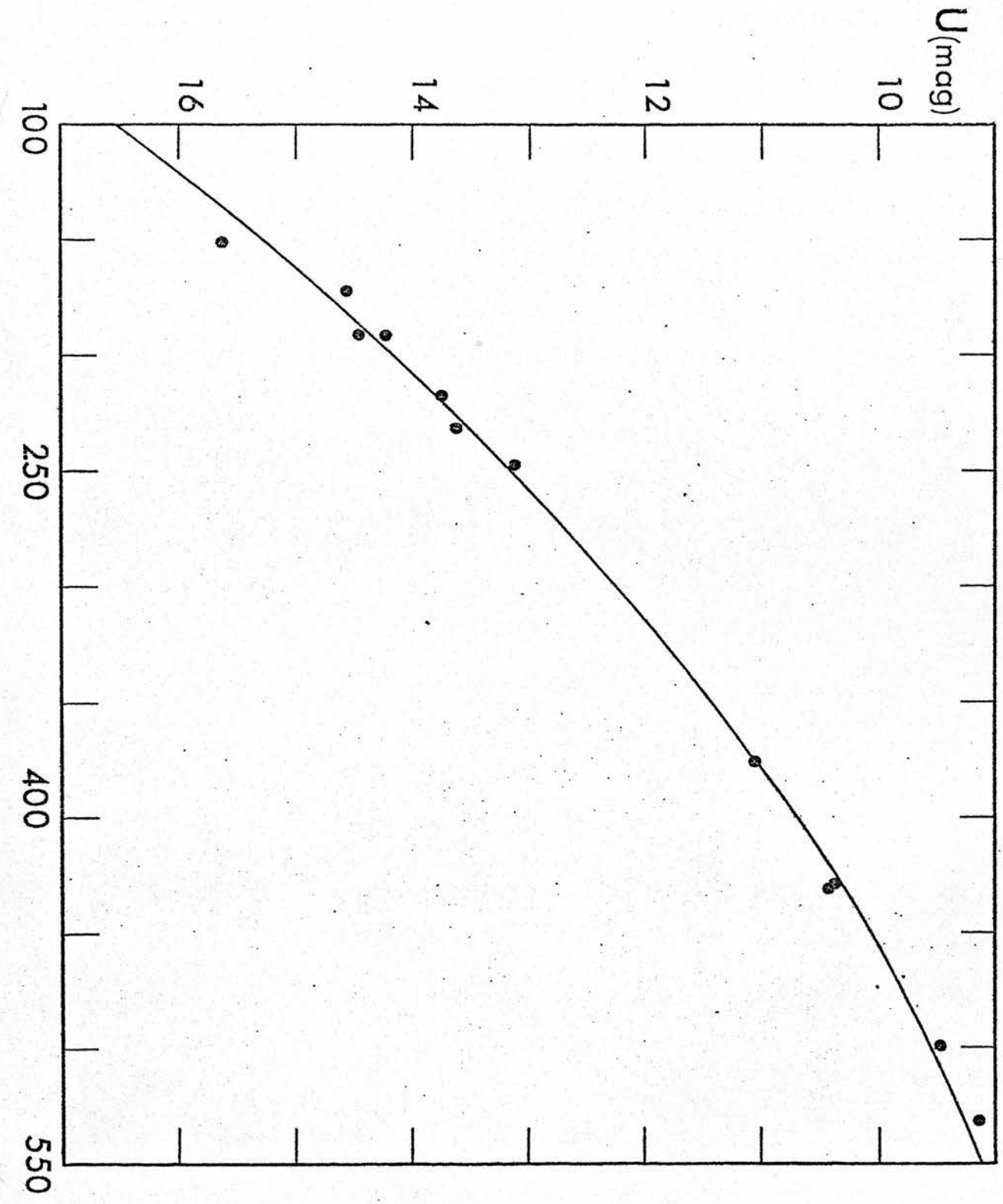

Fig. 4.2c U magnitude calibration curve.

The catalogue positions (epoch and equinox 1950.0) were corrected for proper motions to epoch 1915 and epoch 1968 using the values of proper motion given in the catalogue via a simple computer program PMCOR which solves the equations.

$$\alpha_t = \alpha_0 + t.\,\Delta\alpha$$

$$\delta_t = \delta_0 + t.\,\Delta\delta \qquad 4.4$$

where (α_t, δ_t) is the star position of time t years after the catalogue epoch, (α_0, δ_0) is the catalogue epoch position and $(\Delta\alpha, \Delta\delta)$ the components of annual proper motion of the star.

The corrected positions were converted from equatorial (α,δ) to galactic (ℓ,b) coordinates using the equations given by Torgård (1961).

$$\cos b \cos(\ell - 33^\circ) = \cos\delta \cos(\alpha - 282^\circ.25)$$

$$\cos b \sin(\ell - 33^\circ) = \cos\delta \sin(\alpha - 282^\circ.25) \cos 62^\circ.6 + \sin\delta \sin 62^\circ.6$$

$$\sin b = -\cos\delta \sin(\alpha - 282^\circ.25) \sin 62^\circ.6 + \sin\delta \sin 62^\circ.6$$

4.5

the conversion being effected by computer program CONVEG.

Standard coordinates (x,y) for each of the reference

stars with galactic coordinates (ℓ, b) were computed for plate centre (ℓ_o, b_o) using the transformations

$$x = \cos b \sin(\ell - \ell_o) / (\sin b \sin b_o + \cos b \cos b_o \cos(\ell - \ell_o))$$

$$y = (\sin b \cos b_o - \cos b \sin b_o \cos(\ell - \ell_o)) / (\sin b \sin b_o + \cos b \cos b_o \cos(\ell - \ell_o)) \qquad 4.6$$

In order to make the best possible use of the measurements obtained with the GALAXY measuring machine the normal plate constants equation was generalized. If (x,y) are the standard coordinates of a star whose machine measured coordinates are (X,Y) then a general, magnitude and colour independent, expression may be used to relate them such that

$$x = \sum_{S=0}^{n} \sum_{r=0}^{n-S} \left\{ A_{\frac{S}{2}(2n-S+3)+r} X^r Y^S \right\}$$

$$y = \sum_{S=0}^{n} \sum_{r=0}^{n-S} \left\{ B_{\frac{S}{2}(2n-S+3)+r} X^r Y^S \right\} \qquad 4.7$$

where the A_j, B_j are the fitted plate constants. It is evident that the number of plate constants generated by the equations 4.7, for an nth order fit is, for each coordinate, m where

$$m = \tfrac{1}{2}(n+1)(n+2) \qquad 4.8$$

The plate constants A and B are found, by using the method of least squares, from the matrix equations

$$\underset{\sim}{M} \cdot \underset{\sim}{A} = \underset{\sim}{k} \qquad 4.9$$

The solution of this set of linear equations is found by the Gauss-Jordon procedure outlined by Hawgood (1965).

The elements of $\underset{\sim}{M}$ and $\underset{\sim}{k}$ are determined as follows: firstly the elements of the first row of $\underset{\sim}{M}$ are computed:

$$M_x(1,j) = \sum_{i=1}^{\rho} X_i^r Y_i^s \qquad 4.10$$

where

$$j = \frac{s}{2}(2n - s + 3) + r + 1 \qquad 4.11$$

and ρ is the number of reference stars. The elements of the first column are equated to those of the first row so that

$$M_x(\ell,1) = \sum_{i=1}^{\rho} X_i^{r'} Y_i^{s'} \qquad 4.12$$

where

$$\ell = \frac{s'}{2}(2n - s' + 3) + r' + 1 \qquad 4.13$$

For these $M_{l,j}$, $M_{l,1}$ any element $M_{l,j}$ is found by

$$M_x(l,j) = M_x(1,j)\, M_x(l,1) \qquad 4.14$$

similarly the vth element of the vector $\underset{\sim}{k}$ is given by

$$k_x(v) = \sum_{i=1}^{p} X_i^r\, Y_i^s\, x_i \qquad 4.15$$

Identical expressions may be computed for the M_y and k_y

The first set of computed plate constants is used with the (X,Y) coordinates of the reference stars to give their standard coordinates and thence their galactic coordinates via

$$\tan(l-l_o) = x/(\cos b_o - y \sin b_o)$$

$$\tan b = (\sin b_o + y \cos b_o)\cos(l-l_o)/(\cos b_o - y \sin b_o) \qquad 4.16$$

which may then be directly compared (in decimal degrees) with the input galactic coordinates. The residuals

$$\Delta l = (l_{catalogue} - l_{computed})\cos b_{catalogue}$$

$$\Delta b = b_{catalogue} - b_{computed}$$

$$R = \left[(\Delta l)^2 + (\Delta b)^2\right]^{1/2} \qquad 4.17$$

were calculated and three rejection criteria used in successive redeterminations of the plate constants. The first being that a reference star is not used in subsequent redeterminations of the plate constants if $R > 1^{o}.0$, the second, $R > 0^{o}.03$ and the third $R > 0^{o}.001$. The set of plate constants determined after the third rejection loop in the program (named XYLB) is then output for use in the computation of the galactic coordinates of the programme stars.

Using the method outlined above plate constants for 1st, 2nd and 3rd order fits were determined for each of the plates. The plate centre used for both plates had galactic coordinates $\ell = 140^{o}.5$, $b = -0^{o}.2$. Both $\overline{\Delta\ell}$ and $\overline{\Delta b}$ were very small and not significantly different from zero for each of the plates. Tables 4.2 and 4.3 give summaries of the results obtained. Column 1 gives the order of the fit (the n in equations 4.7), column 2 gives the number of plate constants determined, ($= m = \frac{1}{2}(n + 1)(n + 2)$), column 3 gives the standard deviation of the mean residual in galactic longitude in seconds of arc, column 4 gives the standard deviation of the mean residual in galactic latitude in seconds of arc, column 5 gives the number of reference stars used in the third loop determination of the plate constants, and columns 6 and 7 give the maximum residuals observed in seconds of arc in galactic longitude and latitude.

TABLE 4.2

ASTROGRAPH PLATE

1	2	3	4	5	6	7
1	3	0.35	0.44	24	0.80	0.69
2	6	0.29	0.38	24	0.83	0.90
3	10	0.26	0.37	24	0.69	0.94

TABLE 4.3

SCHMIDT PLATE

1	2	3	4	5	6	7
1	3	0.40	0.30	25	0.80	0.94
2	6	0.33	0.32	25	0.72	0.94
3	10	0.30	0.29	25	0.69	0.72

In order to ascertain whether increasing the order of fit significantly decreases the standard deviation of the position residuals the following F-test was carried out. F is defined by

$$F = \frac{n_1 s_1^2}{n_1 - 1} \cdot \frac{n_2 - 1}{n_2 s_2^2} \qquad 4.18$$

where s_1 ($= \sigma_\ell^2 + \sigma_b^2$) is the larger variance of the two being compared and s_2 is the smaller, n_1 is the number of reference stars used to derive s_1, and n_2 the number used to derive s_2. The value of $F_{k\%}(v_1, v_2)$ is found from tables where v_1 ($= n_1 - 1$) and v_2 ($= n_2 - 1$) are the number of degrees of freedom. The hypothesis that there is no

significant difference between the sample variances is accepted at the appropriate level of testing if

$$F_{calculated} < F_{tabulated}$$

For the astrograph plate the tabulated value of F is

$$F_{1\%}(23,23) = 2.70$$

Comparing the first and second order fit variances gives

$$F_{12} = 1.92$$

Comparing the second and third order fit variances gives

$$F_{23} = 1.06$$

and comparing the first and third order fit variances gives

$$F_{13} = 2.03$$

Thus, since $F_{1\%}(23,23) > F_{13} > F_{12} > F_{23}$ the hypothesis that no significant reduction is achieved in the standard deviations of the residuals by increasing the order of the fit from one to three, at the 1% level of testing is accepted.

Similarly for the Schmidt plate the appropriate inequalities are

$$F_{1\%}(24,24) = 2.64 > F_{13} = 1.71 > F_{12} = 1.25 > F_{23} = 1.22$$

so the above hypothesis is again accepted.

On the basis of this test linear plate constants were used to convert measured (X,Y) coordinates on both the Schmidt and astrograph plates to galactic coordinates. The difference between the Schmidt and astrograph plate galactic coordinates was divided by the epoch difference between the plates to give directly the proper motion components μ_ℓ and μ_b in arc seconds per year.

4.5 Proper Motion Reduction by Mapping one Plate onto the other

To map the measured coordinates (X,Y) at a given star on one plate to those (X′, Y′) on another equations 4.7 were rewritten thus:

$$X' = \sum_{s=0}^{n} \sum_{r=0}^{n-s} \left\{ A_{\frac{s}{2}(2n-s+3)+r} X^r Y^s \right\}$$

$$Y' = \sum_{s=0}^{n} \sum_{r=0}^{n-s} \left\{ B_{\frac{s}{2}(2n-s+3)+r} X^r Y^s \right\} \qquad 4.19$$

The A , B were found for faint stars with B ≥ 15.15 (corresponding to an arbitrary M-number of 130, cf.

Fig. 4.3 for a B magnitude histogram) by solving equations 4.19 by least squares as described in the preceding section. For this reduction rejection criteria based on multiples of the computed residual standard deviations were used rather than fixed values, where the residuals R_x, R_y and R_{xy} are defined by

$$R_x = X_{measured} - X_{computed}$$

$$R_y = Y_{measured} - Y_{computed}$$

$$R_{xy} = \left(R_x^2 + R_y^2\right)^{1/2} \qquad 4.20$$

After the preliminary determination of the plate constants the standard deviation of the positional residuals of the stars used in the fit were calculated. All stars with $R_{xy} \geq 0.7\,\sigma_{\bar{R}_{xy}}$ were rejected for the subsequent recomputation. The successive rejection levels thereafter were $1.4\,\sigma_{\bar{R}_{xy}}$ and $2.1\,\sigma_{\bar{R}_{xy}}$. This method ensured that no intrinsically faint star with a large proper motion was included in the grid system for the coordinate transform.

Equations 4.19 were solved for first to fifth order data fits and the results given in Table 4.4 in which column 1 gives the order of the fit, column 2 the number of plate constants, columns 3 and 4 the mean values of R_x and R_y, columns 5 and 6 the standard deviations $\sigma_{\bar{R}_x}$ and $\sigma_{\bar{R}_y}$, all in microns and column 7 the number of stars used in the fit after the final rejection loop.

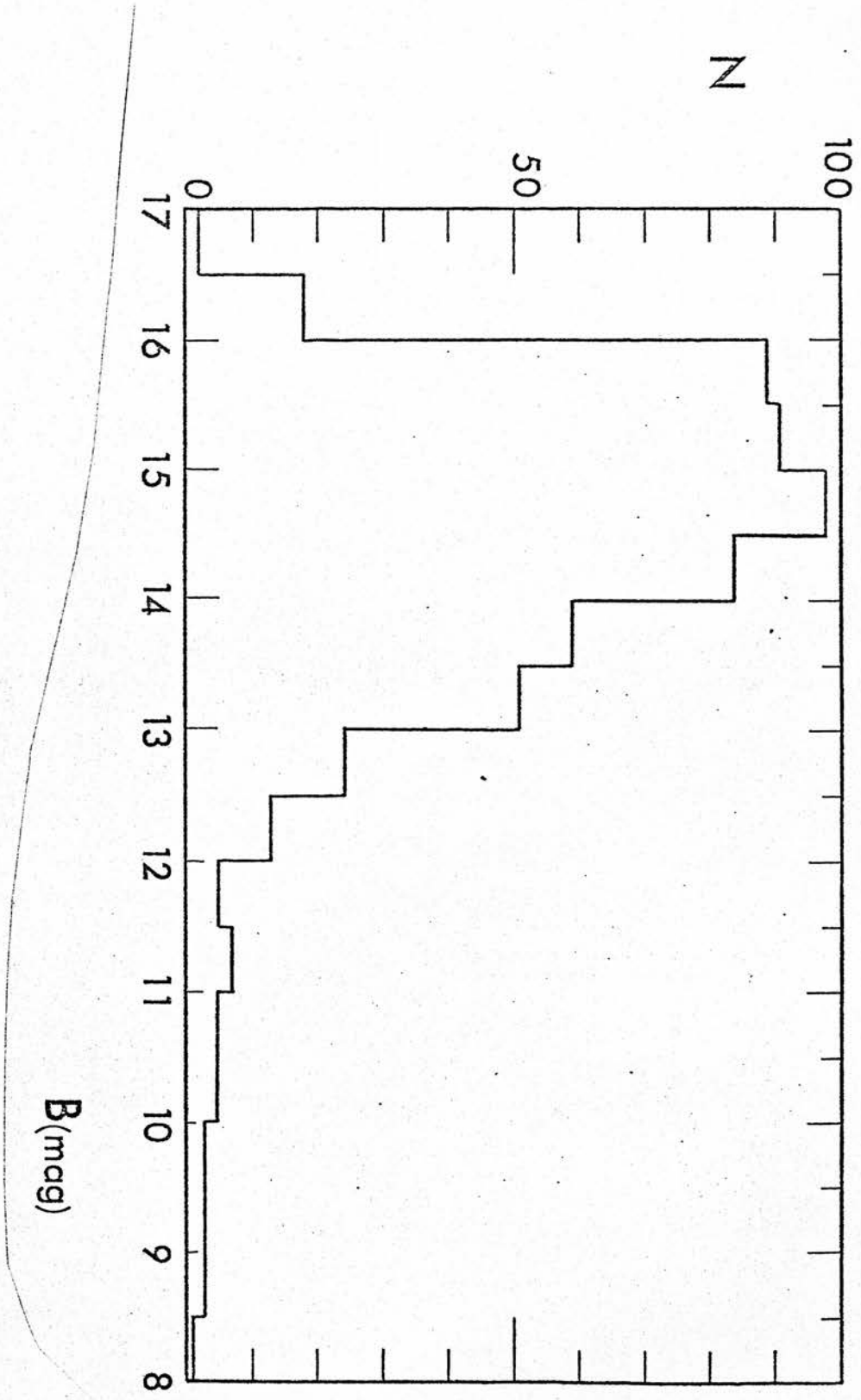

Fig. 4.3 Histogram of B magnitudes from ROE Schmidt plate 741.

TABLE 4.4

1	2	3	4	5	6	7
1	3	0.0	0.0	2.4	2.6	147
2	6	0.0	0.0	2.3	2.5	148
3	10	0.0	0.0	2.2	2.4	141
4	15	0.0	0.0	2.2	2.4	146
5	21	0.0	0.0	2.1	2.3	131

A similar F-test to that described above was used to test the significance of the results from the various orders of fit, and the following results obtained where the suffixes refer to the compared orders of fit:

$F_{12} = 1.085$ $\quad F_{1\%}(146,147) = 1.55$

$F_{13} = 1.180$ $\quad F_{1\%}(146,140) = 1.55$

$F_{14} = 1.180$ $\quad F_{1\%}(146,145) = 1.55$

$F_{15} = 1.289$ $\quad F_{1\%}(146,130) = 1.55$

Thus since $F_{1\%}(\nu_1,\nu_2) > F_{15} \geq F_{14} \geq F_{13} > F_{12}$ the hypothesis that no significant reduction is achieved in the standard deviations of the residuals by increasing the order of fit from one to five, at the 1% level of testing, is accepted.

The linear plate constants were used to convert astrograph coordinates to Schmidt plate coordinates for all the well measured stars. The difference between the

Schmidt measured coordinates and the astrograph transformed coordinates was multiplied by the Schmidt plate scale ($7.4\mu m$ arcsec^{-1}) to give a difference in arc seconds $(\Delta x, \Delta y)$. The rotation angle at the assumed plate centre between the measured Schmidt coordinate system and the galactic coordinate system, measured from the Schmidt plate chart, was $30^{\circ}.5$, hence the proper motion components in ℓ and b were give by

$$\mu_\ell \cos b = (\Delta x \cos 30^{\circ}.5 - \Delta y \sin 30^{\circ}.5)/53$$

$$\mu_b = (\Delta x \sin 30^{\circ}.5 + \Delta y \cos 30^{\circ}.5)/53 \qquad 4.21$$

where 53 is the epoch difference between the Schmidt plate and the astrograph plate in years.

4.6 Comparison of Reduction Methods and Residuals Analysis

The reduction methods described in Sections 4.4 and 4.5 differ essentially in that the analysis of section 4.4 is based on stars brighter than m = 11 whilst that of section 4.5 is based on stars fainter than B = 15.5. Plots of the components of proper motion determined using the different methods are illustrated in Figures 4.4 and 4.5. In galactic longitude the mean residual between the two methods of reduction and its standard deviation, in arc seconds per annum, was + 0.003 $\pm$ 0.005 and in galactic latitude - 0.003 $\pm$ 0.009. These standard

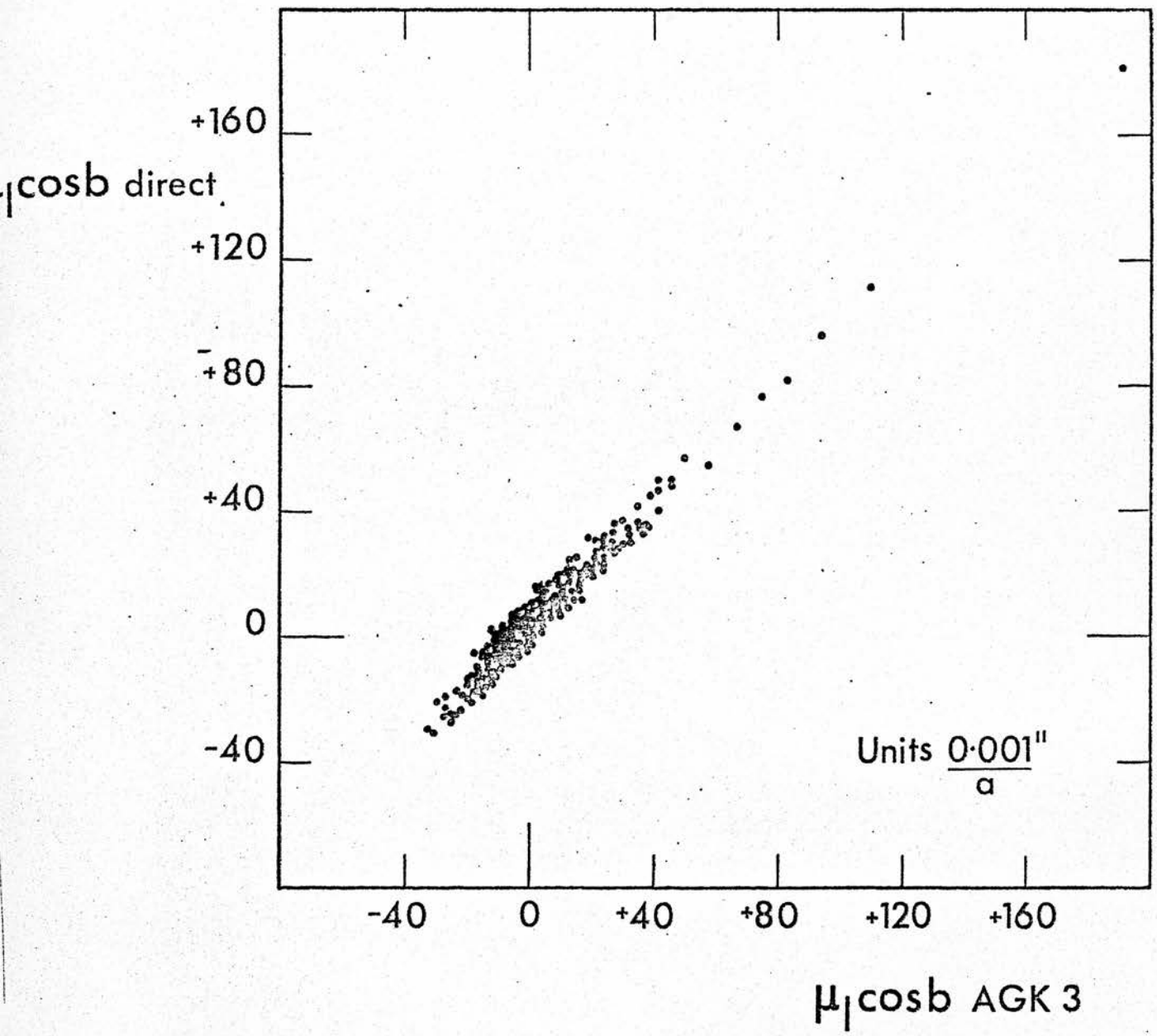

Fig. 4.4 Plot of $\mu_l \cos b$ measured by two distinct methods.

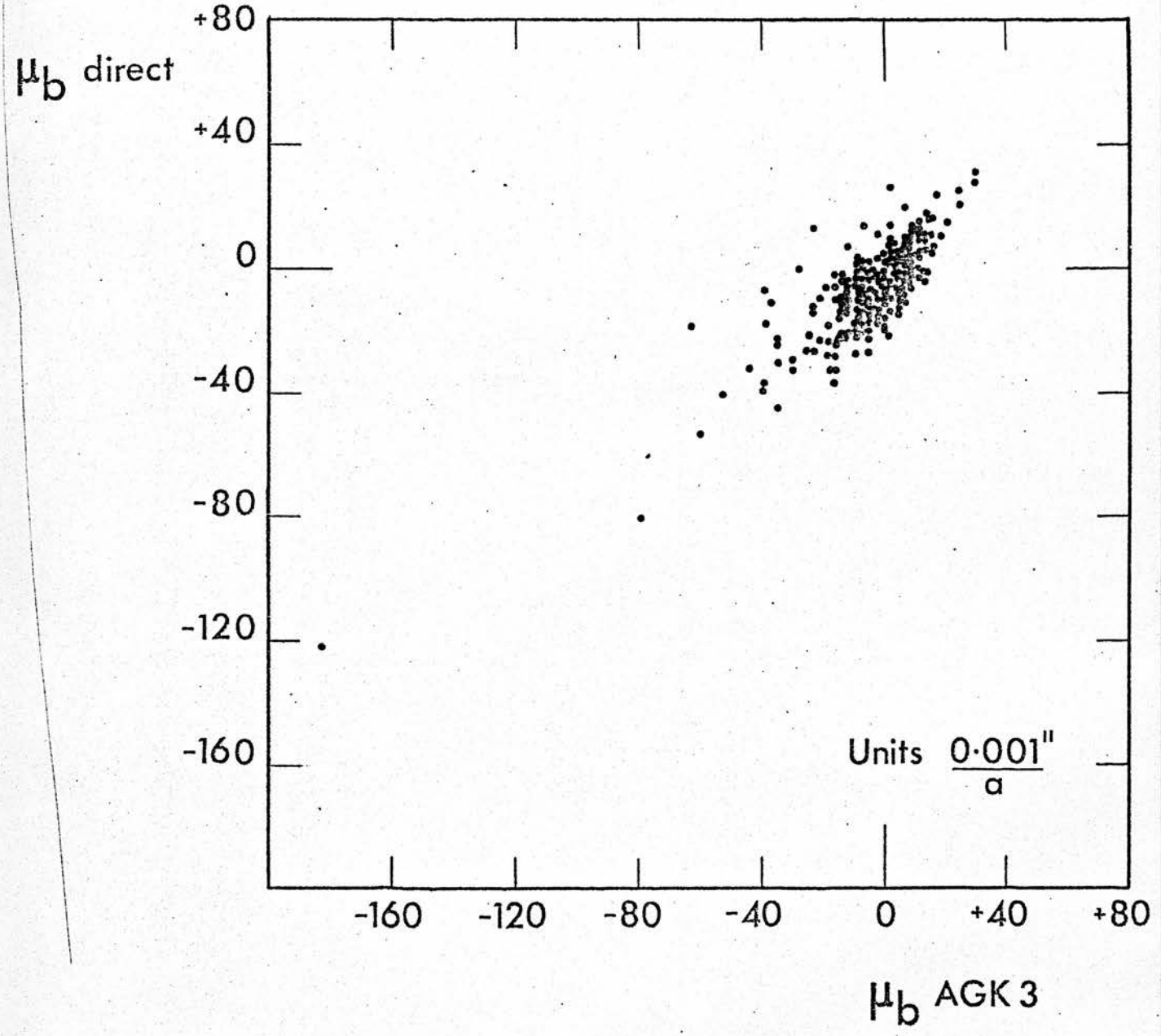

Fig. 4.5 Plot of μ_b measured by two distinct methods.

deviations are approximately the same as those found for the separate fitting techniques.

In order to make a comparison between the given AGK3 catalogue stars' proper motion and those computed for the same stars from GALAXY measures the equatorial proper motion components given in the catalogue had to be converted to galactic coordinate components, this was achieved by substituting μ_α and μ_δ in the following relations, which were derived by differentiating equations 4.5 with respect to time.

$$\mu_\ell \cos b = \operatorname{cosec}(\ell - 33^\circ)\left[\sin\delta \cos(\alpha - 282^\circ.25)\mu_\delta + 15\mu_\alpha \cos\delta \sin(\alpha - 282^\circ.25)\right]$$

$$\mu_b = \sec b\left[\left(\sin\delta \sin(\alpha - 282^\circ.25)\sin 62^\circ.6 + \cos\delta \sin 62^\circ.6\right)\mu_\delta - 15\mu_\alpha \cos\delta \cos(\alpha - 282^\circ.25)\sin 62^\circ.6\right] \qquad 4.22$$

The component residuals in galactic longitude $\Delta\mu_\ell \cos b$ and galactic latitude $\Delta\mu_b$ were defined by

$$\Delta\mu_\ell \cos b = (\mu_\ell \cos b)_{AGK3} - (\mu_\ell \cos b)_{computed}$$

$$\Delta\mu_b = (\mu_b)_{AGK3} - (\mu_b)_{computed} \qquad 4.23$$

For the fourteen AGK3 stars with proper motions in both systems the following mean residuals and standard deviations were obtained:

$$\Delta\mu_\ell \cos b = +0.004 \pm 0.010\ ''/a$$

$$\Delta\mu_b = -0.005 \pm 0.010\ ''/a$$

The standard deviations are again similar to those found from the individual fitting techniques.

Plots of component residuals against magnitude and spectral type were made to seek possible relations between these quantities. The magnitudes were taken from the AGK3 catalogue as were most of the spectral types (those marked o in Fig. 4.6), however, some stars without spectral types in the catalogue had them individually determined as follows: an objective prism plate, details of which are given in Table 4.5 was taken using a prism in front of the corrector plate of the Royal Observatory Edinburgh's Schmidt telescope (see Fig. 4.7) at Monte Porzio Catone, Italy. Selected stars of known spectral type from B to M and those stars whose spectral type was needed were traced, using the 50:1 ratio arm, by a Joyce-Loebl microdensitometer, these tracings were subsequently intercompared visually and spectral types (those marked + in Fig. 4.6) assigned to the unknown stars.

TABLE 4.5

OBJECTIVE PRISM PLATE

Date	Plate No.	Plate centre α	Plate centre δ	RLD at Hγ
1970 Dec 2	MP 1453	3^h05^m	$58^\circ07'$	400Å/mm

Emulsion	Filter	LST	Exposure Time
IN	GG13	5^h02^m	20^m

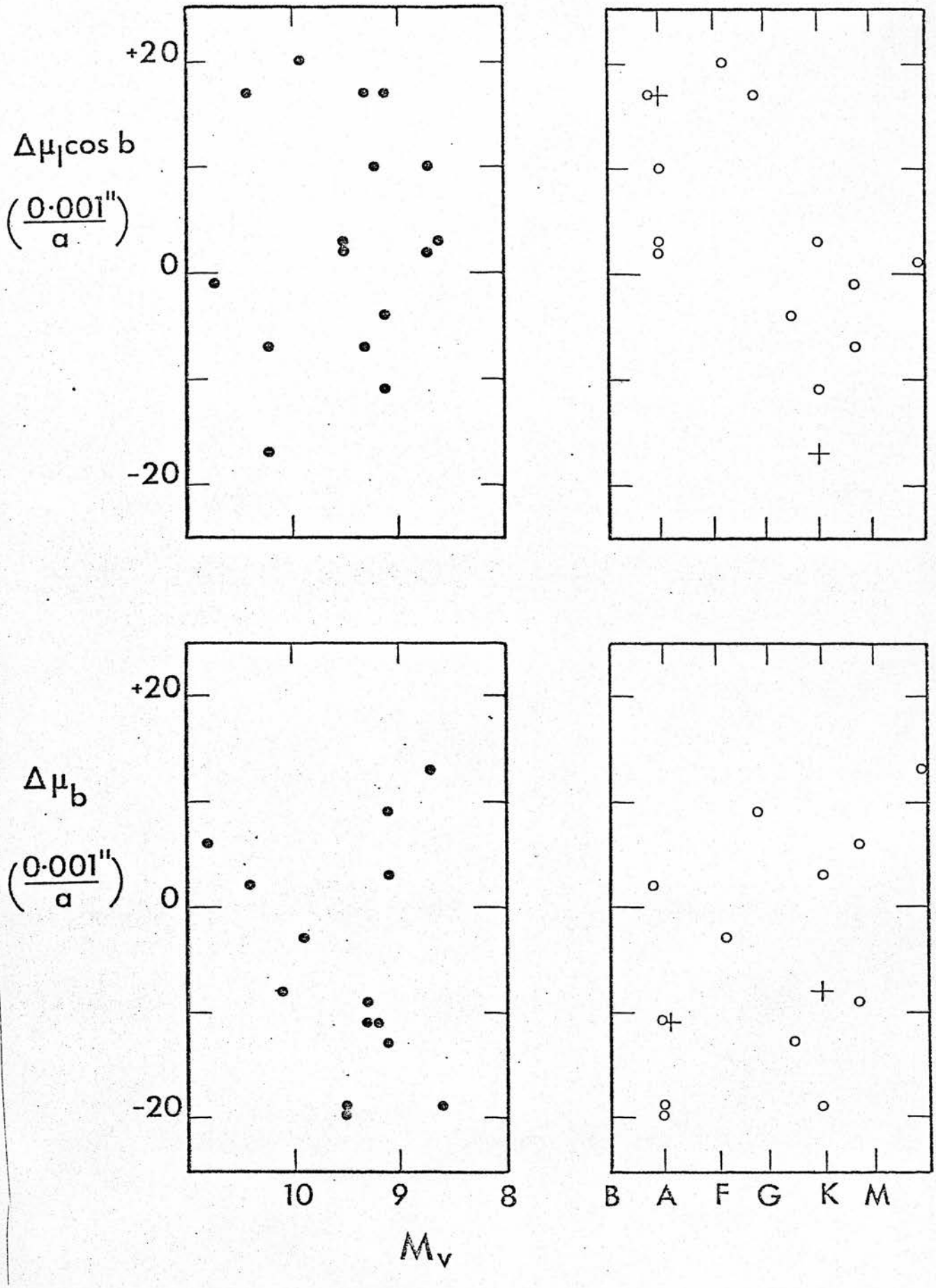

Fig. 4.6 Comparison between AGK3 and measured proper motions.

Fig. 4.7 R.O.E. 40/60/150cm Schmidt telescope at Monte Porzio outstation.

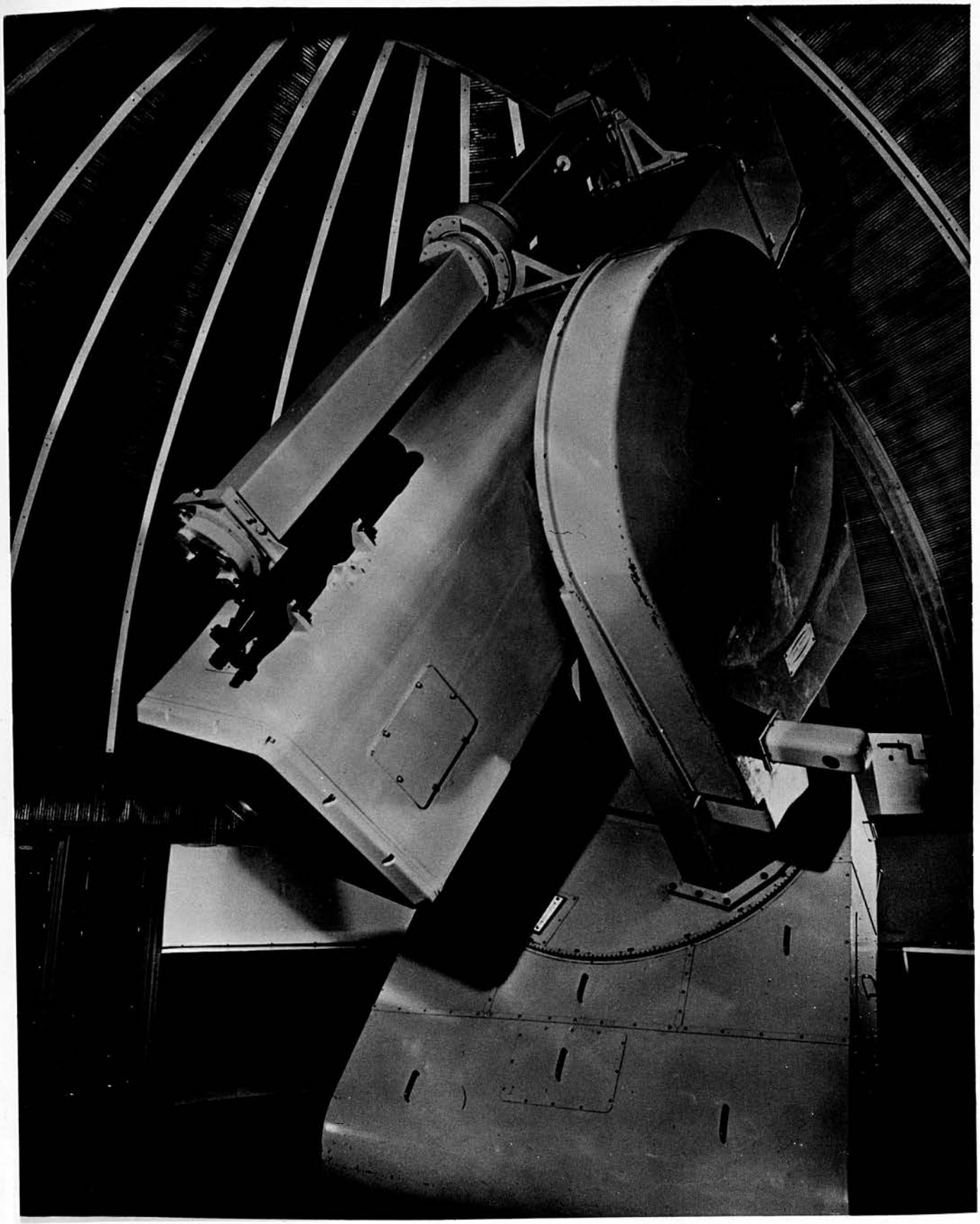

For the limited magnitude range considered there appears to be no correlation of residuals with magnitude in either galactic longitude or latitude, the same being true of latitude residuals with spectral type, but it does seem that the longitude residuals decrease in moving along the spectral sequence from B to M. No correction for this trend has been made in the given list (Table 4.6) of proper motions.

No correlation was found between residuals and the distance from plate centre.

TABLE 4.6

POSITIONS AND PROPER MOTION COMPONENTS

ROE No.	ℓ	b	$\mu_\ell \cos b$	μ_b
42	140.27060	-0.76496	-0.016	-0.001
43	140.24249	-0.85622	-0.001	-0.005
44	140.25108	-0.86853	0.005	-0.011
45	140.26734	-0.87692	0.005	-0.003
46	140.25245	-0 3141	0.020	-0.045
47	140.29709	-0.86155	0.011	-0.004
48	140.31589	-0.82287	0.020	0.003
49	140.34911	-0.79759	0.017	-0.013
50	140.28200	-0.74709	-0.010	-0.006
51	140.32023	-0.74361	0.002	-0.008
52	140.34552	-0.75438	0.003	-0.029
53	140.23581	-0.65295	0.004	-0.006
55	140.17628	-0.54775	0.004	-0.009
56	140.15673	-0.50512	-0.004	0.002
57	140.17631	-0.50513	-0.003	-0.000
58	140.19844	-0.52604	0.001	-0.003
59	140.20761	-0.49319	-0.006	-0.010
60	140.11403	-0.45683	-0.000	-0.002
61	140.10491	-0.43528	-0.004	-0.004
62	140.13782	-0.47780	-0.001	-0.003
64	140.13748	-0.47339	0.009	-0.012
67	140.11585	-0.33541	0.005	-0.003
88	140.15156	-0.29806	0.016	-0.007
89	140.17767	-0.28405	0.000	-0.001
90	140.19190	-0.41938	0.004	-0.002
91	140.20968	-0.39277	-0.000	-0.001
92	140.23119	-0.39884	0.001	-0.006
93	140.23977	-0.38386	0.004	0.001
94	140.23333	-0.49524	-0.006	-0.015
95	140.23590	-0.48809	-0.002	-0.006
96	140.28995	-0.46426	-0.019	-0.010
97	140.30188	-0.58025	-0.000	-0.005
98	140.28605	-0.53071	-0.004	-0.001
100	140.30965	-0.53501	0.005	-0.004
101	140.31654	-0.55535	-0.007	-0.011
102	140.32847	-0.57729	-0.002	-0.004
104	140.33544	-0.66660	-0.011	-0.021

ROE No.	ℓ	b	$\mu_\ell \cos b$	μ_b
108	140.34334	-0.63904	0.006	-0.008
109	140.35069	-0.63747	0.014	-0.008
110	140.36608	-0.63931	0.000	-0.005
111	140.36243	-0.58745	-0.006	-0.017
114	140.42347	-0.69975	0.000	-0.009
115	140.42996	-0.70350	0.002	-0.008
116	140.41827	-0.77947	0.004	-0.007
117	140.44013	-0.73964	0.000	-0.009
118	140.47342	-0.75700	0.004	-0.010
119	140.48003	-0.62482	0.023	-0.007
120	140.37500	-0.59654	-0.008	-0.004
121	140.38145	-0.60537	0.000	-0.003
123	140.41842	-0.61715	0.003	-0.004
125	140.38693	-0.53541	0.001	-0.002
127	140.40448	-0.51474	0.008	-0.004
128	140.41866	-0.52161	0.003	-0.001
129	140.29947	-0.38808	0.002	-0.001
130	140.32865	-0.39157	0.005	0.003
132	140.33624	-0.38133	-0.004	-0.002
135	140.17173	-0.23760	-0.002	-0.008
136	140.20869	-0.19645	-0.001	-0.000
137	140.23993	-0.24071	0.020	-0.000
138	140.11113	-0.14893	0.035	-0.081
139	140.15520	-0.12451	0.008	-0.012
141	140.13416	-0.03794	-0.021	-0.013
148	140.12467	0.08423	-0.005	-0.005
150	140.12575	0.04341	-0.003	0.003
151	140.16737	-0.05997	-0.003	0.002
152	140.21799	-0.06616	-0.007	-0.003
153	140.20287	0.00097	-0.031	0.005
154	140.20173	0.00723	-0.005	-0.005
155	140.22229	-0.13003	0.010	0.003
156	140.25381	-0.22238	0.002	-0.001
157	140.24633	-0.20030	0.007	-0.004
158	140.24184	-0.18460	-0.004	0.009
159	140.25066	-0.16569	-0.006	0.006
160	140.28055	-0.19174	0.004	-0.002
161	140.33307	-0.21198	-0.004	-0.006
163	140.31725	-0.33183	0.001	-0.003

ROE No.	ℓ	b	$\mu_\ell \cos b$	μ_b
164	140.36229	-0.36426	-0.275	0.235
165	140.34495	-0.32088	0.002	-0.000
166	140.34441	-0.29866	-0.003	0.002
167	140.37616	-0.33826	-0.002	0.001
168	140.41221	-0.45955	0.017	0.005
169	140.45960	-0.46464	-0.002	-0.003
170	140.45361	-0.44625	-0.005	0.003
171	140.47665	-0.46907	0.009	-0.016
172	140.46421	-0.54790	0.004	-0.001
173	140.46245	-0.53254	0.028	-0.004
175	140.50296	-0.64251	0.003	-0.006
176	140.50824	-0.63463	-0.000	-0.010
177	140.50582	-0.61056	0.008	0.001
178	140.52083	-0.63822	0.003	-0.004
179	140.53790	-0.64939	-0.010	-0.004
180	140.53568	-0.63915	0.001	-0.011
181	140.60662	-0.67474	0.002	-0.006
182	140.61401	-0.66121	0.006	-0.009
183	140.65035	-0.68366	0.003	-0.008
184	140.64916	-0.64442	0.002	-0.009
188	140.40672	-0.30317	-0.006	-0.001
189	140.40139	-0.27824	0.001	-0.016
190	140.46990	-0.29434	0.008	0.001
191	140.38632	-0.25476	0.005	-0.005
192	140.33109	-0.12041	0.003	0.000
193	140.35915	-0.12024	0.004	0.024
194	140.25977	-0.07562	-0.000	0.003
195	140.27995	-0.09307	-0.002	-0.011
196	140.28073	-0.05393	0.011	-0.000
197	140.29952	-0.07264	0.006	0.005
213	140.27510	0.07241	-0.003	-0.004
214	140.24773	0.12833	-0.009	-0.002
215	140.31444	0.08300	-0.011	-0.004
217	140.34859	0.04627	-0.007	0.005
218	140.34653	-0.05380	-0.003	-0.002
220	140.37298	-0.07308	-0.009	-0.002
221	140.42642	-0.09826	-0.002	-0.007
222	140.44909	-0.09008	-0.003	-0.003
223	140.44206	-0.14098	0.003	-0.006

ROE No.	ℓ	b	$\mu_\ell \cos b$	μ_b
225	140.47797	-0.26279	0.001	-0.005
226	140.45980	-0.22558	0.012	-0.027
227	140.47532	-0.22677	0.009	-0.001
228	140.53391	-0.30539	0.006	-0.011
229	140.54974	-0.28402	0.003	0.001
230	140.56092	-0.29541	-0.013	-0.033
232	140.59599	-0.39426	0.003	-0.011
233	140.60991	-0.39885	0.067	-0.018
234	140.60075	-0.38190	0.001	-0.005
235	140.59851	-0.34420	-0.007	-0.004
236	140.65550	-0.45528	0.022	-0.006
237	140.62314	-0.51481	0.013	-0.024
238	140.67302	-0.57192	-0.004	0.000
240	140.65714	-0.49556	0.003	-0.007
241	140.66449	-0.50459	0.001	-0.015
242	140.68643	-0.50063	0.012	-0.011
244	140.68154	-0.60460	-0.006	-0.006
245	140.73263	-0.61159	-0.002	-0.002
246	140.78026	-0.54190	0.019	-0.007
247	140.66274	-0.36928	0.015	-0.006
248	140.68963	-0.33654	0.006	-0.007
250	140.60189	-0.27784	-0.016	-0.005
251	140.64106	-0.26622	0.033	-0.006
252	140.56533	-0.23137	-0.010	-0.002
253	140.57695	-0.20509	0.021	-0.009
254	140.59163	-0.22387	0.008	-0.005
255	140.50589	-0.11380	0.021	-0.004
256	140.45741	-0.06457	-0.013	-0.002
257	140.48763	-0.08079	-0.003	-0.000
258	140.50856	-0.09391	-0.016	-0.021
259	140.50084	-0.06687	-0.003	-0.003
260	140.51358	-0.08095	-0.001	-0.005
261	140.50798	-0.03936	0.006	-0.001
263	140.40553	-0.03043	0.028	-0.006
264	140.49350	-0.00537	0.000	-0.008
265	140.41905	0.05186	0.015	-0.006
266	140.42143	0.09560	0.033	0.007
268	140.32838	0.13372	0.003	-0.001
269	140.26176	0.24973	-0.019	-0.009
270	140.23271	0.30068	-0.007	0.001

ROE No.	l	b	$\mu_l \cos b$	μ_b
271	140.26806	0.32640	-0.015	0.010
272	140.29047	0.33046	0.181	-0.122
273	140.34827	0.30027	-0.013	0.003
274	140.36100	0.30933	0.012	0.020
275	140.43456	0.18116	-0.014	-0.009
278	140.48975	0.09339	0.006	-0.005
282	140.51891	0.06923	-0.003	-0.006
284	140.53234	0.01094	0.001	-0.002
285	140.56725	-0.05574	-0.008	-0.006
286	140.57685	-0.09401	0.001	-0.005
287	140.59292	-0.10569	0.012	0.006
288	140.61886	-0.17453	0.005	-0.003
290	140.61902	-0.14008	0.002	-0.003
291	140.66864	-0.18218	-0.009	-0.011
292	140.66396	-0.16659	0.004	-0.005
293	140.65857	-0.23244	-0.007	-0.011
294	140.68405	-0.25377	0.004	-0.003
295	140.66902	-0.19874	0.016	-0.007
296	140.69388	-0.22197	0.001	-0.009
297	140.69145	-0.28868	0.008	-0.006
298	140.76342	-0.35374	-0.005	0.001
300	140.81287	-0.38190	-0.003	-0.004
301	140.80591	-0.46690	-0.029	-0.030
304	140.85358	-0.55419	0.002	-0.018
305	140.94730	-0.47352	0.037	-0.005
307	140.88094	-0.38273	0.017	-0.016
308	140.80785	-0.25816	0.030	-0.001
309	140.64665	-0.04249	0.020	-0.003
310	140.67450	-0.06334	0.004	-0.009
311	140.69769	-0.07813	0.036	-0.010
313	140.67178	0.01048	0.002	-0.003
315	140.51578	0.14608	-0.011	0.003
316	140.52528	-0.14402	-0.005	0.015
317	140.56005	0.20737	-0.005	-0.005
318	140.50877	0.19721	-0.007	-0.004
319	140.49464	0.22273	-0.003	0.002
320	140.52878	0.24690	0.035	0.014
323	140.37513	0.38317	-0.009	-0.003
324	140.42042	0.34641	-0.002	0.004

ROE No.	ℓ	b	$\mu_\ell \cos b$	μ_b
325	140.42999	0.35263	0.009	0.002
326	140.54681	0.37581	-0.013	0.013
327	140.54579	0.38528	-0.003	-0.004
328	140.53835	0.27619	-0.006	0.009
330	140.58853	0.25239	0.007	0.001
331	140.58025	0.19909	0.019	-0.038
332	140.66100	0.14699	0.029	-0.013
333	140.68914	0.11629	0.008	-0.001
334	140.67651	0.03535	0.000	0.010
335	140.72659	0.08622	0.001	-0.004
336	140.73322	0.08076	-0.005	0.004
337	140.79555	-0.03182	0.010	0.000
340	140.86290	-0.22305	0.018	-0.010
341	140.90406	-0.29240	0.002	-0.017
342	140.92487	-0.38041	-0.006	-0.016
343	140.94962	-0.37509	0.003	-0.003
344	140.96775	-0.34640	0.011	-0.015
345	140.98075	-0.34097	0.077	-0.011
346	140.97110	-0.43955	0.007	-0.022
347	141.02676	-0.42279	0.004	-0.006
349	141.01709	-0.25912	0.004	-0.006
350	140.91656	-0.14822	0.003	-0.006
352	140.90112	-0.14453	0.003	0.001
353	140.92547	-0.07876	0.003	0.007
354	140.86210	-0.02823	0.023	0.007
355	140.78494	0.04383	0.012	0.007
356	140.79532	0.03026	-0.001	-0.002
359	140.64014	0.29706	0.022	-0.002
361	140.67718	0.30520	0.001	-0.004
362	140.67900	0.31273	-0.006	0.003
363	140.62733	0.40641	0.011	-0.022
364	140.54486	0.43726	-0.025	0.002
365	140.54836	0.44291	0.012	0.011
367	140.54850	0.48232	-0.009	0.002
368	140.64411	0.46891	-0.004	-0.003
371	140.65110	0.53195	-0.028	0.004
373	140.68766	0.39920	-0.012	0.003
375	140.72989	0.41713	-0.001	-0.015

ROE No.	l	b	$\mu_l \cos b$	μ_b
376	140.81545	0.21414	0.001	-0.001
377	140.83873	0.14451	0.008	-0.007
379	140.89497	0.04089	0.022	-0.039
380	140.94588	-0.05975	0.012	0.003
381	141.00856	-0.13785	-0.006	0.001
383	141.08585	-0.28670	-0.001	-0.003
384	141.11763	-0.28611	-0.001	-0.004
385	141.15000	-0.29063	0.029	-0.004
386	141.12540	-0.32843	-0.021	-0.004
387	141.15766	-0.37853	0.010	0.002
388	140.71111	0.55425	-0.007	-0.000
390	140.73708	0.51359	-0.010	-0.001
391	140.76816	0.45067	-0.006	0.005
392	140.77533	0.40378	-0.016	-0.009
393	140.82679	0.28974	-0.015	0.001
394	140.83033	0.36416	-0.007	0.002
395	140.85551	0.36184	0.000	-0.004
396	140.84371	0.38525	0.001	0.004
397	140.85015	0.26271	0.005	-0.001
399	140.88580	0.27047	0.036	-0.054
401	140.88791	0.20670	0.003	-0.005
402	140.93995	0.17297	0.012	0.002
403	140.92569	0.11322	0.002	0.000
404	140.94006	0.10772	0.006	-0.001
405	140.94566	0.09848	0.004	-0.005
406	140.94372	0.14316	0.003	-0.001
409	141.08962	-0.03611	0.005	-0.005
410	141.05787	-0.09541	-0.003	-0.007
411	141.07607	-0.10701	-0.001	-0.000
412	141.08955	-0.11329	-0.018	-0.009
413	141.07950	-0.08924	0.007	-0.004
415	141.14114	-0.17515	0.007	-0.002
416	141.15894	-0.16234	0.001	0.004
417	141.13970	-0.23233	-0.007	-0.001
418	141.27930	-0.21267	0.025	-0.009
419	141.21452	-0.11916	0.020	-0.001

ROE No.	l	b	$\mu_l \cos b$	μ_b
420	141.13881	-0.08086	0.005	-0.006
421	141.14000	-0.06939	0.082	0.013
422	141.17029	-0.03821	-0.003	-0.000
424	141.16043	0.00522	0.048	-0.032
429	141.04385	0.20913	0.009	-0.001
430	140.97316	0.26548	-0.005	0.002
431	140.92689	0.29121	0.022	-0.014
432	140.97869	0.32399	0.001	0.002
433	140.87474	0.40427	0.002	0.006
434	140.90816	0.39051	-0.002	0.003
435	140.84871	0.44266	-0.006	0.003
436	140.86211	0.44449	-0.009	-0.011
437	140.83566	0.49044	-0.002	-0.015
438	140.85846	0.50776	0.009	0.014
440	140.78193	0.60417	0.001	-0.001
441	140.81035	0.58812	-0.015	0.001
442	140.83388	0.59410	-0.012	0.001
443	140.86775	0.66728	-0.019	-0.001
444	140.88822	0.56784	-0.008	0.005
445	140.91471	0.59240	-0.001	-0.003
448	140.90455	0.46759	0.040	-0.041
449	140.92033	0.46258	0.005	0.009
450	140.92777	0.51529	0.030	0.026
451	140.95911	0.37344	0.001	0.001
452	140.94131	0.42652	0.003	0.003
453	140.96485	0.45004	-0.005	-0.015
454	140.98143	0.42510	-0.015	0.002
455	141.01993	0.41728	-0.001	0.012
456	141.03886	0.33605	0.008	-0.004
457	141.03772	0.35147	0.005	0.005
458	141.04234	0.35154	-0.014	0.005
459	141.05439	0.34820	0.003	-0.008
460	141.02480	0.29181	-0.001	-0.000
461	141.10711	0.17567	0.004	0.004
463	141.11483	0.14126	0.019	0.002
464	141.10659	0.15430	0.006	0.001
465	141.17172	0.12570	-0.007	0.009
466	141.21066	0.08051	-0.014	0.010
467	141.19894	0.09965	0.011	0.005

ROE No.	l	b	$\mu_l \cos b$	μ_b
468	141.21283	-0.05227	0.005	-0.006
469	141.20068	0.00969	0.003	0.001
470	141.31742	-0.14772	0.009	0.002
471	141.32417	-0.14682	0.050	-0.023
472	141.39655	-0.16232	0.016	0.003
473	141.46281	-0.17986	0.019	-0.001
475	141.44054	-0.14325	0.042	0.002
476	141.35532	-0.11016	0.018	-0.001
477	141.36903	-0.10719	0.027	-0.011
478	141.33700	-0.05355	-0.019	-0.001
479	141.33158	-0.02877	0.017	-0.003
480	141.25512	0.03829	-0.013	0.007
481	141.27346	0.03632	-0.007	-0.002
482	141.25964	0.08112	0.015	-0.000
484	141.21130	0.13557	0.001	-0.008
485	141.20044	0.27014	0.012	-0.002
487	141.09236	0.32285	-0.014	0.011
488	141.07391	0.37711	-0.004	-0.001
489	141.07044	0.38517	0.006	-0.011
490	141.08558	0.38759	-0.016	-0.016
491	141.07604	0.40370	0.006	-0.005
492	141.11192	0.39737	-0.008	0.006
494	140.98958	0.52819	-0.004	-0.001
495	140.99485	0.54072	-0.003	-0.001
496	141.02948	0.50349	-0.025	0.028
497	140.91632	0.61768	-0.003	0.008
498	140.94670	0.58630	-0.026	0.005
499	140.94306	0.60682	-0.020	-0.001
500	140.96929	0.59078	-0.011	0.006
501	140.96912	0.62940	-0.006	0.018
502	140.97330	0.61473	-0.007	-0.001
503	140.99415	0.62148	-0.011	0.004
504	140.89175	0.65655	-0.016	-0.000
505	140.89793	0.65789	-0.002	-0.002
506	140.90490	0.67500	-0.003	0.004
507	140.94909	0.67089	-0.017	0.011
510	140.97905	0.70875	-0.021	0.002
511	140.99058	0.69766	-0.011	-0.008

ROE No.	l	b	$\mu_l \cos b$	μ_b
512	141.01950	0.60810	-0.011	0.006
514	141.03873	0.60736	-0.007	-0.001
517	141.05602	0.57247	0.000	-0.007
520	141.11113	0.53951	-0.005	-0.005
521	141.12893	0.42314	-0.012	0.003
522	141.17159	0.39598	-0.007	0.004
523	141.18150	0.46300	0.008	0.005
525	141.15406	0.37130	0.009	0.007
526	141.17186	0.37577	0.006	-0.015
527	141.18110	0.38904	0.025	-0.004
528	141.19278	0.36863	-0.018	-0.004
529	141.26191	0.28301	0.009	-0.001
530	141.28248	0.28001	0.001	0.004
531	141.29998	0.25580	0.007	0.002
534	141.33171	0.11566	0.022	0.002
535	141.32726	0.16739	0.011	0.006
536	141.38135	0.07964	0.111	-0.019
537	141.37596	0.09324	0.007	-0.007
538	141.41698	-0.07314	0.007	0.006
539	141.46905	-0.08379	0.027	0.002
542	141.38641	0.17999	0.012	-0.005
543	141.40750	0.15951	0.022	-0.001
545	141.32892	0.27488	0.010	0.002
546	141.34732	0.27923	0.009	0.009
549	141.37804	0.30347	0.007	0.009
550	141.27352	0.41016	-0.008	0.007
551	141.30055	0.42519	0.009	0.011
556	141.28403	0.46159	-0.016	0.025
558	141.20271	0.56052	0.014	0.004
559	141.20612	0.56145	-0.030	-0.001
560	141.19872	0.57721	-0.005	0.003
561	141.16151	0.59264	-0.003	0.005
563	141.13725	0.64921	0.003	-0.033
564	141.08627	0.65144	-0.010	0.007
565	141.11775	0.66662	-0.006	-0.001
568	141.15178	0.85060	-0.017	0.012
570	141.17724	0.76793	-0.005	-0.006
571	141.21877	0.61941	-0.005	0.001

ROE No.	ℓ	b	$\mu_\ell \cos b$	μ_b
573	141.20002	0.69140	0.054	-0.000
574	141.20851	0.69673	-0.004	-0.001
576	141.25057	0.68508	-0.013	-0.005
578	141.26632	0.51393	0.027	-0.002
579	141.28710	0.49375	-0.011	-0.021
581	141.31786	0.46674	-0.002	0.001
582	141.37427	0.47004	0.023	0.003
583	141.44718	0.30523	-0.003	0.016
584	141.44468	0.25994	0.017	0.000
586	141.36567	0.57040	-0.005	0.001
587	141.36403	0.58429	-0.011	0.010
588	141.34745	0.58956	-0.026	-0.004
589	141.29388	0.62596	0.003	0.003
590	141.36384	0.64517	-0.002	0.010
591	141.26485	0.70133	-0.005	0.014
592	141.28880	0.68839	-0.008	0.005
593	141.29572	0.71301	-0.009	0.003
594	141.21338	0.76813	0.010	-0.010
595	141.18131	0.85800	-0.024	0.031
596	140.29946	-0.93740	0.007	-0.011
597	140.32018	-0.96703	0.007	-0.008
598	140.31500	-0.94076	0.005	-0.004
599	140.36870	-0.97852	-0.001	-0.009
601	140.39090	-1.09739	0.004	-0.005
602	140.39725	-1.05941	0.009	-0.013
603	140.41513	-1.07682	0.008	-0.009
604	140.42519	-1.02802	0.045	-0.010
605	140.42947	-1.13700	0.003	-0.006
606	140.47946	-1.13314	-0.003	-0.024
607	140.51903	-1.26086	0.004	-0.014
609	140.53428	-1.34490	0.018	-0.017
616	140.60824	-1.30315	0.006	-0.008
620	140.60658	-1.28679	-0.000	-0.011
622	140.53989	-1.19443	0.006	-0.007
624	140.47724	-1.08842	0.010	-0.007
625	140.52085	-1.05962	0.006	-0.008
626	140.55744	-1.10510	0.008	-0.006
629	140.46049	-0.92247	-0.001	-0.015
631	140.40521	-0.88939	0.008	-0.009

ROE No.	l	b	$\mu_l \cos b$	μ_b
632	140.48019	-0.79445	0.096	-0.007
633	140.46463	-0.90124	0.007	-0.010
634	140.49667	-0.89444	0.016	-0.010
635	140.51342	-0.88230	0.012	-0.029
636	140.54031	-0.93724	-0.003	-0.013
637	140.52609	-1.00629	-0.003	-0.003
638	140.53855	-1.01562	0.003	-0.013
639	140.54982	-1.00638	0.002	-0.020
640	140.57333	-1.00956	0.014	-0.014
641	140.59728	-1.00442	0.007	-0.004
643	140.58894	-1.06423	0.018	-0.022
644	140.59069	-1.05731	0.002	-0.005
646	140.64395	-1.11172	-0.001	-0.013
647	140.67092	-1.13373	-0.001	-0.012
649	140.65721	-1.20832	0.003	-0.019
650	140.68903	-1.28596	0.006	-0.007
652	140.74406	-1.33377	0.007	-0.016
653	140.79354	-1.32625	0.002	-0.015
654	140.83661	-1.26110	0.016	-0.017
655	140.80491	-1.22707	-0.005	-0.022
658	140.71888	-1.10196	0.006	-0.004
659	140.71002	-1.06164	0.010	-0.005
660	140.73985	-1.10690	0.004	-0.012
661	140.64576	-1.00014	0.002	-0.012
662	140.66408	-0.98290	0.007	-0.008
663	140.61914	-0.92766	0.000	-0.008
664	140.64461	-0.94323	0.004	0.001
666	140.55863	-0.82945	0.007	-0.012
667	140.55285	-0.75247	0.011	-0.015
668	140.57948	-0.75864	-0.001	0.006
669	140.64017	-0.76563	0.011	-0.003
670	140.62734	-0.80888	-0.002	-0.001
671	140.66726	-0.86706	-0.001	0.000
672	140.68021	-0.82373	-0.002	-0.012
673	140.67951	-0.89167	0.002	-0.008
674	140.72449	-0.98699	0.010	-0.010
675	140.75000	-0.95324	0.010	-0.013
676	140.74736	-1.06004	0.009	-0.004
678	140.83351	-1.19398	0.007	-0.016

ROE No.	ℓ	b	$\mu_\ell \cos b$	μ_b
679	140.95989	-1.14309	0.008	-0.028
680	140.90998	-1.10466	0.005	-0.012
681	140.88767	-1.06799	0.022	-0.025
682	140.91450	-1.08703	0.007	-0.009
684	140.87200	-1.01388	0.003	-0.008
686	140.76247	-0.92354	-0.000	-0.003
688	140.71770	-0.79845	0.005	-0.008
689	140.74113	-0.74504	0.003	-0.010
690	140.63342	-0.70802	0.005	-0.011
691	140.68744	-0.75026	0.003	-0.006
692	140.72222	-0.73142	0.010	0.011
695	140.78972	-0.78243	0.013	-0.015
696	140.80680	-0.74638	0.003	-0.004
697	140.83876	-0.77276	0.032	-0.027
698	140.85995	-0.90614	0.012	-0.018
699	140.85109	-0.86914	0.008	-0.014
700	140.88967	-0.91693	0.025	-0.001
703	140.95560	-0.97191	0.011	-0.018
704	140.93352	-1.04888	0.009	-0.012
705	140.94859	-1.06455	0.015	-0.016
706	140.93842	-1.01376	0.020	-0.015
707	140.97639	-1.11645	0.005	-0.014
708	140.99438	-1.15245	0.017	-0.016
709	140.97826	-1.10244	0.024	-0.015
710	140.98701	-1.11243	-0.000	-0.020
711	141.02721	-1.13241	0.016	-0.018
712	141.03481	-1.11335	0.011	-0.012
713	141.08435	-1.02052	0.031	-0.015
714	140.99133	-0.97195	0.007	-0.013
715	141.04222	-1.02919	0.016	-0.033
717	141.07470	-1.00369	0.020	-0.013
719	140.96862	-0.94402	0.015	-0.013
720	141.01735	-0.94569	0.011	-0.017
722	140.95602	-0.85081	0.012	-0.014
723	140.89553	-0.81756	-0.001	-0.010
724	140.91811	-0.79656	0.009	-0.009
725	140.85808	-0.71498	0.022	-0.014
726	140.88518	-0.72999	0.006	-0.009

ROE No.	l	b	$\mu_l \cos b$	μ_b
727	140.86862	-0.67430	0.001	0.015
728	140.79083	-0.61622	0.004	-0.011
729	140.94632	-0.60259	0.002	-0.005
730	140.92123	-0.66610	0.007	-0.021
731	140.94391	-0.65682	-0.005	-0.006
733	140.99543	-0.78515	0.002	-0.002
734	141.06839	-0.80824	0.011	-0.014
735	141.06122	-0.85573	0.022	-0.007
736	141.06495	-0.84097	0.008	-0.017
737	141.05907	-0.83817	0.019	-0.023
739	141.07314	-0.93718	0.015	-0.009
740	141.15157	-0.94562	0.015	-0.017
741	141.15565	-0.94981	-0.006	-0.028
742	141.10310	-1.00881	0.018	-0.015
743	141.14048	-0.89854	0.011	-0.018
744	141.15470	-0.91401	0.030	-0.015
745	141.15415	-0.88391	0.007	-0.017
746	141.14364	-0.82687	0.012	-0.022
747	141.15399	-0.80436	0.009	-0.010
748	141.06394	-0.76240	0.057	-0.025
749	141.09244	-0.77683	0.050	-0.031
752	141.03186	-0.67805	0.004	-0.009
756	140.96688	-0.54966	-0.004	-0.008
758	141.06705	-0.55250	0.008	-0.000
759	141.13583	-0.63374	0.030	-0.010
760	141.13088	-0.63039	0.013	-0.002
761	141.21364	-0.75492	0.036	-0.013
763	141.22028	-0.85000	0.018	-0.018
764	141.24729	-0.83832	0.009	-0.021
765	141.27810	-0.75945	0.005	-0.014
766	141.24041	-0.71684	0.002	-0.037
767	141.24932	-0.65018	0.014	-0.007
770	141.15806	-0.56556	0.018	-0.004
771	141.19276	-0.53630	0.007	-0.007
772	141.20147	-0.54292	0.014	-0.012
774	141.10359	-0.50497	0.008	-0.002
775	141.11575	-0.50341	0.004	-0.005
776	141.13328	-0.45618	0.000	-0.009
777	141.17599	-0.46566	0.012	-0.012
778	141.20145	-0.52889	0.016	-0.008

TABLE 4.7
MAGNITUDES AND COLOURS

ROE No.	V	B - V	U - B
42	14.02	1.52	0.15
43	13.92	1.24	0.06
44	13.61	1.39	0.57
45	12.35	2.48	1.69
46	11.92	0.79	-0.08
47	14.23	1.52	-0.43
48	12.44	0.93	-0.21
49	14.10	1.40	0.00
50	8.01	-0.80	2.01
51	13.46	2.00	0.72
52	8.15	0.64	1.51
53	11.22	0.90	-0.19
55	12.54	1.96	1.65
56	14.08	1.17	0.51
57	14.67	1.20	0.36
58	13.92	1.37	0.28
59	12.44	0.77	0.15
60	10.00	1.16	-0.47
61	13.79	1.25	-0.02
62	14.34	1.16	0.17
64	14.13	1.08	0.20
67	14.05	1.28	0.24
88	13.48	0.89	0.05
89	13.41	1.30	0.42
90	13.94	1.18	0.20
91	14.02	1.02	0.60
92	13.23	1.77	1.25
93	14.10	1.44	0.39
94	13.74	0.92	0.75
95	13.53	1.09	0.19
96	14.13	1.03	0.04
97	14.05	1.20	0.07
98	10.74	0.76	-0.32
100	10.16	1.63	1.45
101	13.11	0.97	0.34
102	13.28	0.84	0.52

ROE No.	V	B - V	U - B
104	9.53	0.59	0.20
108	14.34	1.32	0.10
109	14.26	1.53	-0.10
110	14.45	1.55	0.05
111	13.11	1.14	0.17
114	14.05	1.11	0.37
115	13.51	0.95	0.44
116	13.48	1.10	-0.01
117	12.33	1.04	2.13
118	13.64	1.02	0.47
119	11.16	0.84	0.05
120	13.56	0.85	0.43
121	13.94	0.89	0.46
123	13.81	1.02	0.12
125	11.38	1.08	0.08
127	12.56	1.15	-0.47
128	13.92	1.33	0.39
129	14.10	1.36	0.40
130	14.45	1.51	1.00
132	12.65	0.76	0.23
135	13.21	0.83	0.33
136	12.94	2.06	1.08
137	11.43	0.90	-0.11
138	12.17	0.83	0.03
139	12.47	0.99	0.68
141	13.18	1.15	-0.11
148	11.79	2.04	2.13
150	13.94	0.97	0.55
151	13.23	1.35	0.71
152	9.06	0.27	0.57
153	14.42	1.45	-0.01
154	14.37	1.38	0.26
155	13.53	0.88	0.27
156	14.05	0.99	0.35
157	12.56	0.94	0.53
158	14.42	1.70	0.13

ROE No.	V	B - V	U - B
159	13.61	0.76	0.02
160	14.02	1.48	0.26
161	13.31	1.90	0.94
163	12.24	1.05	0.27
164	13.48	3.14	-0.15
165	14.00	1.21	0.36
166	13.81	1.19	0.57
167	13.33	1.17	0.72
168	12.61	1.43	0.77
169	13.74	1.26	0.41
170	14.37	1.84	-0.23
171	14.21	1.54	0.23
172	13.84	1.78	0.43
173	13.41	1.05	0.67
175	14.64	1.48	-0.16
176	12.08	1.38	0.76
177	14.37	1.50	0.09
178	13.94	0.97	0.06
179	10.53	0.88	0.26
180	14.58	1.63	-0.03
181	13.33	1.96	0.79
182	13.23	0.77	0.42
183	13.43	1.07	0.05
184	13.11	1.14	0.34
188	13.74	1.84	0.67
189	14.21	1.62	0.10
190	11.41	1.75	0.93
191	14.15	1.51	0.30
192	13.43	0.94	0.05
193	14.10	1.19	0.03
194	14.26	1.32	0.28
195	11.04	2.75	2.41
196	14.21	1.41	0.46
197	14.45	1.55	-0.21
213	11.32	2.22	2.22
214	14.34	1.62	0.09
215	13.13	1.16	0.73
217	14.05	1.03	0.47

ROE No.	V	B - V	U - B
218	13.94	1.06	0.60
220	14.42	1.54	0.07
221	14.02	1.14	0.27
222	13.94	1.39	0.34
223	14.02	0.98	0.57
225	13.94	1.18	0.48
226	12.17	0.74	0.10
227	14.10	1.73	0.05
228	14.67	1.66	-0.15
229	14.15	1.31	0.21
230	11.73	0.98	-0.28
232	12.28	0.93	-0.11
233	13.71	1.16	0.49
234	12.19	0.93	0.12
235	14.13	1.53	-0.11
236	12.44	0.97	0.05
237	14.15	1.35	0.10
238	14.37	1.75	-0.16
240	13.28	0.72	0.29
241	13.92	1.41	0.17
242	12.92	0.79	0.45
244	14.47	1.53	0.05
245	12.54	0.96	0.06
246	10.21	0.83	0.13
247	11.64	1.19	0.25
248	11.97	1.69	0.95
250	13.64	2.40	0.54
251	12.84	0.95	0.35
252	13.84	1.74	0.52
253	13.51	1.07	0.53
254	11.32	1.84	0.98
255	11.81	1.90	1.77
256	14.61	1.60	-0.25
257	12.80	0.91	-0.21
258	13.21	0.83	0.05
259	14.18	1.53	0.20
260	12.51	1.36	0.63
261	14.21	1.37	0.26

ROE No.	V	B - V	U - B
263	12.75	0.91	0.06
264	13.53	2.05	0.89
265	9.46	-0.09	0.59
266	13.21	0.75	0.37
268	14.39	1.48	0.09
269	14.45	1.13	0.28
270	12.35	1.40	1.31
271	12.80	0.91	0.68
272	11.90	1.31	1.34
273	14.13	0.99	0.48
274	13.81	1.15	0.43
275	13.71	2.16	0.68
278	12.01	1.70	1.61
282	14.02	1.73	0.50
284	14.10	1.27	0.13
285	13.64	2.40	0.64
286	13.09	1.03	0.54
287	14.18	1.48	0.08
288	13.43	1.78	0.77
290	13.81	1.27	0.28
291	11.24	2.09	1.89
292	13.11	1.01	0.56
293	13.46	1.33	1.00
294	14.02	1.31	0.53
295	12.01	1.53	1.32
296	13.51	0.86	0.20
297	13.23	0.98	0.34
298	14.89	0.36	1.50
300	14.37	1.46	0.22
301	12.56	1.10	-0.02
304	14.15	1.81	0.32
305	8.47	0.36	1.55
307	13.53	1.18	0.04
308	10.27	1.52	1.14
309	13.21	1.08	0.30
310	7.57	1.22	4.20
311	13.23	1.14	0.22

ROE No.	V	B - V	U - B
313	13.74	1.34	0.61
315	14.45	1.59	-0.03
316	13.89	0.82	0.68
317	12.56	0.81	0.60
318	13.31	0.77	0.38
319	13.66	1.13	0.69
320	13.18	0.86	0.20
323	12.82	0.80	0.54
324	13.11	0.76	0.77
325	13.92	1.24	-0.14
326	13.94	1.60	0.51
327	13.11	1.26	1.42
328	12.47	2.28	2.00
330	13.56	0.90	0.29
331	8.49	-0.24	1.27
332	12.19	0.68	0.06
333	13.69	0.93	2.13
334	13.94	1.52	0.26
335	10.20	0.59	-0.22
336	13.61	1.05	0.66
337	13.71	1.45	0.41
340	8.85	1.56	2.32
341	14.34	1.24	0.06
342	14.05	1.24	0.28
343	13.92	1.37	0.31
344	14.02	1.14	0.41
345	13.79	1.21	0.96
346	12.01	1.11	0.95
347	13.81	0.73	0.41
349	12.82	1.72	1.22
350	13.43	0.98	0.58
352	14.08	1.58	0.13
353	13.87	0.79	0.66
354	12.01	1.40	0.92
355	12.24	1.72	1.52
356	12.70	0.96	0.16
359	12.82	1.39	1.01

ROE No	V	B - V	U - B
361	14.50	1.37	0.01
362	14.02	1.44	0.04
363	11.68	1.03	0.87
364	14.29	1.46	0.33
365	14.23	1.23	0.40
367	13.01	0.86	0.61
368	13.84	0.82	1.10
371	13.41	0.59	0.64
373	14.26	1.36	0.22
375	12.35	0.56	0.49
376	13.76	0.86	0.24
377	10.05	0.78	0.22
379	12.94	0.89	0.48
380	14.02	1.44	0.40
381	13.51	0.90	0.25
383	13.74	1.55	0.89
384	13.81	1.77	0.40
385	13.31	0.81	0.65
386	13.84	0.35	1.10
387	12.94	2.22	1.07
388	10.29	0.08	-0.08
390	13.04	1.46	0.98
391	14.37	1.09	0.52
392	12.10	0.76	-0.00
393	14.26	1.49	-0.20
394	12.65	0.89	0.12
395	13.18	0.69	0.74
396	14.15	1.60	0.35
397	13.23	0.73	0.37
399	11.92	0.58	-0.01
401	14.31	1.40	0.34
402	13.53	1.09	0.79
403	12.63	0.66	0.25
404	13.76	1.32	0.52
405	12.82	0.80	-0.00
406	13.53	0.97	0.82

ROE No.	V	B - V	U - B
409	12.94	0.93	0.44
410	14.26	1.40	0.03
411	14.02	1.19	0.46
412	13.94	0.93	0.17
413	12.75	1.54	1.45
415	12.42	0.95	0.52
416	11.75	1.12	0.65
417	13.48	2.06	0.81
418	12.92	0.62	0.35
419	11.83	0.79	0.09
420	13.71	0.91	0.49
421	13.64	1.07	0.84
422	12.47	0.53	-0.07
424	11.86	0.60	0.25
429	13.51	1.03	0.59
430	14.23	1.35	-0.01
431	13.26	1.03	1.03
432	13.97	1.03	0.48
433	14.10	0.73	1.80
434	13.09	0.78	0.63
435	14.23	1.39	-0.05
436	13.04	0.67	0.20
437	12.92	0.83	0.73
438	11.34	1.41	1.49
440	14.15	1.31	0.18
441	14.34	1.37	0.37
442	14.00	0.54	0.64
443	11.83	1.00	1.03
444	13.71	0.83	0.66
445	12.84	0.32	0.38
448	11.92	0.54	0.03
449	13.87	1.09	1.00
450	13.01	0.82	0.65
451	13.66	1.13	0.60
452	13.61	1.05	0.36
453	11.38	1.49	1.27
454	14.15	1.14	0.50

ROE No.	V	B - V	U - B
455	12.61	0.68	0.19
456	14.23	1.52	0.01
457	14.02	1.44	0.28
458	12.72	0.86	0.22
459	12.65	0.68	0.39
460	12.82	0.76	0.56
461	12.82	0.72	0.20
463	12.47	0.57	0.18
464	13.64	0.98	0.58
465	14.15	1.06	0.18
466	14.26	1.15	0.19
467	14.02	0.94	0.61
468	12.17	0.83	0.50
469	11.24	1.34	1.47
470	11.92	0.58	0.21
471	12.70	0.84	0.32
472	13.74	0.84	0.67
473	13.61	0.30	0.48
475	10.47	1.57	1.78
476	12.51	0.53	0.24
477	13.71	0.70	0.52
478	13.71	1.87	0.65
479	14.13	1.03	0.51
480	10.36	1.05	0.79
481	13.74	0.63	0.49
482	12.06	1.27	1.00
484	12.37	0.59	0.28
485	14.05	1.70	0.23
487	14.00	1.21	0.29
488	11.83	1.46	1.28
489	12.08	0.88	0.28
490	12.89	0.48	0.41
491	13.53	0.97	0.25
492	13.36	0.97	0.60
494	14.21	1.33	0.22
495	14.23	1.06	0.55

ROE No.	V	B - V	U - B
496	13.51	0.95	0.35
497	13.84	0.78	0.40
498	14.45	1.55	-0.07
499	14.42	1.29	0.15
500	14.15	1.26	0.64
501	13.94	1.60	0.06
502	12.68	0.82	-0.02
503	13.69	0.93	0.24
504	13.92	1.66	0.57
505	14.15	1.31	0.14
506	13.84	0.87	0.44
507	14.34	1.32	0.47
510	13.74	0.88	0.40
511	13.71	0.95	0.49
512	13.81	1.06	0.33
514	13.41	1.05	0.47
517	13.16	1.92	1.27
520	14.67	1.37	0.61
521	13.89	1.15	0.30
522	14.15	1.01	0.51
523	13.21	0.66	0.46
525	13.94	0.89	0.58
526	13.09	0.70	0.41
527	13.43	0.78	0.54
528	11.79	1.25	1.35
529	13.33	0.79	0.67
530	14.10	1.15	0.49
531	12.82	0.55	0.70
534	13.61	0.85	0.29
535	10.02	0.14	-0.06
536	13.33	0.46	0.26
537	12.44	0.60	0.56
538	13.61	1.22	1.05
539	13.21	0.58	0.65
542	13.48	0.77	0.50
543	13.01	1.28	1.38
545	11.66	1.46	1.65
546	12.92	0.58	0.41
549	11.83	0.38	0.22

ROE No.	V	B - V	U - B
550	14.23	1.31	0.32
551	14.45	0.88	0.65
556	12.24	2.22	2.12
558	13.21	0.20	0.81
559	13.09	0.07	0.79
560	9.37	-0.25	0.35
561	13.92	0.99	0.50
563	12.44	0.43	0.06
564	13.41	0.59	0.35
565	9.26	1.61	2.55
568	13.94	0.10	0.35
570	10.02	-0.06	0.51
571	12.75	1.21	0.85
573	10.72	0.57	0.57
574	13.11	1.05	1.63
576	14.05	0.86	0.36
578	14.23	1.10	0.58
579	12.33	0.83	0.14
581	13.92	0.79	0.65
582	11.14	0.61	0.13
583	14.42	1.20	0.46
584	13.79	0.96	0.57
586	12.63	0.24	0.23
587	14.02	1.02	0.46
588	14.45	1.05	0.17
589	13.64	0.98	0.40
590	13.61	0.80	0.63
591	14.05	0.95	0.41
592	13.79	0.96	0.52
593	13.64	0.61	0.34
594	8.64	1.23	2.71
595	13.94	0.93	0.45
596	13.74	1.42	-0.03
597	13.33	0.88	0.10
598	13.51	0.82	0.33

ROE No.	V	B - V	U - B
599	13.81	1.19	0.18
601	14.15	1.14	0.10
602	13.04	0.96	0.22
603	13.51	1.11	0.40
604	14.26	1.65	-0.34
605	13.84	1.16	0.08
606	13.33	0.88	0.21
607	12.77	1.73	0.98
609	13.43	1.15	0.01
616	14.02	1.14	-0.19
620	14.10	1.19	0.28
622	14.34	1.45	-0.22
624	13.48	2.06	0.88
625	13.36	0.85	0.25
626	13.71	1.25	0.19
629	12.92	1.12	0.01
631	14.23	1.18	0.26
632	10.84	1.20	0.43
633	12.75	1.91	1.06
634	13.43	1.03	0.47
635	14.53	1.30	0.25
636	12.63	1.74	1.49
637	14.23	1.52	0.04
638	14.26	1.36	0.29
639	12.56	0.90	-0.10
640	14.42	1.49	-0.15
641	14.18	1.11	0.10
643	14.08	1.21	0.28
644	13.56	0.73	0.43
646	13.71	1.20	0.66
647	12.37	1.00	0.03
649	12.94	0.85	0.10
650	13.23	1.77	1.18
652	13.13	0.99	0.87
653	12.72	1.82	1.39
654	13.84	1.62	0.40

ROE No.	V	B - V	U - B
655	14.34	1.49	0.03
658	14.05	1.41	0.14
659	13.43	2.15	0.97
660	14.02	1.14	0.32
661	13.33	1.17	0.49
662	14.13	1.24	-0.15
663	14.58	1.17	-0.21
664	14.58	1.88	-0.31
666	14.23	1.77	-0.14
667	12.63	0.91	0.02
668	14.53	1.47	-0.12
669	14.29	1.33	0.14
670	11.73	0.89	-0.20
671	12.89	1.15	0.35
672	13.23	1.06	0.28
673	13.23	0.68	0.23
674	12.84	1.74	1.28
675	12.44	0.85	0.29
676	14.13	1.41	0.20
678	13.53	0.84	0.76
679	14.47	1.57	-0.16
680	12.35	2.44	1.94
681	12.92	0.79	0.32
682	14.13	1.66	0.26
684	13.79	2.29	0.72
686	12.51	1.15	0.50
688	12.28	0.88	-0.27
689	11.22	0.53	-0.08
690	14.39	1.27	0.10
691	14.05	1.70	0.01
692	9.48	0.31	0.15
695	12.72	0.90	-0.14
696	14.26	1.49	-0.01
697	13.64	1.02	0.29
698	13.87	1.92	0.61

ROE No.	V	B - V	U - B
699	13.46	1.41	0.31
700	13.33	0.88	0.03
703	14.13	1.16	0.28
704	13.36	0.60	0.54
705	13.66	1.13	0.53
706	13.33	0.79	0.47
707	13.76	0.74	0.34
708	14.15	1.85	-0.33
709	13.94	1.06	0.20
710	13.92	1.20	0.38
711	13.71	1.66	-0.19
712	14.13	1.83	-0.57
713	9.86	0.51	0.24
714	12.92	1.74	1.01
715	14.34	1.41	-0.06
717	13.28	1.01	0.46
719	14.15	1.51	-0.02
720	12.72	0.90	0.45
722	12.15	1.56	1.06
723	13.71	1.04	0.47
724	14.10	1.19	0.40
725	13.84	0.91	0.20
726	13.28	0.76	0.27
727	13.92	1.83	0.53
728	14.13	1.24	0.02
729	13.71	0.70	0.49
730	12.51	0.78	-0.05
731	10.68	0.78	-0.03
733	15.00	0.91	0.94
734	12.37	0.75	-0.02
735	13.64	0.90	0.32
736	13.64	0.98	0.33
737	14.64	1.32	0.72
739	13.84	0.99	-0.02

ROE No.	V	B - V	U - B
740	13.11	0.93	-0.15
741	14.34	1.28	0.02
742	13.51	1.03	0.32
743	14.02	0.98	0.32
744	12.54	0.58	-0.09
745	14.67	1.45	-0.07
746	14.08	1.00	0.26
747	14.13	1.33	0.14
748	10.92	0.79	-0.28
749	13.43	0.94	0.49
752	13.71	1.00	0.42
756	14.34	1.12	0.02
758	11.99	0.63	0.11
759	13.53	1.18	0.61
760	14.31	1.06	0.23
761	13.74	1.34	0.90
763	12.17	0.66	0.03
764	11.94	1.39	1.26
765	14.29	1.29	0.02
766	12.99	0.67	0.06
767	12.19	1.02	0.68
770	12.96	0.70	0.50
771	14.45	1.01	0.42
772	13.71	0.70	0.45
774	13.79	0.96	0.73
775	11.49	0.84	0.30
776	12.84	1.24	1.21
777	14.21	1.04	0.23
778	13.92	0.49	0.77
779	13.92	0.91	0.49
780	10.38	0.20	-0.11
781	14.05	1.24	0.28
782	12.37	0.79	0.10
783	13.11	0.72	0.22
786	14.00	0.91	0.45
787	13.92	0.79	0.33
788	13.94	0.85	0.50

ROE No.	V	B - V	U - B
789	14.45	1.17	0.17
790	12.58	0.67	0.49
791	13.79	0.71	0.61
792	12.56	1.85	1.62
793	11.55	0.70	0.04
795	13.56	0.73	0.55

4.7 Analysis of Results

The proper motions and magnitudes of the stars in Tables 4.6 and 4.7 were analysed in groups according to magnitude and colour to see if any reddened early type members of either the Perseus or the so-called α - arm, defined by the HI observations of Verschuur (1973), were present.

Using the magnitudes for each of the stars with measured proper motion, calculated from the equations given in section 4.3, two colour plots of U - B against B - V were drawn for one magnitude intervals from V = 10 to 13 and then half magnitude intervals from V = 13 to 14.5. For the analysis described below the range V = 10 to 11 was discarded because it contained too few stars, and those fainter than V = 13.5 were discarded as the computed magnitudes fainter than V = 13.7 were extrapolated from the quadratic least squares fit and as such considered unreliable. The plots used in the analysis are shown in Figures 4.8, 4.9 and 4.10.

The locus of the main sequence in the two colour plot was drawn on a transparent overlay to the same scale and zero point as the plots of the observed stars. A curve with exactly the same shape as that of the main sequence but displaced by twice the measured photometric standard deviation in each of U - B and B - V was also

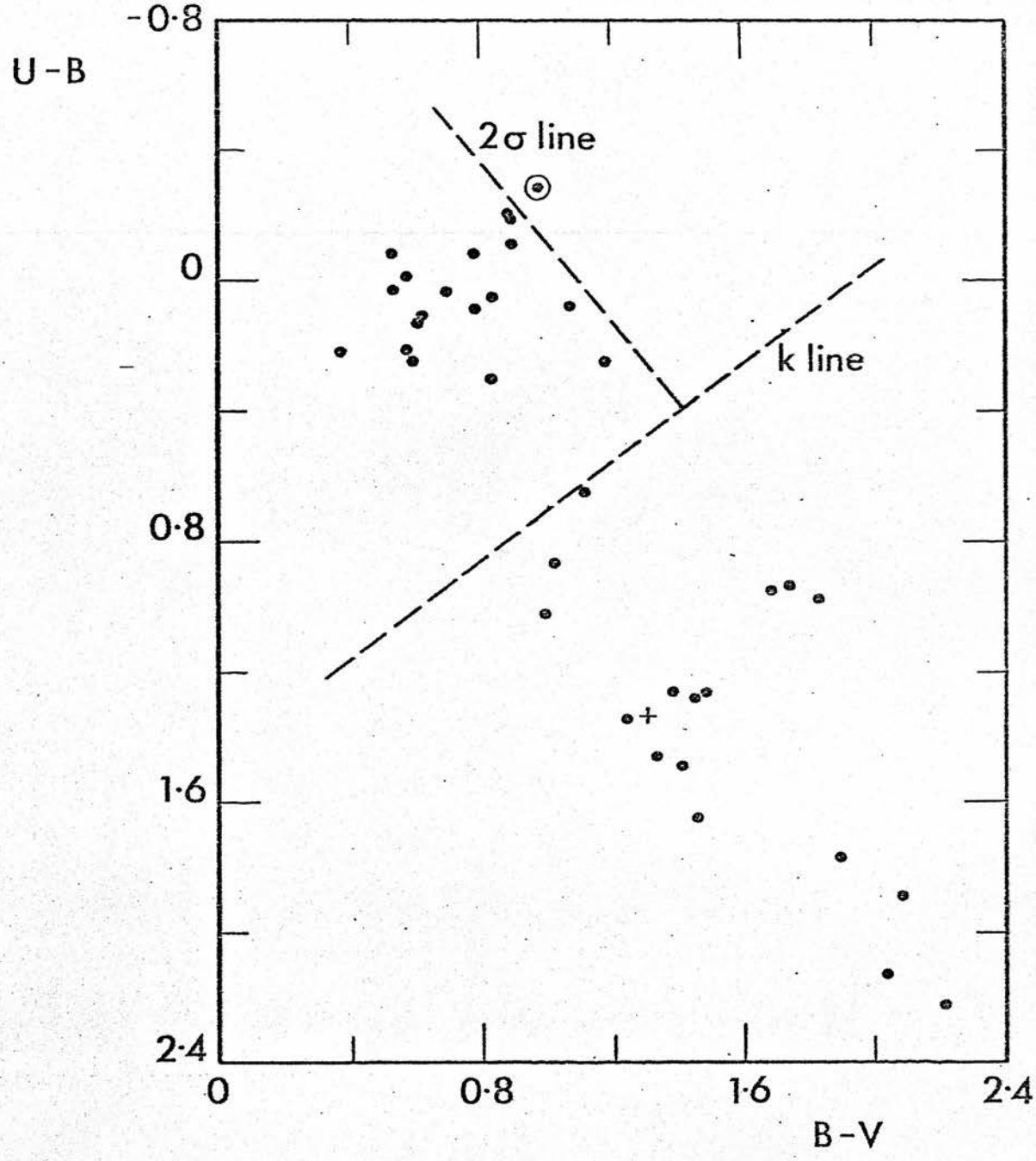

Fig. 4.8 Two colour diagram for proper motion stars with $11 < V \leq 12$.

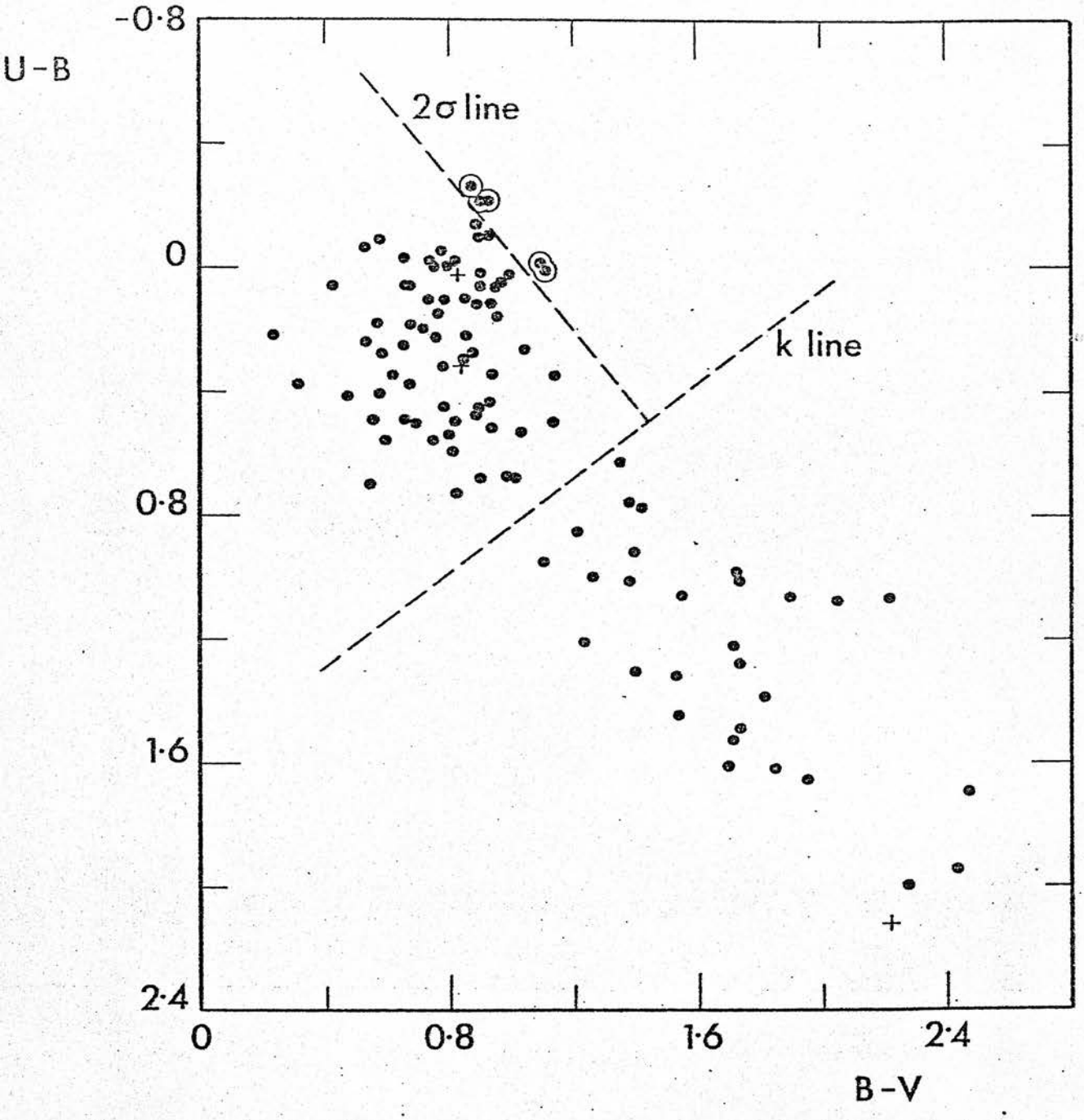

Fig. 4.9 Two colour diagram for proper motion stars with $12 < V \leq 13$.

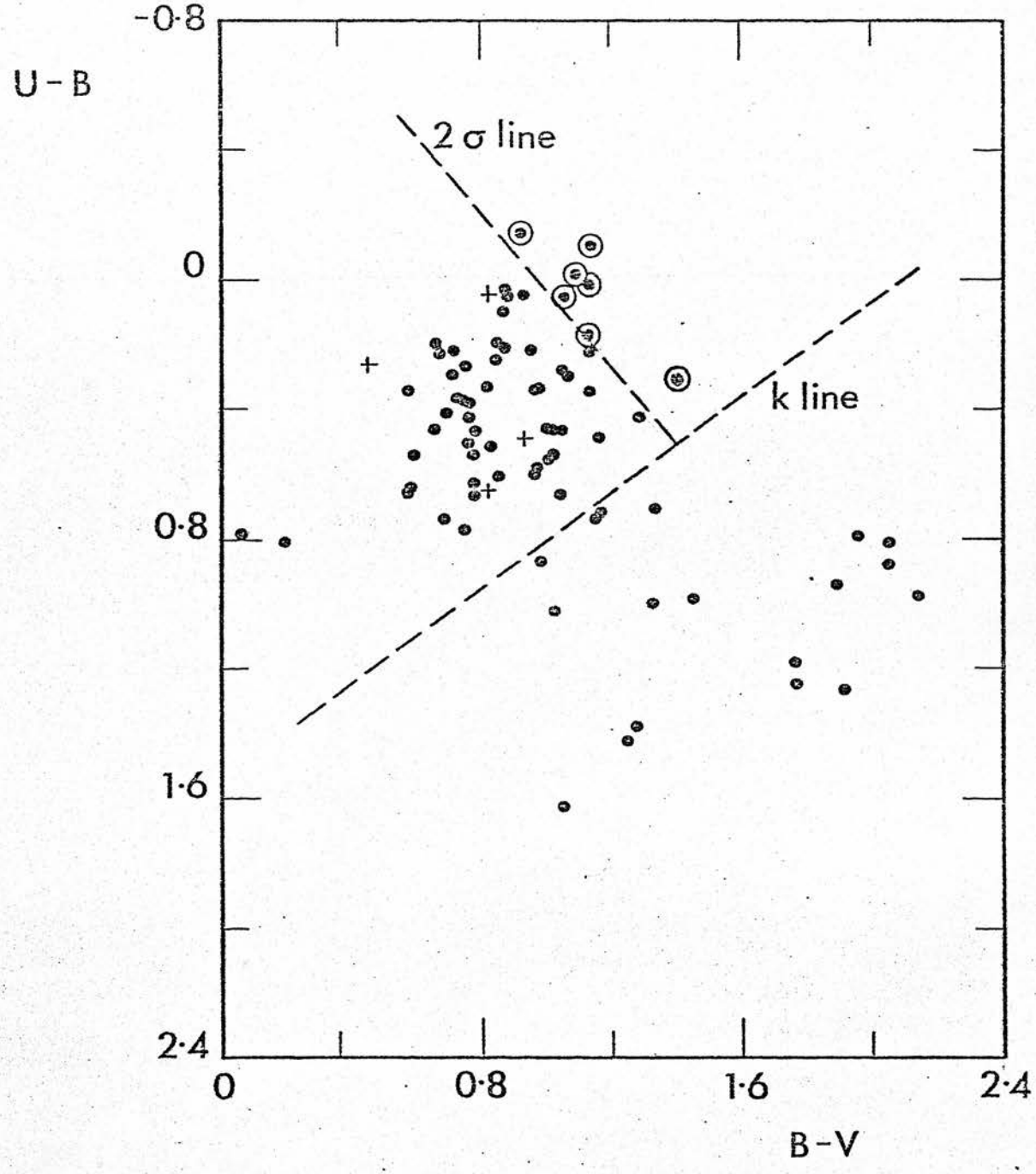

Fig. 4.10 Two colour diagram for proper motion stars with $13 < V \leq 13.5$.

drawn on the overlay (cf. Figures 4.11 and 4.12 which has plotted luminosity class I and III sequences). For each of the magnitude intervals $11 < V \leq 12$, $12 < V \leq 13$ and $13 < V \leq 13.5$ the overlay was placed on the observed plots and stars lying outside the 2σ curve circled as shown in Figures 4.8 to 14.10. The positions of K0 and K5 stars on the mean and displaced theoretical sequences were noted on each of the two colour plots and an arbitrary line drawn by eye between these limits where there seemed to be a natural break in the stellar distribution. Thus each plot was divided into three areas; that below the K-type line, region 3, that above this line and to the left (i.e. blue) of the 2σ line, region 2, and that above the K-type line and to the right (red) of the 2σ line, region 1. For stars in each of these regions in each magnitude range, mean proper motions and their standard deviations were computed.

Stars whose total proper motion exceeded their region's mean proper motion by more than 2.56σ were removed and the region mean proper motion and standard deviations recomputed. For all regions, except region 2 in the magnitude range 13 - 13.5, which had 4 stars removed, the number of stars removed in this way was 2 or less. The results of these computations are set out in Table 4.8.

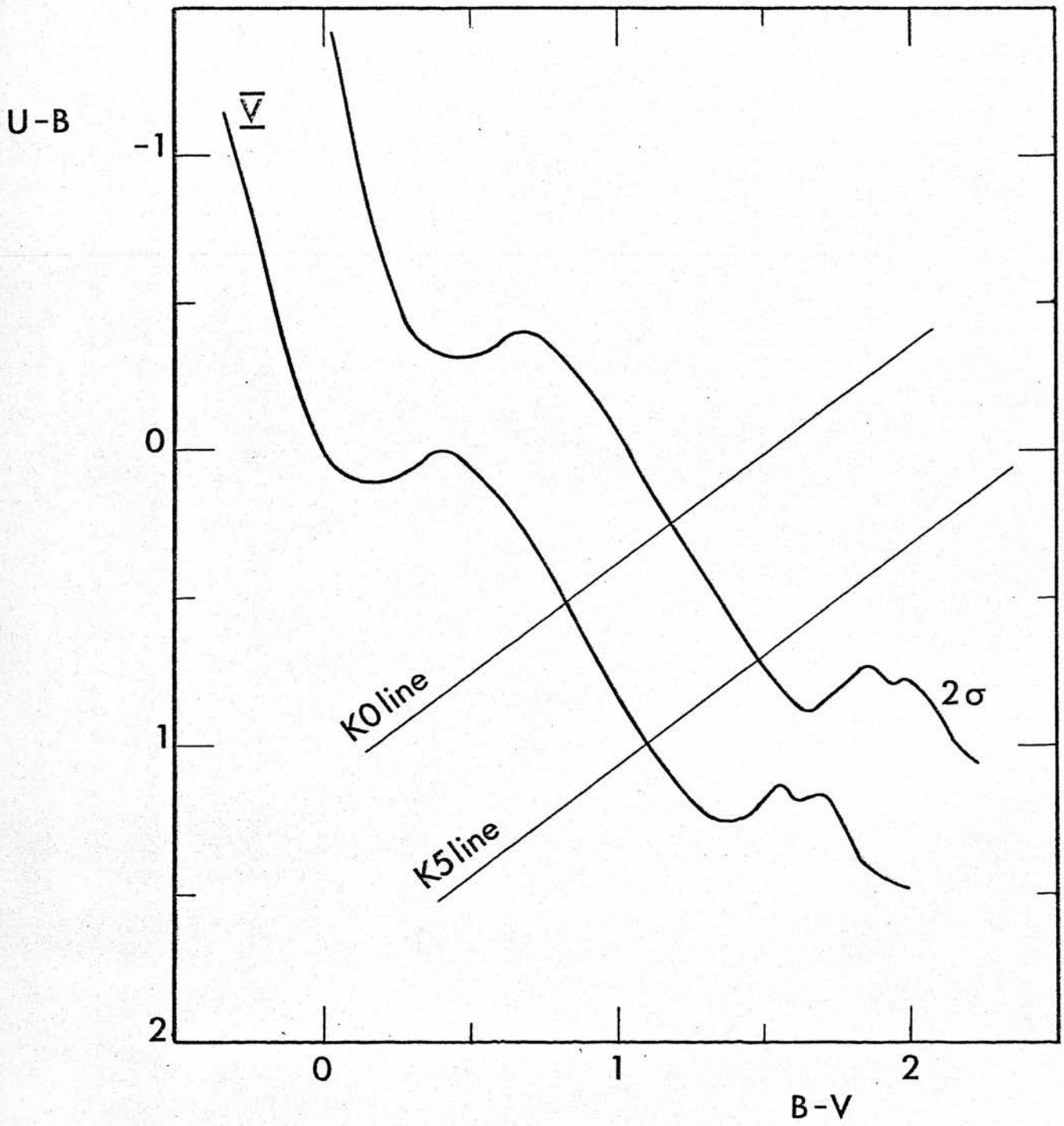

Fig. 4.11 Locus of luminosity class V in the two colour plot showing the positions of the 2σ and K lines.

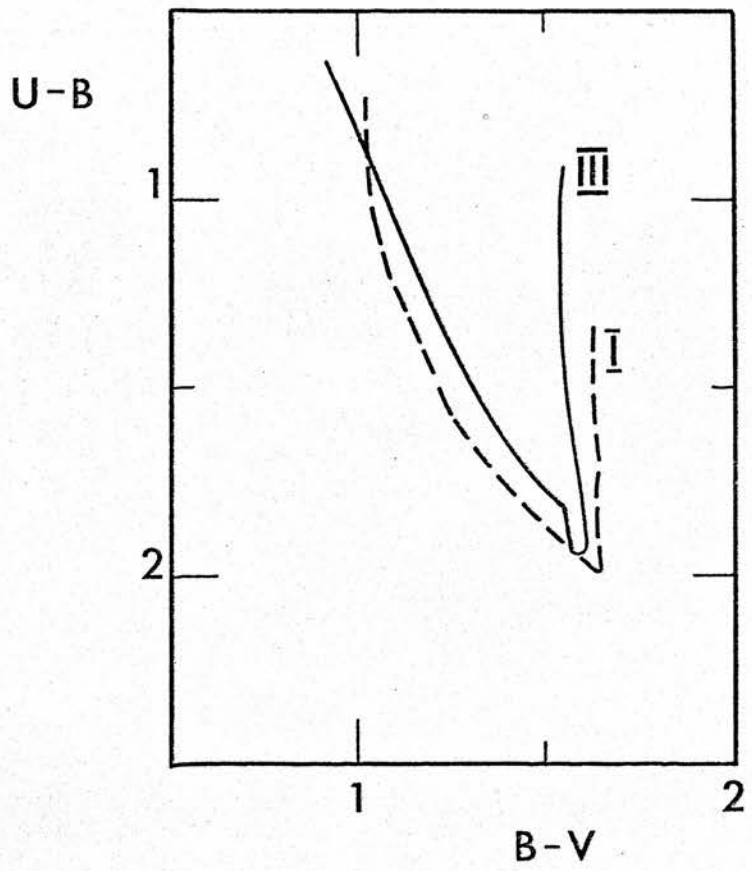

Fig. 4.12 Loci of luminosity classes III and I in the two colour plot.

TABLE 4.8

Group	Magnitude Range	Region	$\overline{\mu_l \cos b}$	$\bar{\mu}_b$	No. of Stars
1	11 - 12	2	0.018 ± 0.015	-0.012 ± 0.018	18
2		3	0.001 ± 0.010	-0.005 ± 0.009	17
3	12 - 13	1	0.010 ± 0.012	-0.010 ± 0.012	5
4		2	0.005 ± 0.011	-0.009 ± 0.010	67
5		3	0.006 ± 0.008	-0.005 ± 0.008	30
6	13 - 13.5	1	0.003 ± 0.012	-0.013 ± 0.004	7
7		2	0.007 ± 0.014	-0.005 ± 0.008	52
8		3	0.002 ± 0.009	-0.005 ± 0.005	20
9*		2	0.044 ± 0.045	-0.001 ± 0.025	4

* stars of large proper motion rejected from Group 7.

For each of the Groups 1 - 9 secular parallaxes were computed. Following the notation of van Rhijn and Bok (1931) mean secular parallax ($\bar{h}/\rho$) is defined by

$$\left(\frac{\bar{h}}{\rho}\right) = \frac{\overline{v \sin \lambda}}{\overline{\sin^2 \lambda}} \qquad 4.24$$

where, in galactic coordinates,

$$v = \mu_l \cos b \sin \chi + \mu_b \cos \chi \qquad 4.25$$

V is the component of the proper motion in the direction of the antapex of the solar motion.

λ is the angular distance of the star from the antapex.

and χ is the position angle of the direction towards the antapex.

λ and χ are related to the position of the solar motion apex (l_A, b_A) and the coordinates (l, b) of a group member star by

$$\sin\lambda \sin\chi = \sin(l-l_A)\cos b_A$$

$$\sin\lambda \cos\chi = \cos(l-l_A)\cos b_A - \sin b_A \cos b \qquad 4.26$$

Substituting from equations 4.25 and 4.26 into 4.24 gives:-

$$\left(\frac{\bar{h}}{\rho}\right) = \frac{\mu_l \cos b \sin(l-l_A)\cos b_A + \mu_b\left(\cos(l-l_A)\cos b_A \sin b - \sin b_A \cos b\right.}{\sqrt{\left(1-\left(\cos(l-l_A)\sin b_A \cos b + \sin b_A \sin b\right)^2\right)}} \qquad 4.27$$

In equation 4.27 $\overline{\mu_\ell \cos b}$, $\bar{\mu}_b$, and (ℓ_A, b_A), taken as Delhaye's (1965) values (56°, $+23^\circ$), are already known and, since all stars in the group occupy a small region on the celestial sphere, mean values for ℓ and b were used. The mean parallax $\bar{\rho}$ was derived from the mean secular parallax by using the following relation:

$$\bar{\rho} = \frac{4.74}{V_o} \left(\frac{\bar{h}}{\rho} \right) \qquad 4.28$$

where 4.74 is a multiplying conversion factor from A.U./yr to km/sec and V_o = 19.5 km/sec for the standard solar motion. On the basis of the standard deviations of single proper motion observations this technique will not produce meaningful results beyond $\bar{\rho}$ = 0."002 (= m - M = $8^m.5$), thus any group with m - M > 8.5 can only be assigned a lower bounded distance of > 500pc. The unreddened distance moduli (m - M) of the groups were calculated using

$$m - M = -5 \left(\log \bar{\rho} + 1 \right) \qquad 4.29$$

In Table 4.9 is listed the calculated values of mean secular parallax in arc seconds per annum, the mean parallax in arc seconds, the unreddened and reddened distance moduli, the total interstellar absorption correction A_V in magnitudes (from Neckel 1967) and the mean absolute magnitude of the group.

TABLE 4.9

Group	$(\bar{h}/\rho)$	$\bar{\rho}$	m - M	A_v	Corrected m - M	$\bar{M}$ Group
1	0.021	0.0051	6.5	0	6.5	+5.0
2	0.003	0.0007	>8.5	>1.4	>10	<+1.5
3	0.013	0.0032	7.5	0	7.5	+5.0
4	0.009	0.0021	8.4	0	8.4	+4.1
5	0.007	0.0017	>8.5	>1.4	>10	<+2.5
6	0.008	0.0019	>8.5	>1.4	>10	<+2.5
7	0.008	0.0019	>8.5	>1.4	>10	<+3.2
8	0.004	0.0010	>8.5	>1.4	>10	<+3.2
9	0.040	0.0097	5.1	0	5.1	+9.1

The following interpretation of Table 4.9, in conjunction with the plotted two colour diagrams and lists of spectral type against absolute magnitude and colour given by Allen (1963), may be made: Groups 1 and 3 are predominantly main sequence stars with spectral types between G0 and G5 situated in the local spiral arm at about 200 to 300 pc from the sun, the significant mean proper motion of Group 3 discounts any possibility of it being a distant group of highly reddened OB stars. Group 4 is most probably a mixture of main sequence, giant and sub-giants stars of late G spectral type, the mean absolute magnitude of the constituent stars being $1^m.7$ too bright to be late G dwarfs, $2^m.6$ too faint to be late G giants and $0^m.8$ too faint to be late G subgiants.

To obtain reasonable agreement between $\bar{M}$, $\overline{m - M}$, V and B - V for Group 9 a mean spectral type between KO and K5 and luminosity class VI is needed, this group is however, too small for any confidence to be placed in its statistical parallax.

For stars with $m - M \geq 10$, the mean absolute magnitude of the group was derived by using a combination of the measured colour - colour and theoretical colour - magnitude relations. This absolute magnitude yielded a spectral type via the Hertzsprung - Russell diagram and, in conjunction with the known mean apparent magnitude of the group, the distance modulus.

Groups 2 and 5 are mainly giant stars between MO and M5 spectral type, Group 2 having a distance modulus of $11^{m}.6$ for a mean spectral type M2III and Group 5 a distance modulus of $12^{m}.8$ for a mean spectral type M5III. Group 8 has the same distance modulus as Group 5 and is composed primarily of giant K5 stars. The distance modulus of Group 7 is very similar to that of Group 2 and consists mainly of giant KO stars. The possibility that the various groups of giants might be supergiants was considered but discounted as the implied distances, for the same total absorption, exceed 20kpc, this objection would be overcome if the total absorption, from circumstellar and interstellar sources, were greatly increased.

The remaining group, number 6, is the only one which, on the basis of its mean position in the two colour diagram and its small mean parallax, could possibly consist of highly reddened early type stars. If Group 6 were composed of such stars, lying at the distance of the α-arm, then, from Fig. 4.10, by measuring along a reddening line of slope 0.72 from the centre of gravity of the Group to the mean theoretical main sequence, $E_{B-V} \sim 1^m.4$. This colour excess in combination with Neckel's value for A_v of $2^m.1$ implies that the ratio of total to selective absorption R ~ 1.6, which contradicts the work of Créze (1972) who has shown that the value of R increases sharply from 3.1 at about $\ell = 130^o$ to 4.5 in the anticentre region. If this is so then the total absorption in the direction of the stars in Group 6 will lie within the limits $4.3 < A_v < 6.3$. The unreddened distance modulus corresponding to 3.5kpc (the mean distance of the α-arm at $\ell = 140^o$) is $12^m.7$, thus the apparent distance modulus would be bounded by $17^m.0 < m_v - M_v < 19^m.0$ and hence the apparent magnitude of a reddened BOV star would lie between $m_v = 13^m.0$ and $15^m.0$. So if $3.1 < R < 3.7$ then it is possible that Group 6 consists of highly reddened early B stars in the α-arm. Such stars would be too faint to have been included in Sim's (1968) OB star survey. If these stars, assumed to be of mean type BOV were in the Perseus arm at $(\ell, r) = (140^o, 2\text{kpc})$ with an apparent distance modulus of $13^m.7$, then, assuming Neckel's value for A_v, they would have a mean apparent magnitude of $V = 9^m.7$ which they do not.

The giant groups appear to fall into two distance groupings, one at around 2.2kpc (Groups 2 and 7) and one at around 3.5kpc (Groups 5 and 8). It is most probably fortuitous that these distances correspond approximately to those of the Perseus arm and the α-arm!

The analysis of the proper motions and magnitudes in Tables 4.6 and 4.7 at best suggests the presence of some highly reddened objects at a distance of 3.5kpc in the α-arm defined by Verschuur's HI observations. More definite results would be obtained by impoving the photometry and going to a fainter limiting magnitude to provide a better statistical sample.

Chapter 5. Star Counts

5.1 Introduction

Star counts in unit B and I magnitude intervals were made in nine regions, each 1.75 square degrees in area; distributed about $(\ell, b) = (140^{\circ}, 0^{\circ})$. The apparent surface distribution of the stars was examined using equal number density contour diagrams. The mean density function and the mean variation of interstellar absorption with distance for various of the areas were determined using a combination of theoretical and observed cumulative Wolf diagrams.

5.2 Observations and Measurements

Two plates, one in each of the colours B and I, were taken with the 60/90/207cm Burrell Schmidt camera at the Warner and Swasey Observatory of the Case Institute of Technology (cf. King (1955) for a more complete description of this telescope). Details of the plates are given in Table 5.1 below.

TABLE 5.1

OBSERVATIONAL MATERIAL

Plate No.		5568	5597
Date		1969 Sept 11	1969 Sept 13
Plate Centre	α	3^h05^m	3^h04^m
	δ	$+58^o.2$	$+58^o.1$
Exposure		20^m	15^m
Emulsion		IN	103aO
Filter		RG8	GG13

Charts were made up from the plates. On these charts all the AGK3 stars present were identified using the transparent overlay described in the previous chapter. Also identified were stars whose photoelectric magnitude was known or had been measured. These two groups of stars were used as the reference block in the GALAXY measures. The area common to both plates was selected to be measured.

The reference block of stars on the B plate were measured using the Grubb-Parsons measuring machine. Two diametrically opposed stars were measured both by the Grubb-Parsons and, manually, by the GALAXY measuring machines for use with the coordinate transform program.

The B plate (No. 5597) was searched to the limit of image detectability by GALAXY. The search tape produced was read into the machine again and the images detected

measured in X, Y and M, and output on the measurement tape.

An independent search to the limit of image detectability was made of the I plate (No. 5568), using the same reference block data as for the B plate. The images found in the search phase were then accurately measured, as described above for the B plate.

The equatorial coordinates of 118 stars, from the AGK3 catalogue, which were identified on the B plate chart were updated for proper motion to the plate epoch and converted to galactic coordinates. Computer program XYLBFULL was used to find the linear plate constants relating the stars' (ℓ, b) coordinates with their measured (X,Y) GALAXY coordinates. The method described in the preceding chapter was used, and after three rejection loops 102 stars were left which were used in the final determination of the plate constants. For these 102 stars the mean residual between the computed and catalogue positions and its standard deviation in each of galactic longitude ($\overline{\Delta\ell}$) and galactic latitude ($\overline{\Delta b}$) were calculated and are given below:

$$\overline{\Delta\ell} = 0^{\circ}.00000 \pm 0^{\circ}.00021$$

$$\overline{\Delta b} = 0^{\circ}.00000 \pm 0^{\circ}.00018$$

The B plate (X,Y) coordinates of the corners of the nine subdivisions of the total area measured were input to the program XYLBFULL and converted, via the linear plate constants determined for the 102 AGK3 stars to (l,b). Table 5.2 lists these coordinates for equinox 1950.0 and epoch 1968.7, X and Y are in microns measured on the B plate and l and b are in degrees and apply to both the B and I plates.

TABLE 5.2
COORDINATES OF THE CORNERS
OF THE SUBAREAS MEASURED

X	Y	l	b
53248	69632	137°.1139	0°.5473
	116053	137.7526	-0.5198
	162474	138.3918	-1.5873
	208896	139.0313	-2.6541
102400	69632	138.2431	1.2246
	116053	138.8826	0.1571
	162474	139.5223	-0.9110
	208896	140.1621	-1.9783
151552	69632	139.3735	1.9018
	116053	140.0133	0.8343
	162474	140.6531	-0.2338
	208896	141.2926	-1.3014
200704	69632	140.5044	2.5781
	116053	141.1441	1.5110
	162474	141.7834	0.4432
	208896	142.4221	-0.6241

5.3 Magnitude Calibration

A calibration curve was drawn, of photoelectric magnitude (cf. Chapter 3), against mean reference block M-numbers for X240 GALAXY optics measurements for the B plate. A least squares straight line fit of the curve (shown in Fig. 5.1) with the standard deviation in the measurement of an individual star is given below.

$$B = 20.88 - 0.010270\,M_B \qquad \sigma_B = \pm 0^m.17 \qquad 5.1$$

For the I plate none of the photoelectric standards was faint enough to appear in the X240 optics mean reference block data, so the reference block of stars were measured with the GALAXY X75 optics. A plot (Fig. 5.2) of X75 optics measures against X240 optics measures was drawn to relate the two sets of measurements, the least squares fitted coefficients are given in equation 5.2.

$$M_{240} = 3.325\,M_{75} - 223 \qquad \sigma_{240} = \pm 14 \qquad 5.2$$

Using equation 5.2 the M_{75} values for the standard stars were converted to M_{240} values which in turn were plotted against photoelectric I magnitudes (Fig. 5.3) to produce a linear least squares relation of

$$I = 15.04 - 0.008713\,M_{240} \qquad \sigma_I = \pm 0^m.10 \qquad 5.3$$

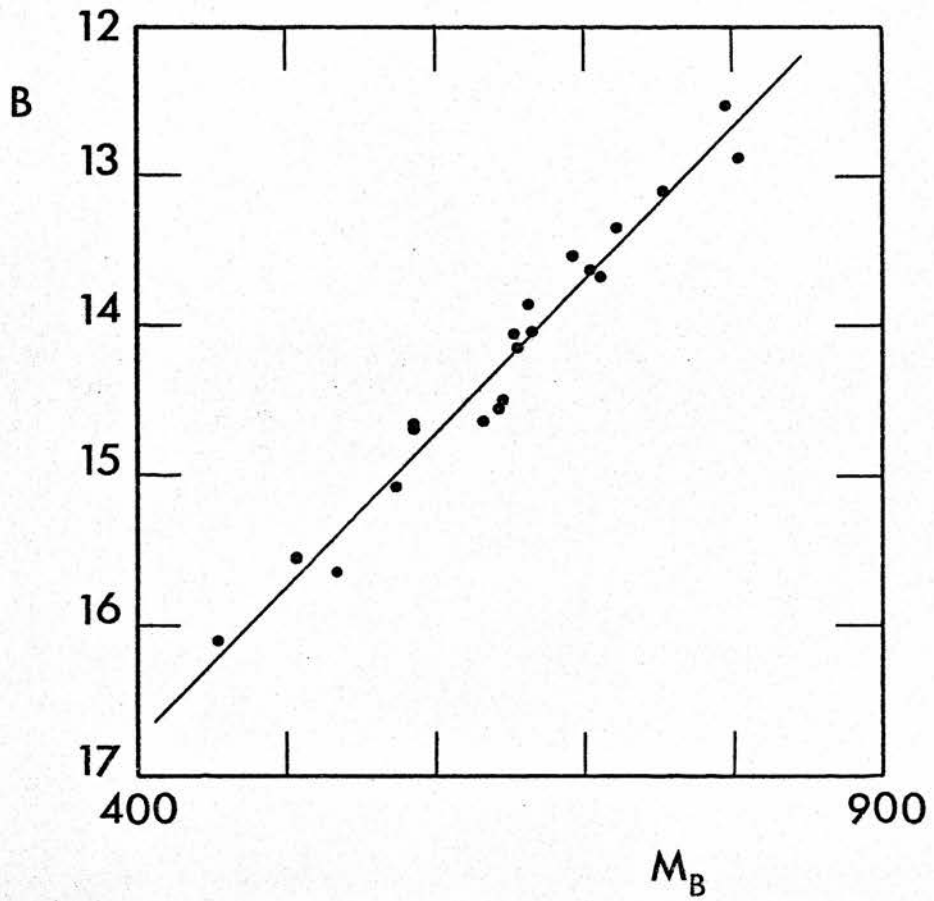

Fig. 5.1 Calibration curve for B plate number 5597.

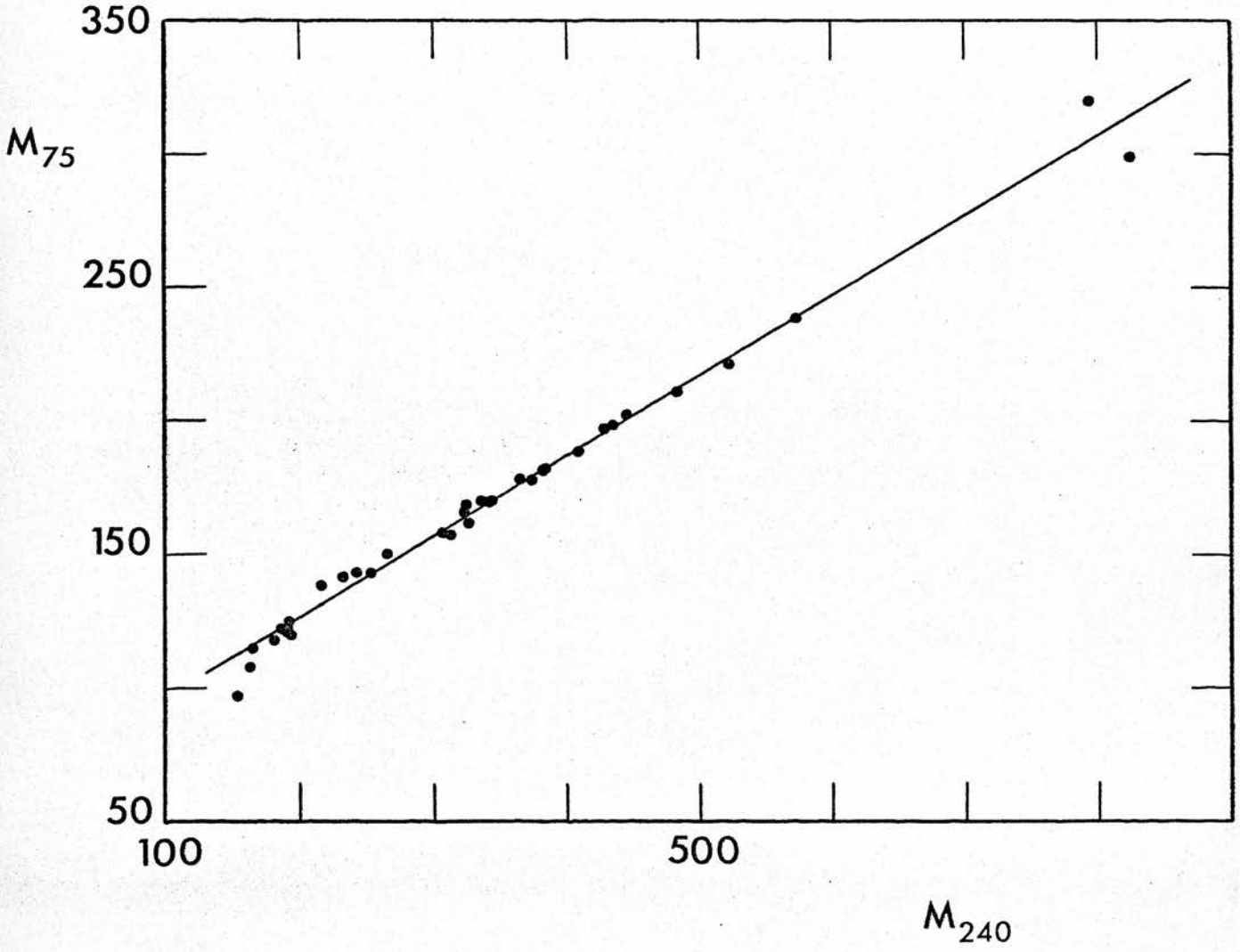

Fig. 5.2 Plot of I plate M-number measures for X75 GALAXY optics against X240 GALAXY optics.

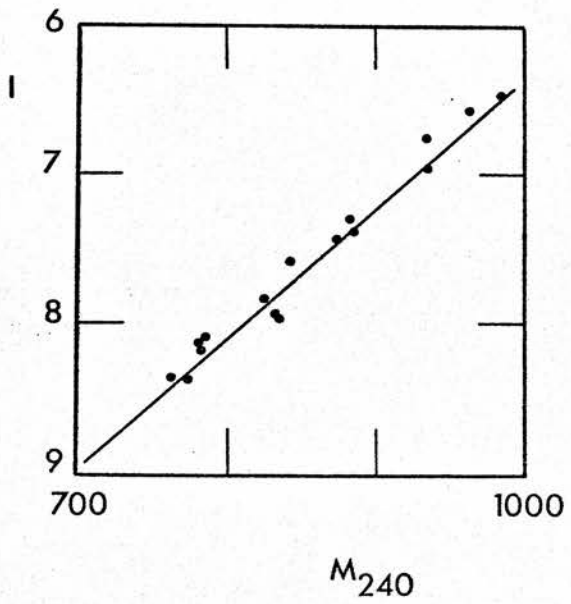

Fig. 5.3 Calibration curve for I plate number 5568.

In each of the above cases the standard deviation was defined as follows:

$$\sigma = \sqrt{\left\{ \frac{\sum (R-\bar{R})^2}{N} \right\}} \qquad 5.4$$

where

$$\bar{R} = \frac{1}{N} \sum \left(M_{obs} - M_{calc} \right)$$

M_{obs} is the observed magnitude, M_{calc} is the magnitude calculated from the calibration curve, and the residual

$$R = M_{obs} - M_{calc}$$

For the I calibration, since two least squares fits, each with its own variance, are involved, the standard deviation of the magnitude of an individual star is taken as $\sigma_I = \pm 0^m.16$.

5.4 Qualitative Analysis

The output for 4791 star images from the GALAXY search and measurement of the I plate was divided into nine areas, defined by the coordinates given in Table 5.2. The M-numbers were converted to I - magnitudes via equation 5.3 and the number of stars in half magnitude ranges counted for each of the nine areas. Table 5.3 lists the results of the counts.

TABLE 5.3

I - MAGNITUDE STAR COUNTS

Magnitude Interval	Region 1	2	3	4	5
5.5 - 6.0	2	0	0	1	1
6.0 - 6.5	2	2	3	1	2
6.5 - 7.0	6	5	3	6	5
7.0 - 7.5	3	5	5	4	6
7.5 - 8.0	9	9	7	6	6
8.0 - 8.5	12	16	5	8	15
8.5 - 9.0	20	18	12	14	22
9.0 - 9.5	21	26	18	22	25
9.5 - 10.0	33	23	32	41	28
10.0 - 10.5	30	41	28	45	36
10.5 - 11.0	62	47	37	48	47
11.0 - 11.5	56	60	42	69	53
11.5 - 12.0	77	46	48	63	68
12.0 - 12.5	70	55	75	66	68
12.5 - 13.0	175	134	103	158	135

TABLE 5.3 Con't.

I - MAGNITUDE STAR COUNTS

Magnitude Interval	Region 6	7	8	9
5.5 - 6.0	0	0	0	2
6.0 - 6.5	0	1	3	0
6.5 - 7.0	2	8	3	0
7.0 - 7.5	4	4	3	2
7.5 - 8.0	8	3	8	5
8.0 - 8.5	9	7	10	7
8.5 - 9.0	11	15	7	6
9.0 - 9.5	18	25	13	12
9.5 - 10.0	30	12	22	16
10.0 - 10.5	31	35	19	28
10.5 - 11.0	42	35	28	32
11.0 - 11.5	60	46	38	26
11.5 - 12.0	44	63	55	32
12.0 - 12.5	55	59	51	46
12.5 - 13.0	137	171	135	97

Contour plots, presented in Fig. 5.4, were drawn of numbers of stars per unit magnitude interval per 1.75 square degrees against galactic coordinates. In the magnitude intervals I = 7 to 8 and I = 8 to 9 there is no evidence of a discontinuity in the apparent surface number distribution.

A definite negative gradient of star numbers against galactic longitude along the equator is apparent by the interval I = 9 to 10 and strengthens to reach a peak in the I = 11 to 12 range, the greatest change in apparent surface number density occurs at $(\ell,b) = (141^{o},0^{o})$. The plot of the magnitude interval I = 12 to 13 shows no well marked discontinuity near $\ell = 141^{o}$ and has its equal number density contour lines more nearly parallel to the galactic equator.

The approximately 45^{o} angle, which the direction at right angles to that of maximum change in apparent star numbers makes with the galactic equator, is similar to that observed for both OB stars (Sim 1968a) and early A stars (McCuskey and Houk 1971). This suggests that, though the majority of stars observed are probably of late spectral type and various luminosity classes, the shapes of the contours are determined by an overlying population of reddened early type stars. If this is indeed the case then the following simple interpretation of the contour plots may be made. From I = 7 to 9 there are few members

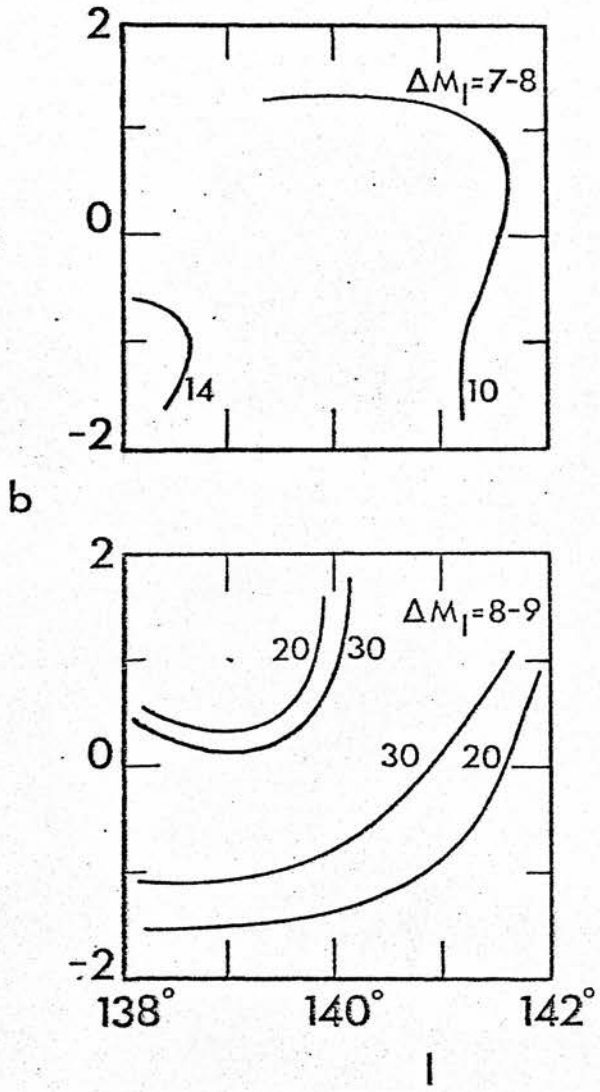

Fig. 5.4 Plots of star numbers per 1.75 square degree area in one magnitude intervals in I, centred on $(\ell,b) = (140^{\circ}0^{\circ})$.

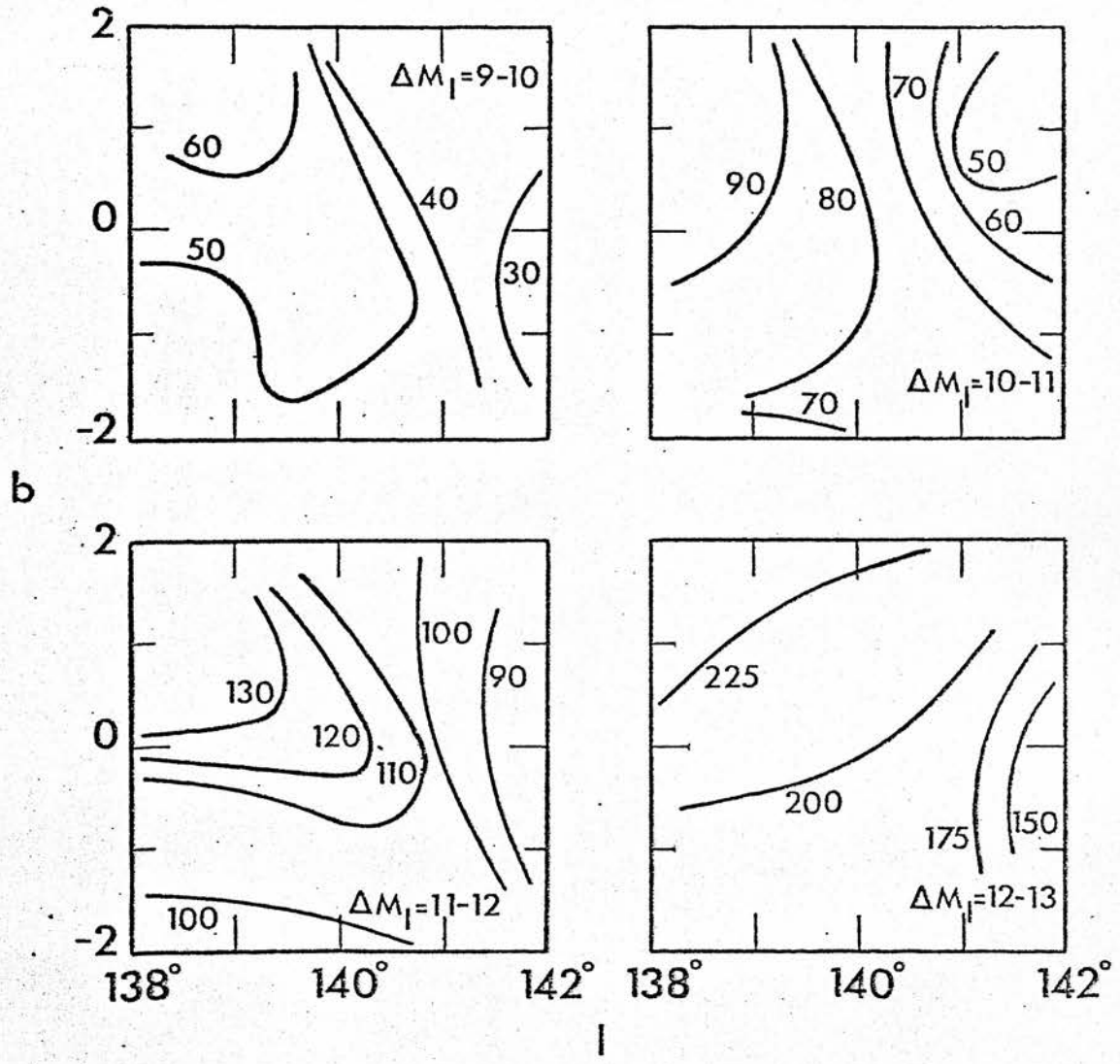
b
2
0
-2
ΔM_l=9-10
60
50
40
30
ΔM_l=10-11
90
80
70
60
50
70
ΔM_l=11-12
130
120
110
100
90
100
ΔM_l=12-13
225
200
175
150
138°
140°
142°
138°
140°
142°
l

of the overlying population present and no well defined structure is apparent. From I = 9 to 12 the overlying population consists mainly of reddened B stars in the Perseus spiral arm. The probability of this being so is strengthened by the following argument: the distance modulus of the Perseus arm is about $11^m.6$ and the absolute I magnitudes of main sequence BO and AO stars are approximately $-3^m.3$ and $+0^m.7$ (Johnson 1966). Assuming that Neckel's (1967) value of $A_V = 2^m.2$ is correct and that the values for R (the ratio of total to selective absorption A_v / E_{B-V}) of 3 and E_{V-I} / E_{B-V} of 1.6 given by Johnson (1968) for stars in Perseus are appropriate it can readily be shown that the apparent I magnitude of a BOV star at the distance of the Perseus arm would be $+9^m.4$ and that of an AOV star at the same distance, $+13^m.4$.

For I = 12 - 13 the equal number contour lines are, except for the region beyond $l = 142^\circ$, more nearly parallel to the galactic equator illustrating the general fall-off in numbers from galactic equator to poles. For this magnitude interval as for I = 7 to 9 there is no way of distinguishing between a reddened B star population and an underlying late type population.

For regions I, V and IX along the galactic equator, and regions III, V and VII at right angles to the galactic equator at $l = 140^\circ$, Wolf diagrams (cf. Wolf 1923) of the logarithm of the cumulative star density per square degree ($\log \Sigma A(m_I)$) against apparent I magnitude were drawn (Figures 5.5 and 5.6).

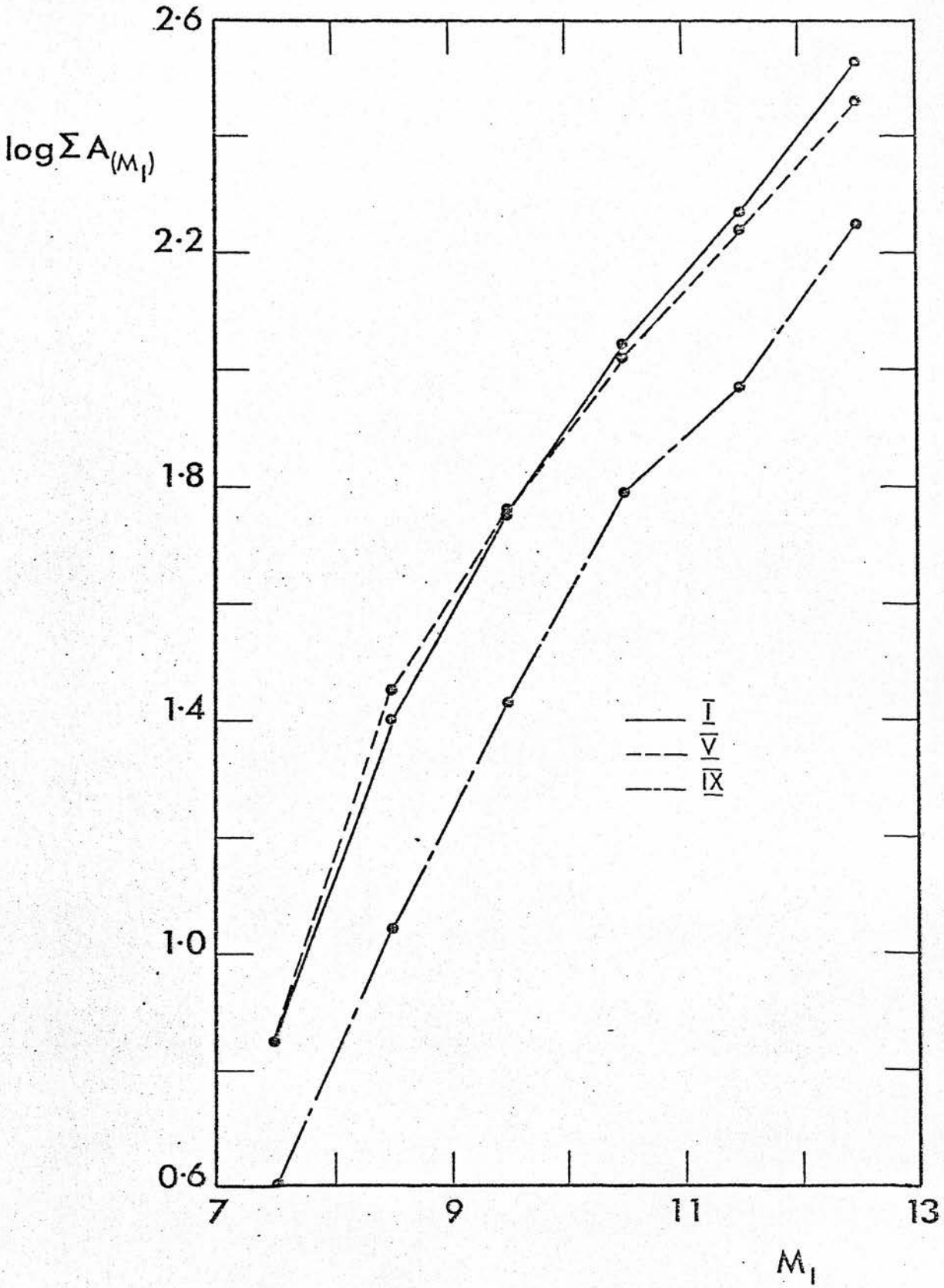

Fig. 5.5 Cumulative I magnitude Wolf diagram for areas I, V and IX.

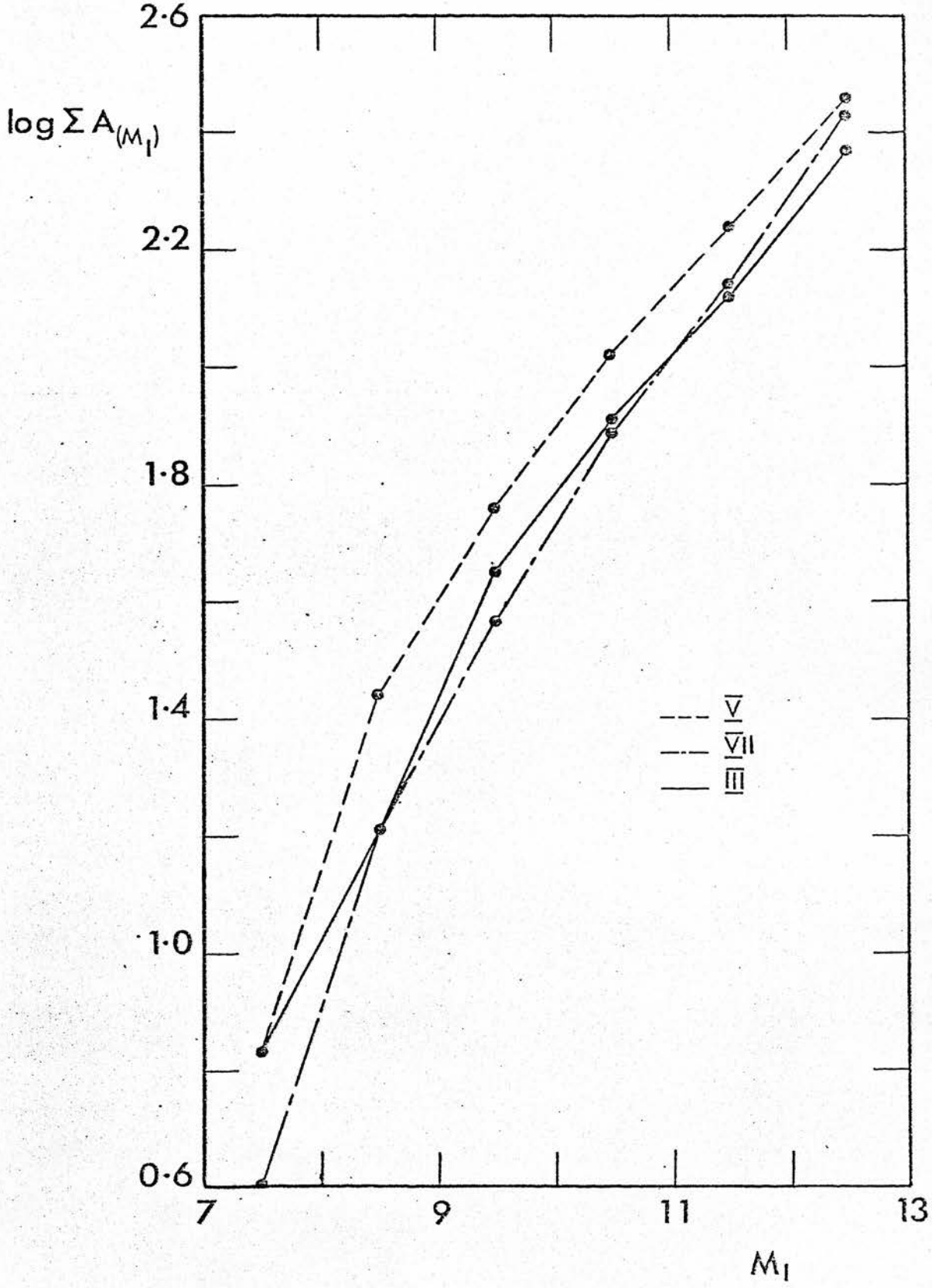

Fig. 5.6 Cumulative I magnitude Wolf diagram for areas III, V and VII.

From Fig. 5.6 it is evident that there is little difference in the cumulative star counts of regions III (centred on $l, b = 139^{o}.3, -1^{o}.8$), V ($l, b = 139^{o}.9, -0^{o}.1$), and VII ($l, b = 140^{o}.4, +1^{o}.7$) implying that there is little difference in the mean star density functions (i.e. number of stars per unit volume) or the mean values for interstellar absorption. However, the corresponding plots taken along the equator, I ($l, b = 138^{o}.0, +0^{o}.3$), V ($l, b = 139^{o}.9, -0^{o}.1$) and IX ($l, b = 142^{o}.0, -0^{o}.5$) do show differences. I and V are, within the expected fluctuations, identical, but IX has apparently fewer stars.

From I = 7.5 to 10.5 in region IX the deficiency of stars is most probably real with the mean density function being smaller than for regions V and I, since the shapes of the curves in the Wolf diagram are similar but displaced (cf. Section 5.5).

Between I = 10.5 and 11.5 the curves are no longer parallel implying an increase in interstellar absorption in region IX of a localised nature since for I = 11.5 to 12.5 curve IX again becomes parallel to curves I and V. The increase in interstellar absorption is due to a cloud with an I magnitude opacity, as measured along the m_I axis of Fig. 5.5, of approximately half a magnitude.

The infrared star counts show that there is a definite drop in star numbers along the galactic equator

with increasing longitude, this effect is due mainly to an overlying population of reddened B stars in the Perseus arm.

The output for 36367 star images from the GALAXY search and measurement of the B-plate was divided into nine areas, defined as before by the coordinates given in Table 5.2 The M-numbers were converted to B magnitudes via equation 5.1 and the number of stars in half magnitude ranges counted for each of the nine areas. The results of the counts are listed in Table 5.4.

TABLE 5.4

B - MAGNITUDE STAR COUNTS

Magnitude Interval	Region 1	2	3	4	5
9.5 - 10.0	0	0	0	0	0
10.0 - 10.5	10	8	2	4	5
10.5 - 11.0	10	13	13	6	8
11.0 - 11.5	20	11	15	14	14
11.5 - 12.0	20	17	19	27	12
12.0 - 12.5	38	35	21	27	23
12.5 - 13.0	56	54	44	45	30
13.0 - 13.5	75	79	51	60	54
13.5 - 14.0	136	118	78	101	79
14.0 - 14.5	169	173	118	122	80
14.5 - 15.0	277	208	149	187	135
15.0 - 15.5	358	283	216	237	208
15.5 - 16.0	461	326	216	279	225
16.0 - 16.5	492	379	219	351	248
16.5 - 17.0	526	328	219	345	227
17.0 - 17.5	459	311	241	314	234
17.5 - 18.0	450	289	229	320	209

TABLE 5.4 Con't

Magnitude Interval	Region 6	7	8	9
9.5 - 10.0	0	0	1	1
10.0 - 10.5	4	5	6	1
10.5 - 11.0	8	9	7	7
11.0 - 11.5	15	13	9	6
11.5 - 12.0	11	19	18	12
12.0 - 12.5	17	32	23	18
12.5 - 13.0	23	41	41	25
13.0 - 13.5	43	54	60	30
13.5 - 14.0	54	75	68	51
14.0 - 14.5	77	107	102	70
14.5 - 15.0	118	130	111	88
15.0 - 15.5	143	183	185	112
15.5 - 16.0	178	221	184	132
16.0 - 16.5	212	277	234	146
16.5 - 17.0	235	268	244	145
17.0 - 17.5	190	261	215	155
17.5 - 18.0	191	232	210	128

Contour plots, presented in Fig. 5.7, were drawn of number of stars per unit magnitude per 1.75 square degrees against galactic coordinates. On all the plots from B = 10 to 18 the apparent star density decreases along the galactic equator in the direction of increasing longitude. In general the lines of equal density are at right angles to the galactic equator. From B = 12 to 18 the greatest rate of change in star density occurs for $l \leq 140^{\circ}$, with the effect being most marked for $B \geq 15^{m}$. Thus the contour plots of apparent star densities offer some evidence for a discontinuity near $l = 140^{\circ}$.

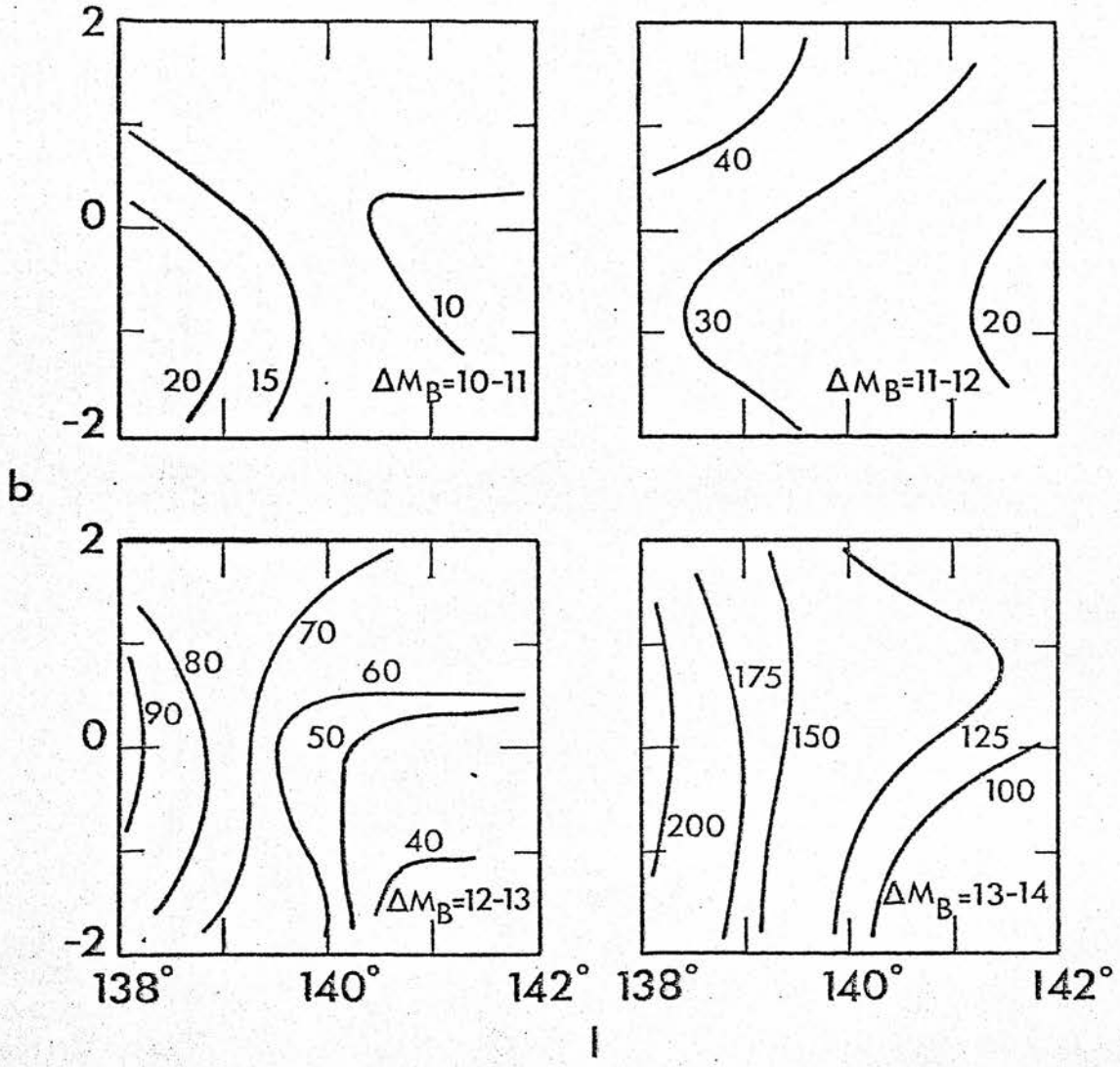

Fig. 5.7 Plots of star numbers per 1.75 square degree area in one magnitude intervals in B centred on $(l,b) = (140^{o},0^{o})$.

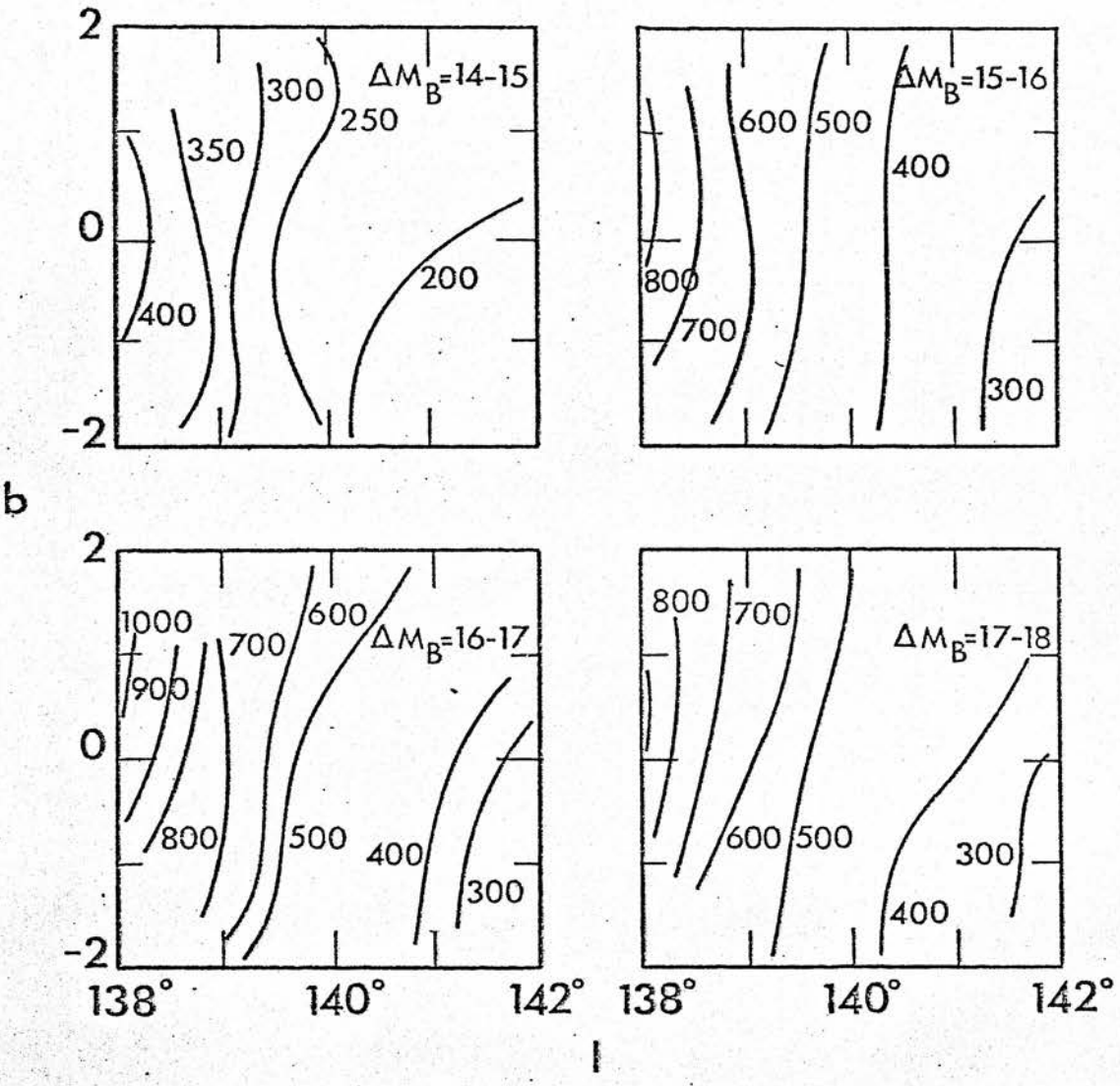
2
0
-2
ΔM_B=14-15
300
250
350
400
200
ΔM_B=15-16
600
500
400
800
700
300
b
ΔM_B=16-17
1000
900
700
600
800
500
400
300
ΔM_B=17-18
800
700
600
500
300
400
138°
140°
142°
138°
140°
142°

Cumulative Wolf diagrams were drawn for the same regions as for the I magnitude analysis, they are shown in Figures 5.11 and 5.12 and are interpreted in the following section (5.5).

5.5 Quantitative Analysis

The fundamental equation of general star count analysis is given by Mihalas and Routly (1968) as

$$A(m) = \omega \int_0^\infty \Phi\left(m + 5 - 5\log r - a(r)\right) D(r)\, r^2\, dr \qquad 5.5$$

where $A(m)$ is the number of stars in the magnitude range $m - \frac{1}{2}$ to $m + \frac{1}{2}$.

ω is the solid angle subtended by 1 square degree $= 4\pi / 41252$

r is the true distance at which a star appears to be of magnitude m

$a(r)$ is the total interstellar absorption in magnitudes to distance r

$\Phi\left(m + 5 - 5\log r - a(r)\right)$ is the stellar luminosity function (i.e. the number of stars per unit absolute magnitude interval).

and $D(r)$ is the density function (i.e. the number of stars per unit volume of space) at distance r.

The use of the general luminosity function is only realistic in the galactic plane since the distribution of early type stars is dependent on galactic latitude.

The observed star counts are dependent on the amount of interstellar absorption present and thus equation 5.5 should be written in terms of apparent luminosity and density functions $D_A(\rho)$ at apparent distance ρ i.e.

$$A(m) = \omega \int_0^\infty D_A(\rho)\, \Phi(m + 5 - 5\log\rho)\, \rho^2\, d\rho \qquad 5.6$$

Now the true density function may be obtained from the apparent density function by:

$$D(r) = D_A(\rho)\, \frac{\rho^2}{r^2}\, \frac{d\rho}{dr} \qquad 5.7$$

or if the absorption law is known

$$D(r) = D_A(\rho) \left\{ 1 + 0.4604\, r\, \frac{da(r)}{dr} \right\} 10^{0.6\, a(r)} \qquad 5.8$$

The method for solving for the stellar density function from the star count integral equation 5.6 follows that of Bok (1937) and is called the $(m, \log \pi)$ method. The star count integral equation is replaced by a sum over finite shells, thus;

$$A(m) = \sum_k \left\{ D_A(\rho_k) \, \Phi(m + 5 - 5 \log \rho_k) \, \delta V_k \right\} \qquad 5.9$$

where δV_k is the volume of the kth shell. The shells are so chosen that their midpoints lie at distances

$$\log \rho_k = - \log \pi_k = \frac{2k}{10} \qquad 5.10$$

The volumes are for a 1^o x 1^o area on the sky and thus are given for $k \geq 2$ by

$$\delta V_k = \frac{4\pi}{123756} \left(\rho^3_{k+\frac{1}{2}} - \rho^3_{k-\frac{1}{2}} \right) \qquad 5.11$$

A table of $\Phi(m + 5 - 5 \log \rho_k) \, \delta V_k$ is constructed for various ρ_k and m in one magnitude steps. Table 5.5 is an extract from the $(m, \log \pi)$ table given by Mihalas and Routly (1968) which was used in the final analysis described below.

TABLE 5.5

$(m, \log \pi)$

$\log \pi_k$	m = 10	11	12	13
-1.0	0	0	0	0
-1.2	0	0	0	0
-1.4	0.01	0	0	0
-1.6	0.03	0.03	0.04	0.06
-1.8	0.10	0.12	0.13	0.16
-2.0	0.32	0.40	0.46	0.51
-2.2	0.85	1.26	1.58	1.82
-2.4	2.29	3.40	5.00	6.30
-2.6	4.18	9.12	13.5	19.9
-2.8	9.14	16.6	36.3	53.8
-3.0	10.5	36.4	66.0	144
-3.2	9.55	41.7	145	262
-3.4	9.55	38.0	166	575
-3.6	12.0	38.0	151	660
-3.8	15.1	47.8	151	604
-4.0	9.55	60.4	190	604
-4.2	4.78	37.9	240	760
-4.4	2.4	15	151	955
-4.6	0	9.6	76	600

TABLE 5.5 Con't

$\log \pi_k$	m = 14	15	16	17
-1.0	0	0	0	0
-1.2	0	0	0	0
-1.4	0	0	0	0
-1.6	0.08	0.09	0.10	0.12
-1.8	0.25	0.30	0.34	0.42
-2.0	0.63	1.00	1.18	1.35
-2.2	2.04	2.52	3.98	4.72
-2.4	7.25	8.14	10.0	15.8
-2.6	25.1	28.9	32.4	39.8
-2.8	79.4	100	115	129
-3.0	214	316	398	458
-3.2	575	853	1260	1580
-3.4	1040	2290	3400	5000
-3.6	2290	4170	9130	13500
-3.8	2630	9140	16600	36300
-4.0	2400	10500	36400	66000
-4.2	2400	9550	41700	145000
-4.4	3020	9550	38000	166000
-4.6	3800	12000	38000	151000

The final step in Bok's method is to try various values for $D_A(\rho)$ until the left hand and right hand sides of equation 5.9 agree. The solution thus derived by trial and error is obviously only one of an infinite family of such solutions as the system of linear equations to be solved is of the mth order with n unknowns where $n > m$.

An attempt was made to solve exactly for the density function for apparent distances greater than about 200pc by assuming that the values of the density function at distances less than 200pc could all be represented by unity or by unity with due allowance for a linear reddening law. In this case the values for the density function are derived by solving the following system of linear equations.

$$\sum_{k=8}^{19} D_A(\rho_k)\,\Phi(m+5-5\log\rho_k)\,\delta V_k = A(m) - \sum_{k=1}^{7} D'_A(\rho_k)\,\Phi(m+5-5\log\rho_k)\,\delta V_k \qquad 5.12$$

The solution vector however, proved physically unrealistic in that some negative values of $D_A(\rho_{k>7})$ resulted. This is probably due to the assumptions about the local values of the density function being incorrect.

The method finally adopted to analyse the B plate star counts was to construct theoretical Wolf diagrams

for distinct values of $da(r)/dr$ the rate of change of interstellar absorption with distance, and $\bar{D}'(\rho)$ the mean theoretical density function. The observational and the theoretical Wolf diagrams were then compared to find the best fit and hence values for $da(r)/dr$ and $\bar{D}'(\rho)$

Using the equation

$$\log \rho = \log r + 0.2\, a(r) \qquad 5.13$$

where ρ is the apparent distance, r is the true distance and $a(r)$ is the total reddening to distance r curves of $\log \rho$ against $\log r$ were drawn for various values of $da(r)/dr$ They are shown in Fig. 5.8. From these curves values of $\log r$ corresponding to the $\log \rho$ in the $(m, \log \pi)$ table were found for the various interstellar reddening gradients.

The true density function $D(r)$ was initially assumed to be equal to unity and to be independent of distance along the line of sight investigated. The values of $da(r)/dr$ varied from 0.5 to 2.5 mag/kpc. The theoretical apparent density function $D'_A(\rho)$ was then calculated from

$$D'_A(\rho) = D(r) \left\{ \left(1 + 0.4604\, r \frac{da(r)}{dr}\right) 10^{0.6\, a(r)} \right\}^{-1} \qquad 5.14$$

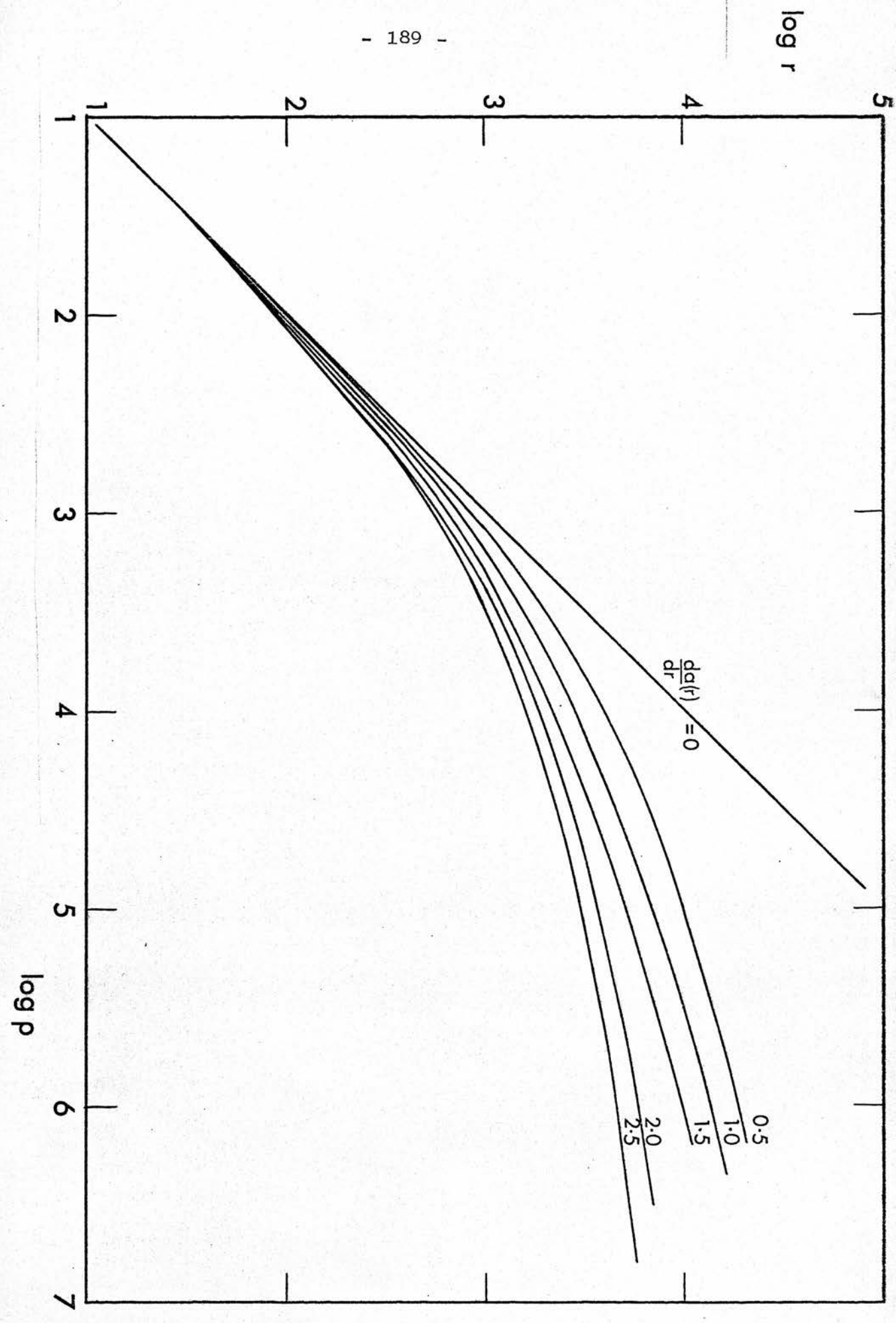

Fig. 5.8 Plot of $\log \rho$ against $\log r$

the values of $D'_A(\rho)$ for various $da(r)/dr$ and $\log \rho$ are listed in Table 5.6.

TABLE 5.6

THEORETICAL APPARENT DENSITY FUNCTIONS

$\log \rho$ \ $\frac{da(r)}{dr}$	0.5	1.0	1.5	2.0	2.5
1.0	1.00	0.99	0.97	0.96	0.96
1.2	0.99	0.97	0.96	0.95	0.94
1.4	0.98	0.95	0.92	0.91	0.89
1.6	0.96	0.93	0.90	0.87	0.84
1.8	0.95	0.89	0.85	0.80	0.77
2.0	0.91	0.84	0.77	0.71	0.66
2.2	0.87	0.76	0.67	0.60	0.54
2.4	0.80	0.65	0.54	0.46	0.41
2.6	0.72	0.54	0.42	0.34	0.28
2.8	0.60	0.41	0.29	0.21	0.17
3.0	0.46	0.28	0.18	0.12	0.092
3.2	0.35	0.17	0.10	0.064	0.048
3.4	0.22	0.096	0.055	0.033	0.023
3.6	0.13	0.050	0.027	0.013	0.0091
3.8	0.069	0.022	0.0113	0.0057	0.0037
4.0	0.033	0.0098	0.0043	0.0024	0.0015
4.2	0.016	0.0032	0.00153	0.00091	0.00060
4.4	0.0065	0.0011	0.00053	0.00029	0.00018
4.6	0.0025	0.00035	0.00015	0.00009	0.00007

Using the $D'_A(\rho)$ in conjunction with the $(m, \log \pi)$ table theoretical star counts $A'(m)$ were computed

from

$$A'(m) = \sum_{k=1}^{19} \left\{ D'_A(\rho_k)\, \Phi(m + 5 - 5\log \rho_k)\, \delta V_k \right\} \qquad 5.15$$

Plots of $\log \sum A'(m)$ the cumulative star count, against apparent magnitude m for the values of $da(r)/dr$ given above are shown in Fig. 5.9.

It is evident from equation 5.14 that the shape of the theoretical cumulative Wolf diagram, for a mean value of $D(r)$, is determined by the adopted value of the change of interstellar reddening with distance. The height of the curve above the m axis is fixed, for a given value of the interstellar reddening slope, by the mean theoretical density function.

The observed cumulative Wolf diagrams (Figures 5.11 and 5.12) were compared with those which had been computed for $D(r) = 1.0$ (Fig. 5.9). From B = 10 to 15, for all the regions studied, the shape of the observed curves lay between those of the theoretical curves for $da(r)/dr = 2.0$ mag/kpc and $da(r)/dr = 2.5$ mag/kpc. Owing to the low resolution of these diagrams a value for $da(r)/dr = 2.2$ mag/kpc was adopted for all the regions, a value which agrees well with that of Neckel (1967) for the range $0 \leq r \leq 1$ kpc.

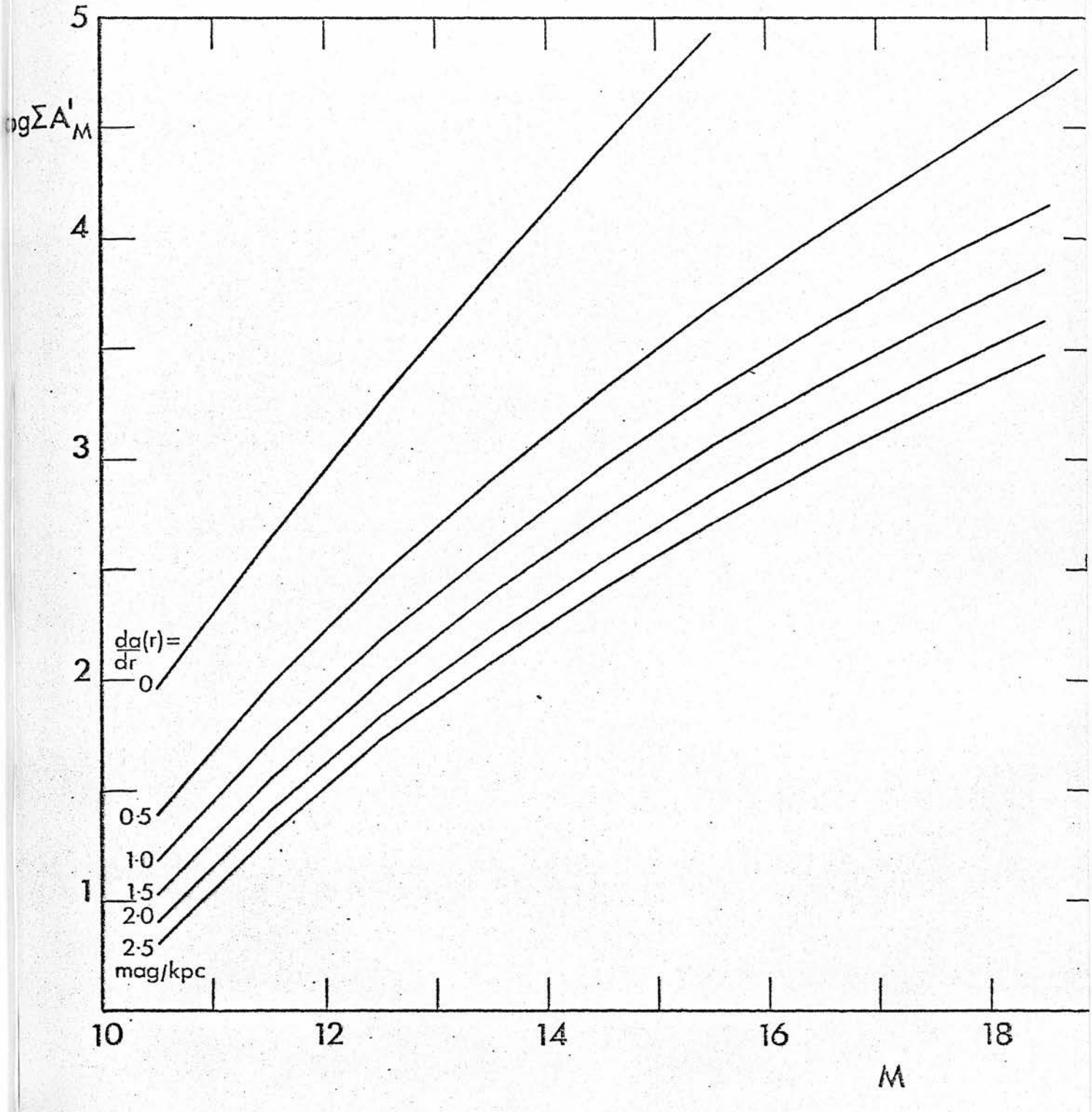

Fig. 5.9 Theoretical cumulative Wolf diagrams for different values of the absorption coefficient.

For this value of the interstellar absorption gradient a further family of theoretical curves of $\log \Sigma A'(m)$ against m were drawn (Fig. 5.10) by varying the value of $\bar{D}(r)$ from 0.2 to 2.0. The observed curves were compared with this set of computed curves to determine a value for $\bar{D}(r)$

Regions III, V and VII (Fig. 5.12) lying across the equator near $\ell = 140^{\circ}$ show no marked differences in either mean gradient of interstellar reddening or mean density function. Similarly regions I, V and IX (Fig. 5.11) show little variations in mean reddening slope, but their mean density functions are very different. The mean density function falls from $\bar{D}(r) = 1.5$ for region I to $\bar{D}(r) = 0.7$ for region IX. The value for $d\bar{D}(r)/d\ell = -0.2$ per degree along the galactic equator through $\ell = 140^{\circ}$ and 0.0 per degree at right angles to the equator through $\ell = 140^{\circ}$. Table 5.7 lists the derived values of interstellar reddening gradient and mean density function.

.../

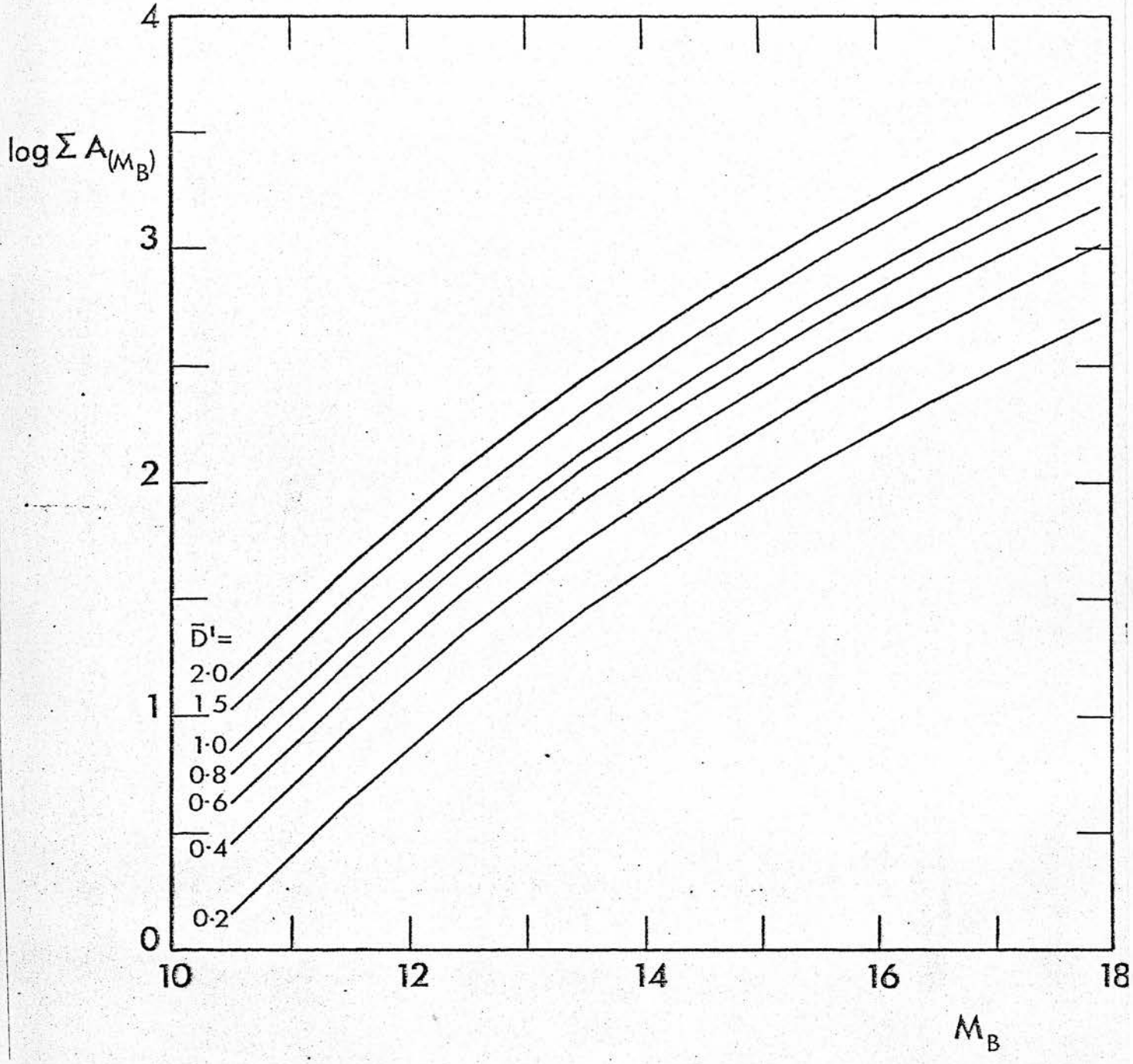

Fig. 5.10 Theoretical cumulative Wolf diagrams for $d\alpha(r)/dr$ = 2.2/kpc and $\bar{D}(r)$ = 2.0, 1.5, 1.0, 0.8, 0.6, 0.4, 0.2.

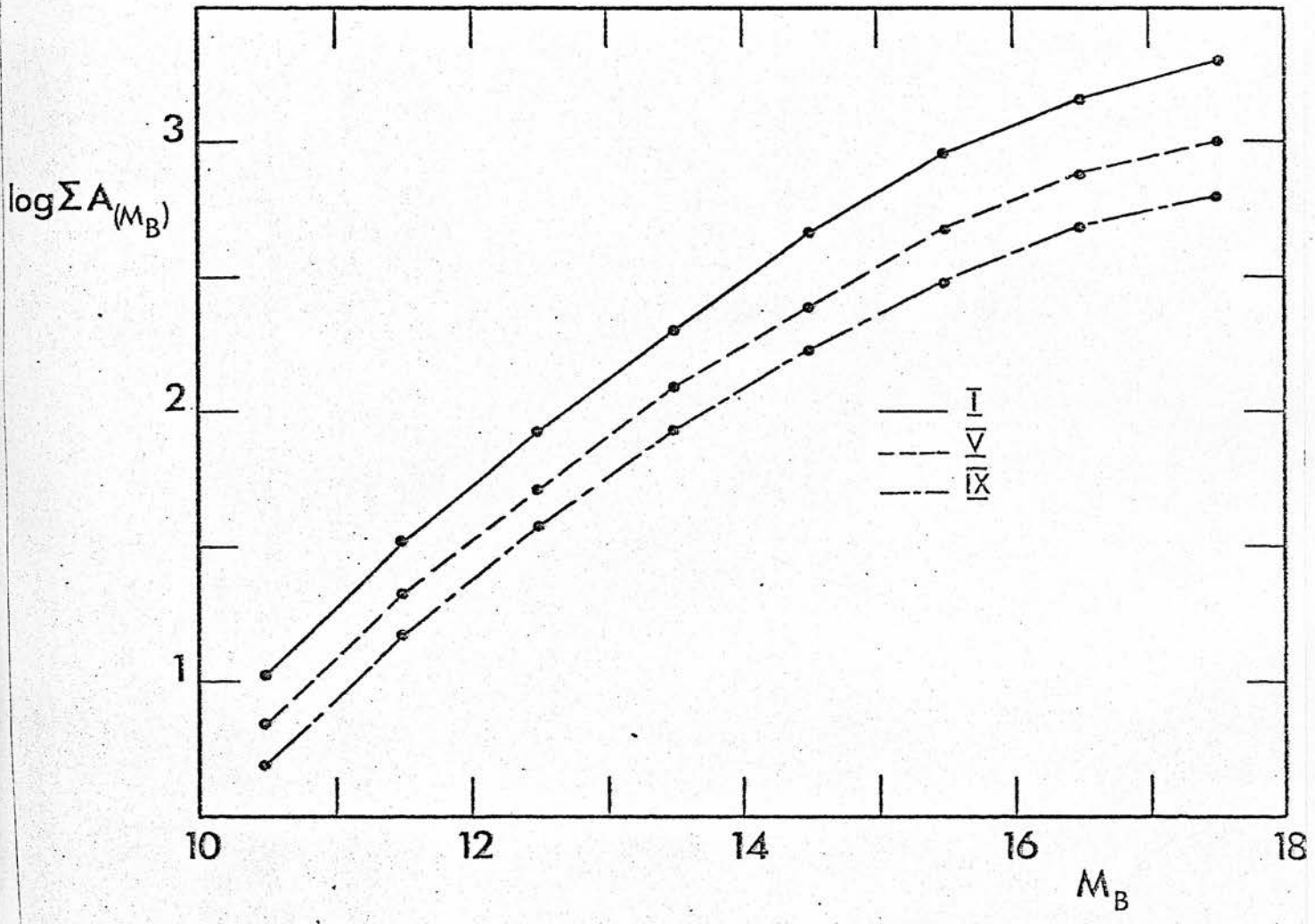

Fig. 5.11 Cumulative B magnitude Wolf diagrams for areas I, V and IX.

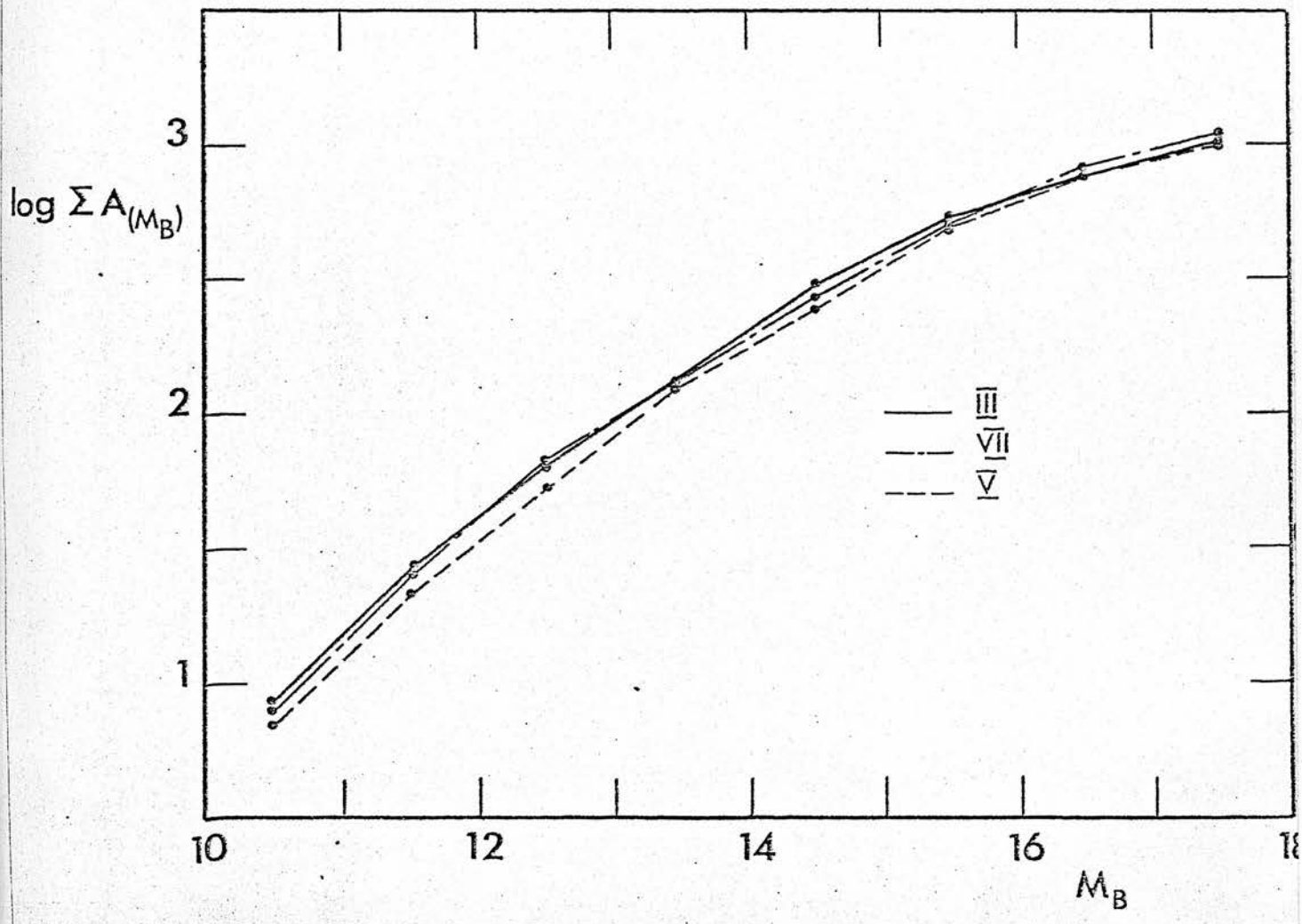

Fig. 5.12 Cumulative B magnitude Wolf diagrams for areas III, V and VII.

TABLE 5.7

MEAN INTERSTELLAR REDDENING GRADIENTS AND MEAN DENSITY FUNCTIONS

Region	ℓ	b	$\frac{da(r)}{dr}$	$\bar{D}(r)$
I	$138^{\circ}.0$	$+0^{\circ}.3$	2.1	1.5
III	$139^{\circ}.3$	$-1^{\circ}.8$	2.0	1.1
V	$139^{\circ}.9$	$-0^{\circ}.1$	2.3	1.0
VII	$140^{\circ}.4$	$+1^{\circ}.7$	2.0	1.1
IX	$142^{\circ}.0$	$-0^{\circ}.5$	2.4	0.7

In the range B = 15 to 18 the fit between the observed and theoretical curves becomes less good and must be due to increasing absorption, i.e $da(r)/dr > 2.2$ mag/kpc, at greater distances as it is not possible to mimic the observed change by varying the values of $\bar{D}(r)$. Since all the observed curves share the same dip this conclusion holds for all the regions.

The above analysis shows that the considerable change with galactic longitude in the numbers of stars observed is due, not to increased interstellar absorption, but rather, to a real reduction in the numbers of stars per unit volume of space.

APPENDIX I

Computer Programs

The following computer programs, written in ALGOL with some NEAT coded segments, were developed for the research programmes described in Chapters 2, 4 and 5.

1) PMCOR

Proper motion correction: this program corrects stellar coordinates for proper motions, the input consists of N sets of (α, δ) and $(\mu_\alpha \cos\delta, \mu_\delta)$ and the epoch difference between the base catalogue and the time of observation, the output is a list of updated equatorial coordinates.

2) GXARW

GALAXY astrometric reduction working version: this program converts rectangular to equatorial coordinates. Sets of (X,Y) and (α, δ) for N_1 reference stars are input from which, in conjunction with an input plate centre (α_o, δ_o), plate constants are computed, these are used to convert N_3 sets of programme star rectangular coordinates to equatorial coordinates. The Gauss - Jordan procedure used to solve for the plate constants was written in NEAT coded double precision segments to reduce the risk of round-off

error. The reference stars' equatorial coordinates, residuals (catalogue - computed) coordinates, and programme equatorial and rectangular coordinates are output.

3) TERF

Test error function: this program was written to test the effect of varying the parameter k in the inverse squared weighting function $E_j = \frac{\sum E_i e^{-kr^2}}{\sum e^{-kr^2}}$

4) ARERC

Astrometric reduction error correction: this program applies corrections generated by the inverse squared weighting function to the programme star equatorial coordinates computed by GXARW. The output is a list of programme star equatorial and rectangular coordinates and the corrections applied.

5) GXARW2

Essentially the same as GXARW but designed for large numbers of reference stars.

6) ARERC3

Essentially the same as ARERC but again designed for large numbers of reference stars.

7) GXCONV

GALAXY conversion: N sets of input GALAXY data are averaged and the running number of stars with differences ($\Delta X, \Delta Y$) between measured runs exceeding $\pm 3\mu m$ printed, with their differences. The averaged data is output on paper tape.

8) RESPLOT

Residuals plot: input is from ARERC in the form of N sets of rectangular coordinates and corrections applied. The graph plotter peripheral is used to plot out vector residuals in arc seconds against GALAXY coordinates.

9) POSRD

Positional reduction: this program was used in testing the position residuals derived from a Schmidt plate for systematic deviations. The input, consisting of N sets of (X,Y) coordinates and position residuals was divided into eight parts defined by a circle of chosen radius and a right angled cross both centred on the plate centre. The output is a set of eight mean residuals and their standard deviations.

10) ASTAN

Astrometric analysis: the input consists of a tape of colours and magnitudes for stars whose position

residuals are derived and input from ARERC or ARERC3. Output is a histogram of residuals in α and δ, mean residual and standard deviations for stars in pre-selected magnitude or colour intervals, and the mean and standard deviations of residuals in α and δ for all the programme stars.

11) TABLE 1

Provided a matched listing of Schmidt and Astrograph plate coordinates, M - numbers, and chart identification numbers.

12) TABLE 4

Makes least squares fits of any order between the (X,Y) coordinates and the M - numbers of a group of stars on one plate with the same group on another. The coefficients of the least squares fits in X, Y and M, the reference plate star coordinates and the residuals (ΔX,ΔY,ΔM) are all output on a lineprinter, the residuals are also output on paper tape.

13) RESPLOT4

Plots (ΔX,ΔY) from TABLE 4 against GALAXY (X,Y) coordinates.

14) GXARN

GALAXY astrometric reduction Nth order: similar to

GXARW but completely general instead of being simply a 3rd order calculation.

15) TABLE 5

Makes a least squares fit between coordinates of reference stars on one plate with those on another, the plate constants thus determined are used to convert all the programme plate star positions to reference plate positions. The reference plate programme star coordinates are output with the residuals between these and the transformed programme plate coordinates. TABLE 6 is similar but has the added refinement of a reference star rejection mechanism based on a multiple of the standard deviation of the mean residual. TABLE 7 results are output on paper tape as well as the lineprinter.

16) CONVEG

Conversion of equatorial to galactic coordinates: equatorial coordinates of N stars and the galactic quadrant in which they appear are input and converted to galactic coordinates using the formulae given by Torgård in Lund Annals 15.

17) XYLB

(X,Y) coordinates to (ℓ,b) coordinates: computes plate constants between (X,Y) and (ℓ,b) for reference stars and outputs them on lineprinter and paper tape.

Rejection of reference stars in three loops set at 1^{o}, 0^{o},03, and 0^{o}.001.

18) PM

Proper motion: uses the output from TABLE 7 with information about the epoch difference between the two plates, the plate scale of the reference plate, and the transformation angle between GALAXY (X,Y) coordinates and galactic (ℓ,b) coordinates to output a list of galactic coordinate proper motion components in arc seconds per annum. Also input are the plate constants from XYLB determined between the two different epoch plates and the AGK3 catalogue and the measured (X,Y) programme coordinates on each of the two plates. The (ℓ,b) coordinates for the programme stars at the later epoch are output with the epoch difference divided differences between the (ℓ,b) of the first and second epoch plates, i.e. the proper motion components. The M - numbers of the reference plate were input with the calibration curve coefficients and converted to and output as magnitudes. Other output includes a running number, a reference number, and the mean and standard deviations of the residuals between the two sets of proper motions.

19) SLLSP

Simple linear least squares program: this program performs a linear least squares fit, recomputes the Y variable, compares it with the original and computes and outputs the mean and standard deviations of the residuals.

20) SQLSP

Simple quadratic least squares program: similar to program SLLSP but the least squares fit is to a quadratic rather than a linear curve.

21) MAGLIST 2

Magnitude list: converts lists of GALAXY M - number or Becker iris photometer readings into magnitudes via input calibration curve coefficients (linear or quadratic), also output are colour differences.

22) DIV, COMB, CUT, FROG, PREPARE 1, PREPARE 2, UNMEAN, GXTAPE:

All these programs were written to modify various data tapes into forms acceptable as input to some of the major programs described above.

APPENDIX II

Astrometry with a Schmidt Camera

A description of the spherical and instrumental corrections which need to be made to star image positions measured on a Schmidt camera plate is given in this Appendix. The theory is developed to third order terms, with the notation and argument following, in part, those of Dixon (1962, 1963a, 1963b).

Spherical Corrections

To find the apparent position of a star just before its light enters the corrector plate of the Schmidt camera it is necessary to apply the following spherical corrections to the catalogue position of the star:

i) The proper motion of the star between the epoch of the catalogue and that of the observation.

ii) Precession.

iii) Nutation.

iv) Aberration.

v) Annual Parallax.

vi) Refraction.

i) Correction for Proper Motion

Let the coordinates of a star at epoch t_0 be (α_0, δ_0)

and let (α_1, δ_1) be the coordinates corrected for proper motion at epoch t_1, then

$$\alpha_1 = \alpha_0 + (\mu_\alpha + \tfrac{1}{2}\Delta\mu_\alpha)\,t \qquad 1)$$

$$\delta_1 = \delta_0 + (\mu_\delta + \tfrac{1}{2}\Delta\mu_\delta)\,t \qquad 2)$$

where

$$t = t_1 - t_0$$

μ_α, μ_δ are the components of proper motion in right ascension and declination, and

$$\Delta\mu_\alpha = 2\mu_\alpha\mu_\delta \sin 1'' \tan\delta_1 \,.\, t \qquad 3)$$

$$\Delta\mu_\delta = -\mu_\alpha^2 \sin 1'' \sin\delta_1 \cos\delta_1 \,.\, t \qquad 4)$$

ii) Correction for Precession

(α_1, δ_1) are the mean equatorial coordinates corrected for proper motion referred to the mean equator and equinox at t_0 . (α_2, δ_2) are the mean equatorial coordinates corrected for proper motion referred to the mean equator

and equinox at t_1 . Thus:

$$\cos\delta_2 \sin(\alpha_2 - z) = \cos\delta_1 \sin(\alpha_1 + \zeta_0)$$

$$\cos\delta_2 \cos(\alpha_2 - z) = \cos J \cos\delta_1 \cos(\alpha_1 + \zeta_0) - \sin J \sin\delta_1$$

$$\sin\delta_2 = \sin J \cos\delta_1 \cos(\alpha_1 + \zeta_0) + \cos J \sin\delta_1 \qquad 5)$$

Definitions of T_0 , and T and values of J, ζ_0 and z are given in the "Explanatory Supplement to the Astronomical Ephemeris", they are as follows:

Initial epoch $t_0 = 1900.0 + T_0$

Final epoch $t_1 = 1900.0 + T_0 + T$

$$J = (2004''.682 - 0''.853\,T_0)\,T - 0''.426\,T^2 - 0''.042\,T^3$$

$$\zeta_0 = (2304''.250 + 1''.396\,T_0)\,T + 0''.302\,T^2 + 0''.018\,T^3$$

$$z = \zeta_0 + 0''.791\,T^2$$

iii) Correction for nutation

If (α_2, δ_2) are the mean coordinates at time t_1 and (α_3, δ_3) are the true coordinates at time t_1 , then

$$\alpha_3 = \alpha_2 + \Delta\Psi(\cos\epsilon + \sin\epsilon \sin\alpha_2 \tan\delta_2) - \Delta\epsilon \cos\alpha_2 \tan\delta_2$$

$$\delta_3 = \delta_2 + \Delta\Psi \sin\epsilon \cos\alpha_2 + \Delta\epsilon \sin\alpha_2 \qquad 6)$$

$\Delta\Psi$ and $-\Delta\epsilon$ ($\Delta\epsilon = -B$ where B is one of the Besselian day numbers) are tabulated for each day of the year in the "Astronomical Ephemeris".

iv) Correction for Aberration

Let (α_3, δ_3) be the true position of the star and (α_4, δ_4) its apparent position, then

$$\alpha_4 = \alpha_3 - \kappa\,(\sin\alpha \sin\lambda_\odot + \cos\alpha_3 \cos\lambda_\odot \cos\epsilon)\sec\delta_3$$

$$- e\kappa\,(\sin\alpha_3 \sin\Pi + \cos\alpha_3 \cos\Pi \cos\epsilon)\sec\delta_3$$

$$\delta_4 = \delta_3 - \kappa\,(\cos\alpha_3 \sin\delta_3 \sin\lambda_\odot + (\cos\delta_3 \sin\epsilon - \sin\alpha_3 \sin\delta_3 \cos\epsilon)\cos\lambda_\odot)$$

$$- e\kappa\,(\cos\alpha_3 \sin\delta_3 \sin\Pi + (\cos\delta_3 \sin\epsilon - \sin\alpha_3 \sin\delta_3 \cos\epsilon)\cos\Pi) \qquad 7)$$

where $\lambda_\odot$ is the celestial longitude of the Sun, Π is the longitude of perihelion, ϵ the obliquity of the ecliptic, κ the constant of aberration and e the eccentricity of the Earth's orbit.

v) Correction for Annual Parallax

(α_4, δ_4) are the heiocentric coordinates of star, (α_5, δ_5) are its geocentric coordinates, then, if π is the parallax of the star

$$\alpha_5 = \alpha_4 + \pi\,(\cos\alpha_4 \cos\epsilon \sin\lambda_\odot - \sin\alpha_4 \cos\lambda_\odot)\sec\delta_4$$

$$\delta_5 = \delta_4 + \pi\,(\cos\delta_4 \sin\epsilon \sin\lambda_\odot - \cos\alpha_4 \sin\delta_4 \cos\lambda_\odot$$

$$- \sin\alpha_4 \sin\delta_4 \cos\epsilon \sin\lambda_\odot) \qquad 8)$$

vi) Correction for Refraction

(α_s, δ_s) are the true geocentric equatorial coordinates of the star, (α_o, δ_o) the observed coordinates, if t_s is the true meridian angle of the star and H_s its true hour angle then

$$t_s = H_s \quad \text{if} \quad 0^\circ \leqslant H_s \leqslant 180^\circ$$

$$t_s = 360^\circ - H_s \quad \text{if} \quad 180^\circ < H_s < 360^\circ$$

If φ is the geocentric latitude of the observer, ζ is the true zenith distance of the star, and R is the coefficient of refraction, then

$$\alpha_o = \alpha_s + R \cos\varphi \sin t_s \sec\zeta$$

$$\delta_o = \delta_s + R (\sin\varphi \sec\delta \sec\zeta - \tan\delta_s) \qquad 9)$$

The effect of atmospheric dispersion shifting the relative positions of stars of different spectral type may be largely eliminated by the use of filters.

(α_o, δ_o) is the apparent position of the star just before its light strikes the corrector plate of the Schmidt telescope.

Instrumental Corrections

i) Corrections due to Improper Telescope Alignment

If the direction of the centre of curvature of the photographic plate is tilted at an angle β (assumed small, cf. Dixon (1963a)) with respect to the optical axis of the telescope then the error in the machine measured coordinates (X,Y) is given by

$$\Delta X = \beta XY$$

$$\Delta Y = \tfrac{1}{2}\beta (Y^2 - X^2) \qquad 10)$$

Both Schmidt telescopes belonging to the Royal Observatory Edinburgh may be adjusted to remove this error and any residual coma.

ii) Correction due to the Deformation of the Photographic Plate from a Sphere

The effect of the plate being deformed from a sphere is the same as if the focal length varied across the plate. At the peaks on the photographic plate the focal length is Δf less than at the points of contact. (see Fig. A2.1).

Let the functional relationship between F, the distance from the primary mirror to the deformed plate, in a

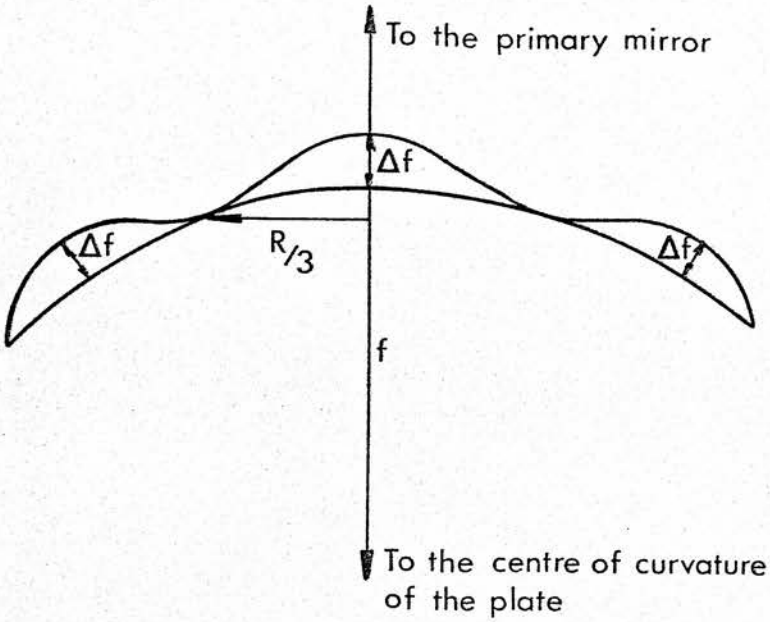

Fig. A2.1 A deformed Schmidt plate.

direction which passes through the centre of curvature of the mirror, and f the true focal length be given by

$$F = f - \Delta f \cos^2 \varphi \qquad 11)$$

If the radius of the plate is R and the distance from the plate centre, measured along the surface of the plate, is r, then, by measurement (cf.Reddish and Purchase 1963), R and r may be related to φ by

$$\varphi = 3\pi r / 2R$$

from which, by substituting for r $(= X^2+Y^2)$ and φ in equation 11),

$$F = f - \Delta f \cos^2 \left(3\pi (X^2+Y^2)^{1/2} / 2R \right) \qquad 12)$$

For the Royal Observatory Edinburgh Schmidt telescopes Δf has a maximum value of about 10μm which would cause a maximum deviation of some 0".05 at the edge of a 4° field, with the largest deviation occurring at 2R/3 from the plate centre (cf. equation 12) the worst expected error due to plate deformation would be about 0."04.

iii) Elastic Deformation of the Schmidt Plate

The correction ϵ , in radians, which has to be applied to star positions on the plate returning to the plane state

was given by Shepherd (1953) as

$$\epsilon = \frac{1}{16}(1-\sigma)\gamma^2\lambda - \frac{1}{48}(1-3\sigma)\lambda^3 \qquad 13)$$

where σ is Poissons ratio for glass, γ is the angular radius of the plate (the angle subtended by the plate radius at the centre of curvature of the plate) and λ is the off-axis angle. To the first approximation γ and λ may be written as:

$$\gamma = R/f \quad \text{and} \quad \lambda = (X^2+Y^2)^{1/2}/f$$

where (X,Y) are the measured Cartesian coordinates of the star on the plate, thus

$$\epsilon = \frac{(1-\sigma)}{16}\frac{R^2(X^2+Y^2)^{1/2}}{f^3} - \frac{(1-3\sigma)}{48}\frac{(X^2+Y^2)^{1/2}}{f^3} \qquad 14)$$

iv) Correction for an error in the Focal Length

Let (x,y) be the standard coordinates of a star with measured coordinates (X,Y) and equatorial coordinates (α,δ) on a plate with centre (A,D). If f is the focal length of the telescope thenthe relations between (x,y) and (X,Y) are given by

$$x = \frac{X}{f} - \frac{X}{6f^3}\left(X^2+Y^2\right)$$

$$y = \frac{Y}{f} - \frac{Y}{6f^3}\left(X^2+Y^2\right) \qquad 15)$$

The relations between the standard and equatorial coordinates are

$$\sin\delta = \sin D\left(1-\tfrac{1}{2}K-K^2\right) + y\cos D$$

$$\sin\left(\alpha-A\right) = x/\cos\delta$$

$$K = \left(x^2+y^2\right) \qquad 16)$$

By differentiating equations (15) with respect to f, equations (16) with respect to x and y, and making suitable substitutions it can readily be shown that for a change Δf in focal length, errors $(\Delta\alpha, \Delta\delta)$ given by equations (17), to the first order of small quantities, result

$$\Delta\alpha = \Delta f \sec\delta \sec\left(\alpha-A\right)\left(G\sin\left(\alpha-A\right)+H\right)$$

$$\Delta\delta = \Delta f\, G \operatorname{cosec}\delta \qquad 17)$$

where

$$H = \frac{X}{18f^4}(X^2+Y^2) - \frac{X}{f^2}$$

$$G = H \tan\delta \left\{ \cos D - \tfrac{1}{2}\sin D(2+K)\left(\frac{X}{f} - \frac{X}{6f^3}(X^2+Y^2)\right)\right\}$$

v) Correction for error due to Non-coincidence of Rectangular and Equatorial Coordinates in the Measuring Machine

Consider a star image whose true Cartesian coordinates in a system in which there is no rotation with respect to the equatorial coordinate system are (X,Y) and whose measured coordinates due to a rotation of θ° between coincident and apparent axes are (X', Y') then the standard transformation between the systems are

$$X = X'\cos\theta - Y'\sin\theta$$

$$Y = X'\sin\theta + Y'\cos\theta \qquad 18)$$

Substituting for (X,Y) in the expressions for the standard coordinates (x,y) yields

$$x = \frac{X'\cos\theta - Y'\sin\theta}{f} - \frac{x'\cos\theta - Y'\sin\theta}{6f^3}.(x'^2+Y'^2)$$

$$y = \frac{X'\sin\theta + Y'\cos\theta}{f} - \frac{X'\sin\theta + Y'\cos\theta}{6f^3}(x'^2+Y'^2) \qquad 19)$$

The differences ($\Delta x, \Delta y$) between equations (19) and those uncorrected for rotation θ are

$$\Delta x = \frac{X'(1-\cos\theta)+Y'\sin\theta}{f} - \frac{x'(1-\cos\theta)+Y'\sin\theta}{6f^3}.(x'^2+Y'^2)$$

$$\Delta y = \frac{Y'(1-\cos\theta)-X'\sin\theta}{f} - \frac{Y'(1-\cos\theta)-X'\sin\theta}{6f^3}.(x'^2+Y'^2) \qquad 20)$$

The equations (16) relating (x,y) to (α,δ) are differentiated with respect to x and y

$$\Delta\delta = \sec\delta\left[y(\cos D - \tfrac{1}{2}y\sin D(2+K)) - \tfrac{1}{2}\sin D(2+K)(x\Delta x + y\Delta y)\right]$$

$$\Delta\alpha = \sec(\alpha-A)\left\{\frac{x+\Delta x}{\cos\delta - \Delta\delta\sin\delta} - \sin(\alpha-A)\right\} \qquad 21)$$

Values for Δx and Δy from equations (20) may then be substituted into equations (21) to produce the errors ($\Delta\alpha, \Delta\delta$) generated in ($\alpha, \delta$) by a rotation of axes.

vi) Corrections for errors due to incorrect Plate Centre

If (α_0, δ_0) are the coordinates of the true field centre, (A, D) those of the assumed field centre (which is the origin of the (x,y) and (X,Y) systems), $(\Delta A, \Delta D)$ the distance between the two centres, $(\Delta x, \Delta y)$ the corresponding distance in standard coordinates, then to the first order of small quantities

$$\Delta A = -\Delta x \sec D$$

$$\Delta D = -\Delta y \qquad 22)$$

The errors $(\Delta\alpha, \Delta\delta)$ in the position of a star of measured coordinates (α, δ) are then given by

$$\Delta\delta = \sec\delta \left[\Delta D \left(\cos D \left(1 - \tfrac{1}{2}K - \tfrac{1}{8}K^2 \right) - y \sin D \right) - \Delta x \left(\sin D \left(x + \tfrac{1}{2} x K \right) \right) \right.$$

$$\left. + \Delta y \left(\cos D - \sin D \left(y + \tfrac{1}{2} y K \right) \right) \right] \qquad 23)$$

$$\Delta\alpha = \sec\delta \sec(\alpha - A)\, \Delta x = \sec\delta \tan\delta \sec(\alpha - A)\, \Delta\delta + \Delta A$$

SUMMARY

The nature of the discontinuity near the galactic equator at longitude 140° was investigated by studying the apparent surface distribution, the mean density functions and the proper motions of stars within an area of approximately 16 square degrees centred on $(\ell,b) = (140^{\circ},0^{\circ})$.

The suitability of the GALAXY machine for measuring precise stellar positions was tested. It was found that, after corrections for proper motions, the mean residuals between the catalogue and computed positions, from a Schmidt camera plate, for 430 stars in the Pleiades were $+0^{s}.002 \pm 0^{s}.009$ in right ascension and $+ 0''.03 \pm 0''.14$ (standard deviation) in declination. The standard deviations of these residuals correspond to 1μm on the plate. No magnitude or colour dependence was found for the GALAXY measures in the ranges of these variables considered.

UBV photoelectric magnitudes for 53 stars and RI magnitudes for 20 stars were measured. The magnitudes are given in the Johnson system.

Measurements were made of two plates taken 53 years apart to determine the proper motions of 553 stars common to both plates. U, B and V magnitudes for each of the stars were measured and the secular parallaxes of distinct

groups of stars, in preselected magnitude intervals, in the two colour diagram were derived in an attempt to identify possible stellar members of the α - spiral arm defined from HI observations by Verschuur. Other than late type giants the only group of objects whose distance corresponded to that of this arm was a small group of reddened early type stars.

Star counts in unit B and I magnitude intervals were made in nine regions, each 1.75 square degrees in area, distributed about $(l, b) = (140^{\circ}, 0^{\circ})$. The apparent surface distribution of the stars was examined using equal number density contour diagrams. The mean density function and the mean variation of interstellar absorption with distance for the various areas were determined using a combination of theoretical and observed cumulative Wolf diagrams. This analysis showed that the considerable change in the number of stars observed with galactic longitude is due, not to increased interstellar absorption, but rather, to a real reduction in the number of stars per unit volume of space.

ACKNOWLEDGEMENTS

I would like to thank my supervisors Professor H.A. Brück and Dr. M.J. Smyth for their encouragement and help.

I am indebted to many staff members of the Royal Observatory Edinburgh for their assistance. In particular to Dr. V.C. Reddish who originated the project, to Professor R.H. Stoy for expert advice on the reduction of photoelectric observations, to Dr. S.V.M. Clube and Dr. K. Nandy for various enlightening discussions and to the GALAXY group (Dr. N.M. Pratt, Mr. A. McLachlan, and Mr. C.K. Barclay).

My thanks are due to Mr. C.A. Murray of the Royal Greenwich Observatory for providing an extract from the AGK3 catalogue, to Dr. R.D. Wolstencroft of the University of Hawaii for making some of the photoelectric observations, to Dr. P. Treanor of the Specola Vaticana for providing the first epoch astrograph plate, and to Miss N. Houk of the Warner & Swasey Observatory for taking some of the photographic plates.

I should like also to thank Miss J.M. Jukes who typed the thesis, Mrs. M. Fretwell who drew the diagrams and Mr. P. Conlon who prepared the photographic prints.

REFERENCES

Adam, G.R., (1971) Publ. Roy. Obs. Edinburgh, 8, 43.

Allen, C.W., (1963) Astrophysical Quantities, University of London, 194.

Andersen, J., (1971) Astron. & Astrophys., 13, 40.

Baker, J.R., and Smith, F.G., (1971) Mon. Not. Roy. Astr. Soc., 152, 361.

Barney, I., (1955) Mitt. Astron. Ges., 7, 38.

Berkhuijsen, E.M., (1972) Astron. & Astrophys Suppl., 5, 263.

Bertiau, F.C., and de Graeve, E., (1967) Spec. Vat. Ric. Astron., 7, 281.

Blanco, V.M., et al. (1968) Publ. U.S.N. Obs., 21.

Bok, B.J., (1937) The distribution of the stars in space, University of Chicago Press.

Bridle, A.H., (1968) Mon. Not. Roy. Astr. Soc., 138, 251.

Brück, M.T., et al. (1968) Nature, 218, 662.

Cooke, B.A., et al. (1969) Nature, 224, 134

Courtès, G., et al. (1970) The spiral structure of our Galaxy, IAU Symposium No. 38, Holland, 209.

Crézé, M., (1972) Astron. & Astrophys., 21, 85.

Davis, L., and Greenstein, J.L., (1951) Astrophys. J., 114, 206.

Debehogne, H., (1968) Bull. Cl. Sci. Acad. Roy. Begique, 54, 42.

Delhaye, J., (1965) Galactic Structure, edited by A. Blaauw and M. Schmidt, University of Chicago Press.

Deupree, R., (1969) Publ. Astr. Soc. Pac., 81, 130.

Dieckvoss, W., (1955) Mitt. Astron. Ges., 7, 40.

Dieckvoss, W., and de Vegt, C., (1966) Astron. Abh. Hamburg Sterw. Bergedorf, 8 (2).

Dixon, M.E., (1962) Mon. Not. Astr. Soc. Sth. Africa, 21, 184.

Dixon, M.E., (1963a) ibid 22, 6.

Dixon, M.E., (1963b) ibid 22, 32.

Dixon, M.E., (1967) Mon. Not. Roy. Astr. Soc., 137, 337.

Dodd, R.J., (1972) Astron. J., 77, 306.

Eichhorn, H., et al. (1970) Mem. Roy. Astr. Soc., 73, 125.

Fellgett, P.B., and Seddon, H., (1963) Observatory, 83, 25.

Fernie, J.D., (1968) Astron. J., 73, 995.

Fernie, J.D., and Hube, J.O. (1968) Astron. J., 73, 492.

FitzGerald, M.P., (1968) Astron. J., 73, 983.

Georgelin, Y.P., and Georgelin, Y.M., (1971) Astron. & Astrophys., 12, 482.

Goss, W.M., (1967) Astrophys. J. Suppl., 15, 131.

Hawgood, J., (1965) Numerical Methods in Algol, McGraw - Hill, London.

Hertzsprung, E., (1947) Ann. Sterrw. Leiden, 19, 1A.

Hughs, E.E., et al. (1969) Bull. Amer. Astr. Soc., 1, 193.

Humphreys, R.M., (1970a) Astron. J., 75, 602.

Humphreys, R.M., (1970b) Contr. Kitt Peak Nat. Obs., No. 554, 41.

Iriarte, B., et al. (1965) Sky and Telescope, 30, 21.

Jefferies, J.T., and Sinton, W.M., (1968) Sky and Telescope, 36, 140.

Johnson, H.L., (1964) Boll. Obs. Tonantzintla Tacubaya, 3, 305.

Johnson, H.L., (1966) Ann. Rev. Astron. & Astrophys., 4, 193.

Johnson, H.L. (1968) Nebulae and Interstellar Matter, edited by B.M. Middlehurst and L.H. Aller, University of Chicago Press, 167.

Kerr, F.J., and Westerhout, G., (1965) Galactic Structure, edited by A. Blaawu and M. Schmidt, University of Chicago Press, 167.

Khavtasi, J.Sh., (1960) An atlas of dark nebulae, Akad. Nauk U.S.S.R., Tbilsi.

King, H.C., (1955) The history of the telescope, Charles Griffin and Co. Ltd., London.

Kohoutek, L., (1972) Astron. & Astrophys., 16, 291.

König, A., (1924) Astron. Nachr., 222, 177.

Kostjakova, E.B., (1970) The Spiral Structure of our Galaxy, IAU Symposium No. 38, Holland, 225.

Kraft, R.P., and Schmidt, M., (1963) Astrophys. J., 137, 249.

Lawrence, L.C., and Reddish, V.C., (1965) Publ. Roy. Obs. Edinburgh, 3, 279.

McCuskey, S.W., and Houk, N., (1971) Astron. J., 76, 117.

Mathewson, D.S., (1968) Astrophys. J., 153, L47.

Mathewson, D.S., and Ford, V.L., (1970) Mem. Roy. Astr. Soc., 74, 139.

Mathewson, D.S., and Nicholls, D.C., (1968) Astrophys. J., 154, L11.

Mavridis, L.N., (1966) Colloquium on late type stars, Trieste, 420.

Mavridis, L.N., (1971) Structure and evolution of the Galaxy, Holland, 110.

Mezger, P.G., (1970) The Spiral Structure of our Galaxy, IAU Symposium No. 38, Holland, 107.

Mihalas, D., and Routly, P.M., (1968) Galactic Astronomy, W.A. Freeman and Co., San Francisco.

Moffat, A.F.J., and Vogt, N., (1973) Astron. & Astrophys., 23, 317.

Morrison, D., and Jefferies, J.T., (1972) Sky and Telescope, 44, 361.

Neckel, Th., (1967) Veröffentl. Landessternw. Heidelberg-Königstuhl, 19.

Neugebauer, G., and Leighton, R.B., (1969) Two micron Sky Survey, N.A.S.A., California.

Perek, L., and Kohoutek, L., (1967) Catalogue of Galactic Planetary Nebulae, Prague.

Pratt, N.M., (1971) Publ. Roy. Obs. Edinburgh, 8, 109.

Racine, R., and van den Bergh, S., (1970) The Spiral Structure of our Galaxy, IAU Symposium No. 38, 219.

Reddish, V.C., (1966) Sky and Telescope, 32, 124.

Reddish, V.C., (1967) Nature, 213, 1107.

Reddish, V.C., and Purchase, D.E., (1963) Ann. Report Roy. Obs. Edinburgh, 3.

Rickard, J.J., (1968) Astrophys. J., 152, 1019.

Rohlfs, K., (1967) Zs.f. Astrophys., 66, 225.

Rudkjøbing, M., (1970) Astrophys. & Sp. Sc., 6, 157.

Ryter, C., (1970) Astron. & Astrophys., 9, 288.

Sato, F., (1970) Ann. Tokyo Ast. Obs. 2nd Ser., 12, 1.

Schmidt, M., (1965) Galactic Structure, edited by A. Blaauw and M. Schmidt, University of Chicago Press, 513.

Schulte, D.H. and Crawford, D.L., (1961) Contr. Kitt Peak Nat. Obs., No.10.

Schwartz, D.A., (1969) Thesis, Dept. of Physics, University of California.

Seaquist, E.R., (1967) Astron. J., 72, 1359.

Seddon, H., (1968) Nature, 217, 932.

Seddon, H., and Jones, W., (1966) Publ. Roy. Obs. Edinburgh, 5, 99.

Seward, F.D., (1973) Sky and Telescope, 45, 220.

Shepherd, W.M., (1953) Mon. Not. Roy. Astr. Soc., 113, 450.

Sim, M.E., (1968a) Publ. Roy. Obs. Edinburgh, 6, 123.

Sim, M.E., (1968b) Observatory, 88, 62.

Smith, L.F., (1968) Mon. Not. Roy. Astr. Soc., 141, 317.

Spoelstra, T.A.Th., (1972) Astron. & Astrophys., 21, 61.

Tammann, G.A., (1970) The Spiral Structure of our Galaxy, IAU Symposium No. 38, Holland, 236.

Torgård, I., (1961) Ann. Obs. Lund, 15.

Van Rhijn, P.J., and Bok, B.J., (1931) Groningen Publ., 45.

Velden, L., (1970) The Spiral Structure of our Galaxy, IAU Symposium No. 38, Holland, 164.

Verschuur, G.L., (1968) Observatory, 88, 15.

Verschuur, G.L., (1969) Astron. J., 74, 597.

Verschuur, G.L., (1973) Astron. & Astrophys., 24, 193.

Walker, G.S., (1971) Publ. Roy. Obs. Edinburgh, 8, 109.

Wolf, M., (1923) Astron. Nachr., 219, 109.